ELECTROCHEMICAL IMMUNOSENSOR FOR RAPID AND SPECIFIC DETECTION OF SARS-COV-2

Viviana Katherine Vásquez Fonseca

Master's thesis submitted for the degree of Master in Materials Engineering.

Director

Jahir Orozco Holguín, PhD in Chemistry

Co-director

Ana María Torres López, PhD in Medical Sciences

University of Antioquia

Faculty of Engineering

Master's Degree in Materials Engineering

Medellín, Antioquia, Colombia

2022

Dedication

I dedicate this master's thesis to all those who died in the COVID-19 pandemic as a symbol of the importance of supporting health research to advance new technologies that allow a rapid response to emerging diseases and even those that still claim millions of lives. I also dedicate this work to my family, who have always supported me in this great challenge. To Jerónimo García for being my pillar in every moment and circumstance of life, and my director Jahir Orozco for his trust and advice. To my colleagues in the Max Planck Tandem Group for their help, advice, teaching, and showing me the wonders of science and research. Finally, I dedicate this work to Alexandra Elbakyan for giving the world the opportunity of free access to science, which as researchers, helps us to achieve new and better results.

TABLE OF CONTENT

LIST OF FIGURES

LIST OF FIGURES ANNEX 1 (SUPPLEMENTARY INFORMATION)

LIST OF TABLES

Academic production

Published articles:

1. V. Vásquez, M.-C. Navas, J. A. Jaimes, and J. Orozco, "SARS-CoV-2 electrochemical immunosensor based on the spike-ACE2 complex," *Anal. Chim. Acta*, p. 339718, Mar. 2022, doi: 10.1016/J.ACA.2022.339718

2. Vásquez, V., Orozco, J. Detection of COVID-19-related biomarkers by electrochemical biosensors and potential for diagnosis, prognosis, and prediction of the course of the disease in the context of personalized medicine. Anal Bioanal Chem (2022). https://doi.org/10.1007/s00216-022-04237-7

E-poster:

3. Maria-Camila López, Viviana Vásquez, Javier A. Jaimes, Mauricio Rojas, Jahir Orozco, Maria-Cristina Navas. “Production and characterization of pseudotyped particles to develop an inmunosensor for SARS-CoV-2”. Congress Biosensors for Pandemics 2021. Spain. February, 2021.

ABSTRACT

COVID-19 is an emerging infection produced by the etiologic agent coronavirus type 2, causing severe acute respiratory syndrome (SARS-CoV-2). It appeared in China in late 2019 and then spread worldwide. Timely detection is imperative to reduce the speed of contagion and contribute to the traceability of the disease. Currently, diagnostics is done by reverse transcription-polymerase chain reaction (RT-PCR) that detects the genetic material of the virus requiring robust equipment and trained personnel, or by antigen and serological tests that detect the structural proteins of the virus and antibodies generated by the host, respectively, but with cross-reactivity and low sensitivity. Biosensors can take advantage of the high affinity of biorecognition molecules and unique material properties for rapid, specific and highly sensitive detection of SARS-CoV-2, offering a promising solution to the limitations of conventional methods. In this work, an electrochemical immunosensor has been developed for the rapid and trustworthy detection of SARS-CoV-2. The immunosensor captured the protein S from the virus between magnetic beads functionalized with primary antibodies and specific secondary antibodies, which were labeled with a reporter enzyme. The system was confined to the surface of screen-printed electrodes, and the enzyme-mediator interaction signal was recorded in a portable potentiostat. The biosensor was characterized in terms of analytical performance and detected commercial protein S and protein S from viral particles, pseudovirions and samples from patients in concentrations of clinical relevance (22.5 ng/mL-2 μg/mL), opening the possibility of SARS-CoV-2 detection at the point of care.

Keywords — **bioengineering, biosensor, SARS-CoV-2, COVID-19, electrochemistry.**

CHAPTER I: Introduction, statement of the problem, justification and objectives

INTRODUCTION

Infectious diseases attract the attention of health care systems worldwide because of their ability to infect one individual to another and create resistance to antimicrobial drugs, leading to a higher mortality rate in the population [1]. Another issue is the sudden appearance of emerging diseases due to zoonotic pathogens such as the current SARS-CoV- 2, which appeared in China at the end of 2019 and spread worldwide in just a couple of months [2]. SARS-CoV-2 is part of the coronavirus family, characterized by having a high infection capacity derived from rapid replication of its genetic material in the host and from a surface protein called protein S (or spike protein) that is responsible for binding with a high affinity to cell receptors and then infecting the cells of the human body, mainly in organs such as the lungs [3].

There are currently three main strategies for detecting the virus in patients. One is based on the RT-PCR to detect the virus genetic material, hindered by high equipment and trained personnel requirements. The other one relies on an antigen test that detects structural proteins of the virus such as S protein or N protein with low sensitivity, and finally, the serological test to detect the antibodies generated by the human body after contact with the virus but lacks sensitivity, frequently having false-positive results and therefore not reliable by itself as a diagnostic tool [3].

Nanotechnology has opened the path to developing new strategies to solve the issues of standard detection technologies. Nanobiosensor-based devices take advantage of the high affinity of biorecognition molecules and the unique properties of nanomaterials to offer alternatives for the highly selective and specific detection of SARS-CoV-2 and rapid and timely screening of infected/healthy people. In addition, the devices hold the potential to be implemented at the point of care to avoid samples and/or patients' displacement, reducing the virus spreading.

PROBLEM STATEMENT

COVID-19 is an infectious disease caused by SARS-CoV-2, first reported in Wuhan (China) in December 2019 [4]. SARS-CoV-2 is a virus belonging to the coronavirus family and is the seventh virus known to infect humans. It can cause severe respiratory illness, leading to death, affecting all people without discrimination of race, gender, age, or social status [5]. This virus has generated significant concern throughout the population because it is highly contagious [6], spreading quickly from person to person via droplets that come out from an infected person's nose or mouth when coughing, sneezing or even talking, or through contact with contaminated surfaces or objects, potentially increasing its spread speed [4] and creating an unprecedented health emergency. Strategies such as strict quarantines, social distancing, frequent hand washing, masks, and timely diagnosis of patients with COVID 19 have been crucial as countermeasures. In this context, rapid, simple and specific detection of the virus is essential to reduce its impact related to spread speed. Standard diagnostic protocols consist of molecular methods of virus detection by an RT-PCR that detects the genetic material (RNA), or through rapid tests for detection of the structural proteins of the virus, and indirectly by serological methods that detect IgG and IgM antibodies generated by the host [5]. However, these methods are time consuming and tedious, requiring hours or even days to obtain results; in addition, rural populations, usually with fewer resources, need to travel (or transport samples) to urban centers for diagnosis, further delaying results and increasing the risk of contagion.

Although researchers and health care systems worldwide have made significant advances in discovering and implementing vaccines and effective treatments, there is still a long way to go, and the best way to contain the virus and decrease the mortality rate remains through prevention and timely, rapid and effective detection. Therefore, new strategies are needed to help screen the population with COVID-19, with or without symptoms. For example, biosensors integrate biorecognition elements with transduction platforms and, sometimes, amplification systems. It is essential to consider which type of transducer offers the most significant advantages, considering the need for timely point-of-care screening, and which type of bioreceptor (immunosensors, genosensor, aptasensor, glycosensors, etc) is required to interact with the target biomarker specifically, considering the mutation rate of the virus

that makes many variants have emerged. There are several ongoing pieces of research on developing biosensors to detect the genetic material or structural proteins of SARS-CoV-2. However, they are at an early stage, so further studies are required to improve their analytical properties and achieve sensitive detection, with limits of detection (LOD) of clinical relevance that can be implemented at the point of care.

Research Question

Can a biosensor functionalized with specific receptors provide a rapid, specific, low-cost, and easy-to-implement alternative for SARS-CoV-2 detection?

JUSTIFICATION

The SARS-CoV-2, which causes coronavirus disease 2019 (COVID-19), has caused great concern worldwide because the rapidly generated health crisis has impacted the economy and society, so countries worldwide have focused on finding strategies to reduce its future effects. One of the alternatives to mitigate its impact is the rapid detection of the virus to identify infected people and screening the population, whether they have symptoms or not, isolating them further, thus reducing the spread speed.

Since the beginning of the pandemic in Colombia, we have gone from analyzing just over 4000 samples in one day to about 50000 samples both by RT-PCR and antigen testing, but further population screening is still required to detect people with the infection rapidly. Although research in biosensors is new in Colombia, it has been decades worldwide. During this time, biosensors have demonstrated to offer a possibility to face the current health crisis related to SARS-CoV-2 diagnosis issues by detecting the virus at the point of care and screening the population regardless of symptoms or not. In addition, as a transversal platform, these devices have potential applications in detecting other biomolecules, biomarkers, and even other possible emerging diseases, being a basis for new technological developments and innovation. Electrochemical biosensors are detection tools that measure electrochemical changes at electrode surfaces from the bioreceptor-target analyte interaction. They are characterized by their ability to produce reliable analytical information more efficiently and faster than other methods. Furthermore, their versatility makes them amenable to being miniaturized and portable for implementation at the point of care, simplifying the processes, avoiding extraction or amplification, and minimizing the displacement of samples or patients.

This project seeks to develop a new strategy for the rapid detection of SARS-CoV-2, with a sensitivity comparable to standard testing methods, at a relatively low cost, and with an easy-to-use point-of-care device to avoid the displacement of samples and/or patients. A biosensor like this will allow rapid population screening to implement measures that decrease the contagion rate. Furthermore, the target analyte could be measured in different matrices thanks to the ability of the modified magnetic beads to capture the target analyte from the medium,

even in the presence of interferents from a real complex matrix. In addition, the detection platform could be readily modified further to detect other emerging diseases.

Furthermore, the project was a joint effort between the BIOMAT research group of the Bioengineering program and the Max Planck tandem group in Nanobioengineering, both from the University of Antioquia. Finally, this work was part of the project "Nanobiosensors for the rapid detection of SARS-CoV-2" from Minciencias Cod. 1115101576765, "Invitation to present projects that contribute to solving current health problems related to the COVID-19 pandemic" [7].

OBJETIVES

A. *General objective*

Develop an electrochemical immunosensor for rapid and specific detection of SARS-CoV-2 that is easy to implement at the point of care.

B. *Specific objectives*

- Determine the components and suitable conditions to assemble the immunosensor by rapidly screening through analysis of its optical and electrochemical responses.

- Evaluate the analytical characteristics of the assembled electrochemical biosensor in terms of specificity, sensitivity, detection limits, reproducibility and stability.

- Study the device's performance in buffered solutions spiked with commercial protein S, pseudovirions and viral particles, and real patient samples.

CHAPTER II: Theoretical framework and state of the art

1. Severe acute respiratory syndrome coronavirus 2 (SARS-CoV-2)

Although zoonotic pathogens (animal origin) have affected humanity since the beginning of the 21st century [1], [3], [8]–[10], the recent emergence of viral infectious diseases caused by coronaviruses has affected the entire world population. Coronaviruses are a group of single-stranded RNA viruses named for the corona-like structure on their outer surface, classified into alpha (α), beta (β), gamma (γ) and delta (δ) genera. Although these viruses infect a wide variety of mammalian (alpha and beta) and avian (gamma and delta) species, only seven are known to have infected humans [8], [11]–[13]. Four of these coronaviruses have low pathogenicity, being endemic in humans, i.e., human coronavirus OC43 (HCoV-OC43), HKU1 (HCoV-HKU1), NL63 (HCoV-NL63) and 229E (HCoV-229E), but the other three, i.e., severe acute respiratory syndrome coronavirus (SARS-CoV), Middle East respiratory syndrome coronavirus (MERS-CoV) and SARS-CoV-2, are highly pathogenic [2], [8], [12]. This last-mentioned is indeed a beta coronavirus responsible for severe and potentially fatal respiratory disease [8], [12].

SARS-CoV, transmitted from civet cats to humans, emerged in China in 2002 and caused a pandemic with more than 8000 infected and 800 deaths. MERS-CoV, transmitted from dromedaries to humans, appeared in 2012 in the Middle East, causing about 2500 cases and 860 deaths worldwide [8], [14]. In December 2019, in Wuhan, Hubei province of China, a new coronavirus, SARS-CoV-2, was found to be responsible for an outbreak of atypical pneumonia defined as coronavirus disease of 2019 (COVID-19) [2], [15]. In January 2020, the virus was sequenced and isolated in China [9] and since then, it has spread rapidly worldwide. The World Health Organization (WHO) declared it a pandemic on March 11, 2020 [12] and about two years later, more than 400 million cases and 5.76 million deaths in the world had been reported [15], even though by February 2022, 54% of people were already fully vaccinated [16].

1.1. Structure

SARS-CoV-2 shares approximately 80% of its genome with SARS-CoV and 96% with the bat coronavirus BatCoV RaTG13 [12], [13], [17], indicating that SARS-CoV-2 most likely originated in bats jumped to humans via an intermedary that seems to have been the pangolín [8]. Its RNA sequence is approximately 30000 bases long and its structure consists of four proteins, i.e., spicule (S protein), membrane (M protein), envelope (E protein) and nucleocapsid (N protein) proteins (see Figure 1) [18].

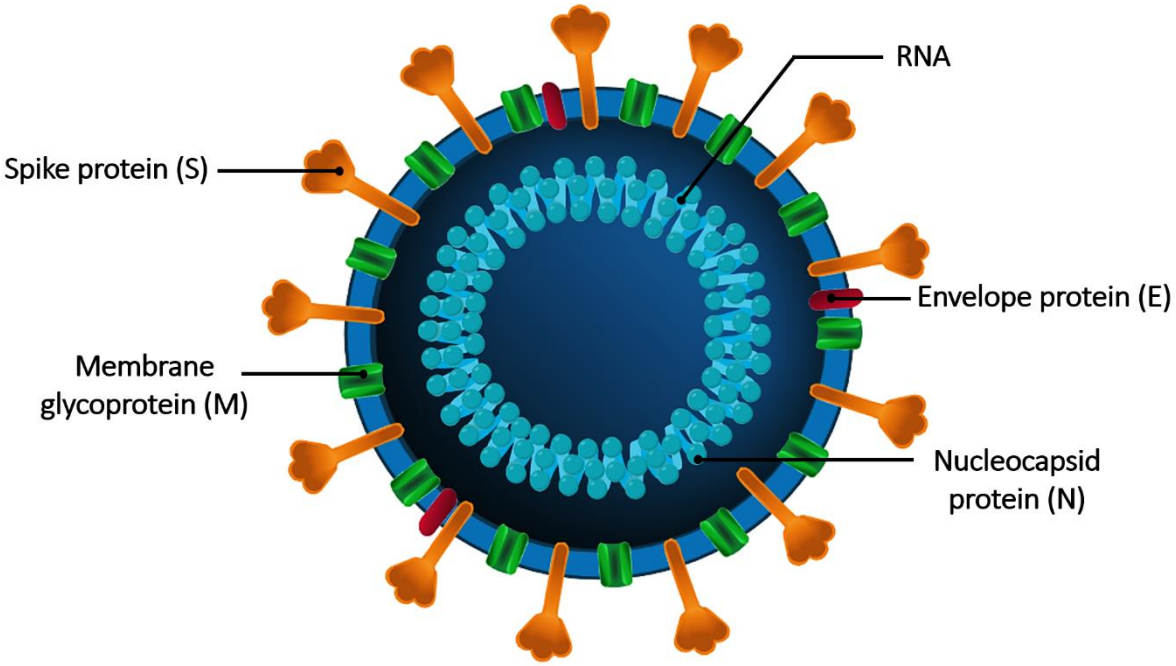

Figure 1. Structure of SARS-CoV-2. Formed mainly by the genetic material (RNA) and the four structural proteins, i.e., nucleocapsid protein (N), an envelope protein (E), membrane protein (M) and spike protein (S). Modified from reference [19].

The SARS-CoV-2 genome contains two 5' and 3' untranslated regions (UTRs), one open reading frame (ORF) encoding the sixteen nonstructural proteins (nsp1-16) and five other ORFs encoding the four structural proteins and eight accessory proteins [12]. The highly immunogenic phosphoprotein N protein is the most abundant in the coronavirus [17]. N protein consists of an N-terminal domain and a C-terminal domain, both of which can bind to the viral RNA and thus help with the packaging of the viral genome [18], responsible for viral RNA transcription and replication [20]. The E protein is an integral membrane protein of 8-12 KDa and regulates virus life cycles, such as virus assembly and release. In addition,

it functions as an ion channel, which is necessary for pathogenesis [12], [18]. The M protein is a dimeric protein with a size of 25-30 KDa, which is responsible for shaping the virion as it maintains the curvature of the membrane and binds to the nucleocapsid [18]. The M and N proteins' binding stabilizes the nucleocapsid and helps complete viral assembly, while the E and M proteins form the viral envelope [21]. S protein is a 150 KDa trimeric class I fusion glycoprotein located on the viral particle surface responsible for binding to the host receptor. It is highly N-glycosylated and forms peaks between 18 and 23 nm long on the virus surface. It consists of S1 and S2 subunits [18], [22]. The S1 subunit is responsible for receptor recognition. It comprises four distinct A-D domains, consisting of the N-terminal region (NTD) formed by the A domain and is also called the receptor-binding domain (RBD) and the C-terminal region (CTD) formed by B, C and D domains. The S2 subunit facilitates virus-cell fusion and forms the stem of the spike [8], [12], [21], [22].

1.2. Mechanism of infection

SARS-CoV-2 is transmitted from person to person by direct inhalation of contaminated droplets released into the environment when an infected person sneezes or coughs. It is also transmitted by direct contact through oral, nasal and ocular mucosa. Other important means of transmission are objects that have been in contact with an infected person [19], [23]. Upon entering the body, SARS-CoV-2 binds to epithelial cells in the mouth or nose and can even migrate through the airways and infect type II alveolar pneumocytes [19]. These cells are characterized by having within their receptors the human angiotensin-converting enzyme 2 (ACE 2), being the main entry point of the virus, even though other SARS-CoV-2 entry receptors have also been reported, e.g., DC-SIGN (CD209), CD147, L-SIGN (CD209L) [23] and AXL [24]. ACE2 is found in various tissues and organs, such as the lungs, heart, kidneys, liver, gastrointestinal tract and blood vessels. This enzyme regulates blood pressure and inflammation by controlling the renin-angiotensin-aldosterone system [8], [23].

The RBD in the S protein from the virus consists of 394 glutamine residues, recognized explicitly by 31 lysine residues of the host ACE2 enzyme [19], [25]. The RBD region of the SARS-CoV-2 binds to the ACE2 receptor with a 10-20 fold higher affinity than SARS-CoV, which facilitates viral entry and explains the easiness of virus spread from person to person [25], [26].

Following the binding between S protein and the ACE2 receptor, the acid-dependent transmembrane protease serine 2 (TMPRSS2), cathepsins and furin enzymes carry out the S protein cleavage precisely in 2 portions of the S2 region. In the first one, the RBD region and the fusion domains of S protein are separated, and in the second one, the fusion peptide is exposed and inserted into the membrane to allow the fusion of the viral and host membranes [6], [18], [21], [27]–[29]. When the virus manages to enter the cell, RNA is released into the cell cytoplasm and initiates its translation and replication process by appropriating the cell's reproductive machinery (endoplasmic reticulum and Golgi complex and the endoplasmic reticulum) to produce more viral copies. Finally, the virus is transported to the membrane, exits the cell by exocytosis, and travels to infect other cells [8], [19], [21], [30].

1.3. Detection of SARS-CoV-2

Pathogen detection aims to identify specific biomolecules of the microorganism or molecular changes in the host [8]. Currently, there are three strategies to detect SARS-CoV-2, i.e., detection of the viral genetic material (RNA), viral antigens (structural proteins) or antibodies generated by the host [3].

The main diagnostic tool for SARS-CoV-2 has been the RT-PCR, a technique that detects the genetic material of the virus by combining reverse transcription of RNA into complementary DNA and amplifying specific targets [8], [31]–[33]. It is initially required to collect the sample from the patient, mainly by nasopharyngeal swabbing, followed by RNA extraction and purification for reverse transcription. Finally, the sample reacts with a cocktail of probes that recognize specific SARS-CoV-2 biomarkers such as the E gene, the RdRp gene and the ORF 1ab gene in a thermal cycler [3], [34], [35]. This technique is the most widely used due to its sensitivity and specificity, allowing the virus to be identified accurately and reliably [12]. However, it requires highly specialized personnel and instrumentation, and two to five hours approximately to obtain the results, but due to the need to transport the samples to specialized laboratories, it can take twenty-four hours or more, increasing the related costs and the possibility of the virus spreading [3], [20].

Another strategy currently used to detect SARS-CoV-2 is rapid antigen detection tests (RADTs) [3] that detect viral particles from their structural proteins, such as S or N proteins.

Although less sensitive than RT-PCR, it is faster and easier to implement, obtaining results in approximately 30 minutes [36].

Serological tests have also been used to detect SARS-CoV-2 infection, an indirect method that detects antibodies generated by the body of infected people. When foreign agents enter the body, such as microorganisms, the immune system responds rapidly to eliminate the foreign agent and creates antibodies that detect these foreign agents to have some immunity in posterity [3], [35]. In the case of COVID-19, the body generates immunoglobulin M (IgM) at the beginning of the infection or when it is acute, and immunoglobulin G (IgG) appears as a response to the acute phase. For their detection, a blood sample is taken from the patient and transferred directly to the test (immunochromatographic, enzyme-linked immunosorbent assay (ELISA) or lateral flow immunoassay), which gives the results in 5-15 minutes or even hours [3], [34]. Yet, these tests are not recommended as diagnostic tools due to their low sensitivity. For example, in asymptomatic cases, the concentration of these antibodies is low, so false-negative results can be obtained in people with the infection [36]. In addition, a positive result only indicates that the person has been in contact with the virus, but it is not known precisely whether the person is still infected [33].

2. Biosensors

Biosensors have been investigated with increased interest due to the growing demand for detecting molecules at low concentrations and with high specificity [37]. They are autonomous devices that integrate materials and biomolecules coupled with transducers that transform the bioreceptor-analyte interaction's physical, chemical or biological interaction into a quantifiable signal for the selective and specific detection of molecular targets [38]–[42]. These devices are characterized by high sensitivity, low detection limit and high specificity derived from the material properties and biological recognition systems. In addition, they can be miniaturized and integrated into portable analysis systems using very small reagents and sample volumes in rapid and straightforward assays [40].

Biosensors consist of a biological component called a biorecognition element, which is in direct contact with a transducer platform and a device for data reading, collecting and evaluating analytical information [39], [43], [44], i.e., the biological components are immobilized on the surface of the transducers to interact with high affinity with the target

molecule. As a result, it generates a physicochemical signal that is converted into a measurable and quantifiable signal [39], amplified and analyzed in a processing system, as shown in Figure 2 [40], [45].

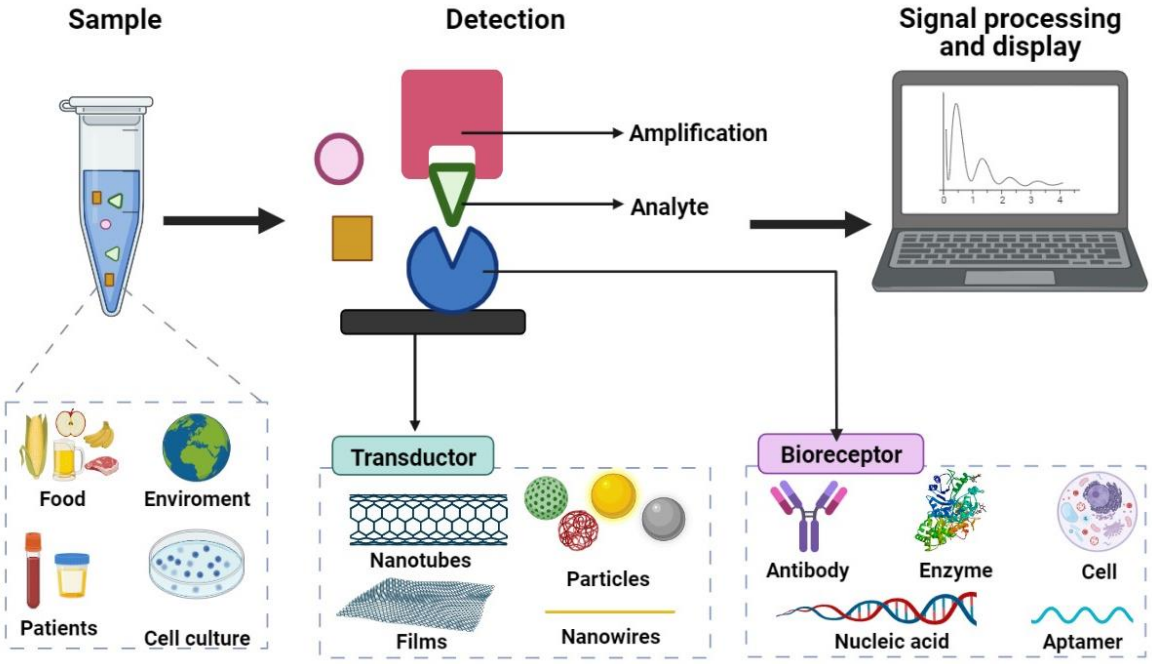

Figure 2. Components of a biosensor. The first component is the detection system, which includes the transducer that can be modified with different nanomaterials and biological receptors that improve sensitivity and specificity, respectively. In some cases, it can also have amplification systems. The second component is the amplification and processing system, which allows the visualization and analysis of the data. This equipment can be portable or with the capacity to analyze multiple samples. The sample can come from cell cultures, patients, food, or the environment and contains the analyte of interest. Modified from reference [40].

Biological recognition elements include enzymes, proteins, antibodies, nucleic acids, cells, tissues, receptor molecules, etc [46]. These molecules are responsible for giving specificity to the sensor and must be in direct contact with the transducer [11], [15]. Depending on the recognition element, biosensors can be catalytic, including enzymes, microorganisms, organelles, cells, or tissues, and affinity-based biosensors, including antibodies, nucleic acids, proteins, peptides, aptamers, etc [39], [40]. In developing biosensors, a wide range of transducers has been investigated to offer different detection and signal conversion strategies,

classified as electrochemical, optical, mass, thermoelectric, piezoelectric, and calorimetric etc [40].

2.1. Classification of biosensors

Biosensors can be classified according to the immobilized biosensing molecule or transduction mode.

2.1.1. According to the bioreceptor biomolecule

Biological receptors are recognition elements responsible for the biosensors' specificity [42], [47]. Biosensors can be catalytic or based on affinity reactions [39], [40]. From catalytic biosensors, the most studied are those based on enzymes. Their principle of work is based on enzyme-substrate catalytic reactions that consume or generate a detectable compound; or on activation or inhibition of the enzymatic activity in the presence of the analyte [40], [48]. Although these biosensors have high sensitivity, they often have low stability and their performance is highly dependent on pH, ionic strength and temperature [40].

Whole cells, such as microorganisms, have also been reported as recognition elements in biosensors [48]. They offer several advantages, such as low cost and the ability to metabolize compounds and release other molecules, such as ammonia, carbon dioxides, and hydrogen ions, measured by the transducer. But it also has several limitations, such as a short lifetime, low reproducibility and low stability. Therefore, this biosensor is mainly used in the environmental and food areas to detect contaminants or pathogens [40].

Affinity biosensors are based on analyte-macromolecule interactions, whose macromolecules have been artificially engineered or isolated from the biological environment [48]. Immunosensors are based on highly selective, specific and rapid antigen-antibody interactions [40], [48]. These biosensors have been widely investigated mainly for diagnosing infectious diseases and monitoring disease-related biomarkers, among many other applications. Nucleic acids have been widely used as bioreceptors when developing genosensors and aptasensors [40], [48]. Genosensor high specificity is due to the ability of the base pair to interact with the complementary sequence by Watson and Crick's pairing. For its design, a short synthetic probe called a capture probe is immobilized on the transducer and hybridizes with the RNA or DNA of the sample, straightforwardly generating changes in the electrical properties of the transducer or a sandwich-like format through enzymatic reactions by a labeled signal probe. This interaction is of high affinity and can be reversible.

One of the main issues of this type of system is that the concentrations of nucleic acids in samples are usually too low, requiring highly sensitive biosensors with very low detection limits to detect these concentrations [40]. Unlike genosensors, aptasensors bind to other target molecules, such as proteins, ions, toxins or small organic molecules. They are characterized by a unique three-dimensional shape that significantly improves their affinity to the analyte [49].

2.1.2. According to the transducer

A wide range of transducers has been investigated in developing biosensors to provide different detection strategies of high performance. These biosensors can be classified as electrochemical, optical, piezoelectric, and calorimetric [40].

Electrochemical biosensors are among the most studied biosensors because they can be portable and amenable to miniaturization, offering new venues for point-of-care solutions. In addition, these biosensors measure electrochemical changes at the electrode sensing surface upon interaction with the analyte of interest [40], [41].

Optical biosensors measure light based on optical diffraction, i.e., an optical device emits a beam of light that is directed at the sensing surface, part of the light is reflected according to the surface properties and the equipment measures changes in the properties of the light, which indicate changes in mass, concentration or number of molecules of interest. Optical signals of most interests in biosensor design include absorbance, fluorescence, chemiluminescence, and surface plasmon resonance [40], [41]. These biosensors can analyze many samples at once but require robust equipment for detection and miniaturization and use at the point of care is more limited.

Piezoelectric biosensors or mass sensors use a piezoelectric quartz crystal as a detection principle. The bioreceptor is immobilized on the crystal and upon interaction with the analyte, changes in the crystal resonance frequency are correlated with mass changes. These sensors also require robust equipment for their use to be of interest at the point of care [40], [41].

Calorimetric or thermal sensors measure heat generation in a reaction and are mainly used in enzyme-based biosensors with clinical and environmental applications [40].

2.2. Electrochemical biosensors

Electrochemical biosensors are widely explored due to their amenability to miniaturize, offering portability and thus new opportunities for point-of-care detection. These biosensors measure physicochemical or biological changes at the electrode surface when interacting with the analyte of interest, producing an electrical signal [40], [41]. Advances in their development include modifying carbon, gold and platinum-based electrodes with a wide variety of nanomaterials to improve their electroanalytical properties [50], increasing the surface area/volume ratio, creating stable and favorable microenvironments for the maintenance of the analytical biomolecule's structure, reducing detection limits and response times and increasing the biosensors stability.

Electrochemical biosensors can be amperometric, potentiometric or impedimetric, depending on the technique for recording the response signal. The most common techniques to follow the performance of biosensors are cyclic voltammetry, chronoamperometry, and Electrochemical Impedance Spectroscopy (EIS) [46]. Amperometric biosensors measure the current from an electroactive species' oxidation or reduction processes in a biochemical reaction [51]. In chronoamperometry, a fixed potential is applied and the resultant current is measured upon a time, depending on the analyte diffusion to the electrode surface [51]–[53]. Although this technique is less selective presents a higher sensitivity for detecting redox reactions [52]. This type of sensor is mainly used in enzymatic sensors, in which the enzyme catalyzes the redox reaction. However, they have also been widely used in immunosensors, labeling the analyte or a secondary antibody with an enzyme or nanozyme to catalyze the redox reaction [51].

Among the most studied nanomaterials to modify electrodes, metallic nanoparticles, carbon nanotubes, graphene, metal oxide nanostructures and conductive polymers have been reported [54]. Although nanomaterials offer excellent benefits, they also present challenges related to the biocompatibility of some nanomaterials like metal- and semiconductor-derived nanomaterials and quantum dots. Other materials doped with dyes are harmful to the environment and degrade rapidly. Yet, nanomaterials have been developed with better biocompatibility and stability while maintaining their excellent electrochemical properties [55].

2.2.1. Nanomaterials in electrochemical biosensors

Nanomaterials are attractive in developing biosensors because they exhibit enhanced physicochemical properties concerning the corresponding bulk counterparts, classified according to their nanometer-sized dimensions. 0D materials have dimensions in the nanometer interval (1- 100 nm), e.g., nanoparticles, quantum dots, and fullerenes. 1D materials have one of their dimensions within the nanometric scale. In this group, we find nanotubes, nanofibers and nanowires. In comparison, 2D materials can be monolayers and thin films of, for example, graphene, nanosheets, phosphorene and molybdenum disulfide. The 3D materials can be polycrystals, composites, or nanomaterials dispersed in a matrix [56].

Among the most used materials for designing nanobiosensors are noble metals such as gold, silver and platinum since they have excellent conductivity and stability properties. Semiconductors such as indium and tin oxide have also been studied because they have good conductivity properties and are inexpensive. Other materials of great interest are those based on carbon, such as graphene and polymers, mainly as a flexible platform or for their optical transparency to be implemented in surface detection platforms combined with other more conductive materials [42], [57].

These nanomaterials confer to the biosensor improved properties such as stability, biocompatibility, selectivity, or enhanced optical, electrical, or catalytic properties [56]. Some examples of nanomaterials used in the development of biosensors are described in more detail as follows.

2.2.1.1. Magnetic beads (MBs)

Magnetic structures such as iron oxide nanoparticles in the form of magnetite (Fe_3O_4) or maghemite (γ-Fe_2O_3) offer significant advantages for pre-concentration of the analyte on the electrode surface by applying an external magnetic field and minimizing interferences from the sample matrix. Also, they can present a better signal/noise ratio and, when coated with other materials such as polymeric composites or ceramic matrices, maintain a high electron transfer capacity, improving biocompatibility and environmental stability [46]. There are currently different commercial references of magnetic particles on the market, with different coating materials, particle sizes, and superficial functional groups for linking a variety of

biomolecules, which broadens their range of applications, mainly in biosensors and macromolecules separation and purification [58]. Biosensors based on MBs have been demonstrated to detect pathogens such as bacteria, viruses, and disease biomarkers. Their high level of use in biosensors lies in their high capacity to separate the analyte of interest from complex samples containing many interferents and allow faster and more efficient washing processes in the manufacturing process, offering fast, low-cost and easy-to-implement detection [59].

2.2.1.2. Carbon quantum dots (CDs)

CDs have emerged as a new zero-dimensional nanomaterial with less than 10 nm diameter. They were first discovered in 2004 [60] and are mainly known for their unique fluorescence properties, with quantum confinement and crystal structure. [55]. They are derived from organic compounds [61] and differ from other nanomaterials by photoluminescence, high stability in aqueous solution, high biocompatibility, and high content of functional groups that can provide abundant binding sites to link specific bioreceptors by diverse straightforward and low-cost synthesis techniques. Additionally, they have rich and high surface areas offering fast electron conduction in the sensing interface, making them good candidates for developing electrochemical biosensors [55].

The carbon source can significantly influence the properties of the CDs, including the detection properties, since it has been reported that CDs made by the same method but from different precursors would have different selectivity, for example, different metal ions [60]. CDs properties may vary with size, morphology and type or amount of doping [61], having many oxygen-containing functional groups on their surfaces, such as carbonyl, hydroxyl, carboxylic acid, epoxy/ether [62]. CDs can be easily doped with elements such as S and N depending on the precursor carbon source. Doping CDs with heteroatoms can influence their intrinsic properties, including electronic, optics, local chemistry and surface reactivity. Doping with nitrogen improves dispersibility in water, decreases toxicity, and increases photostability and fluorescence at different pHs. [60]. Different heteroatoms and metallic elements such as N, S, O, B, Cl, Cu, Zn, Fe have been used, which affect their intrinsic properties by modifying the electronic structure [61], [62].

CDs can be synthesized by top-down and bottom-up techniques. The top-down approach starts from decomposing carbon feedstock such as carbon soot, carbon fiber, activated carbon, carbon black, graphene and CNTs, which go through laser ablation, arc discharge, electrochemical exfoliation or oxidized acidic treatment processes. However, these processes usually require high precision instruments and equipment, high temperature and energy consumption, which leads to high costs, and in most cases, the CDs obtained require an additional surface passivation step [55]. On the other hand, in the bottom-up approach, starting from small carbon-containing molecules such as citric acid, polyols, amino acids, synthetic polymers such as polyethylene glycol (PEG), and natural products such as carbohydrates, polysaccharides, biomass (orange juice, honey, walnut shells, silk, chitosan), these precursors are treated by pyrolysis, solvothermal- and hydrothermal-carbonization and microwave/ultrasonication [55].

CDs have been reported in storage, energy conversion and detection of ions and molecules, mainly in optical sensing formats and many other applications. For example, they have been reported to detect glucose, vitamin B12, trace metal elements in organisms and microRNA of cancer biomarkers. In addition, CDs incorporated in electrochemical biosensors have been reported to detect dopamine, alpha-fetoprotein, carcinoembryonic antigen and vitamin D2 [55]. And also for bioimaging, nanomedicine, photocatalysis and electrocatalysis applications [50]. Furthermore, they have been reported to be able to load drugs, prevent β-amyloid aggregation for the treatment of Alzheimer's disease, hepatitis control, and promote wound healing. They also have high antimicrobial activity by generating reactive oxygen species (ROS) that trigger oxidative stress, functioning as radiosensitizers in cancer therapy [63].

Different nanocomposites based on CDs have been reported as electrochemical sensors. For instance, CDs with AuNPs and AgNPs have demonstrated increasing the chemical reactivity and decreasing the oxidation potential of metallic nanoparticles with low chemical reactivity and high oxidation potentials, providing excellent electronic, optical, catalytic and analytical properties with high stability and reproducibility [54]. Pd-Au @CDs nanocomposites have also been reported to detect colitoxin DNA, with excellent electrochemical properties [64] and an α-MnO2/GQD nanocomposite for quantifying glucose and L-tyrosine and detecting diabetes and diabetic foot ulcer using a micro-fluidic platform [65]. In addition, au-

GQDs@AgPt nanostructures have been designed as an electrocatalytic agent for methanol oxidation [66].

2.2.1.3. Conductive polymers

Conductive polymers are incorporated in biosensing platforms as they enhance the analytical characteristics of biosensors, such as electrochemical activity, electrical conductivity, mechanical elasticity, surface area, biocompatibility and environmental stability [67]. Among the most widely used conductive polymers in biosensor research are polypyrrole (Ppy), polyaniline (PANI), polythiophene (PTH) and poly(3,4-ethylenedioxythiophene) (PEDOT), with exceptional properties that extend their applicability in the design of rechargeable batteries, coatings that prevent corrosion, electromagnetic shielding, solar cells, and superconductors [68].

Most reported synthesis strategies are based on polymers' chemical, electrochemical, and biochemical formation. Chemical synthesis is based on strong oxidizing compounds such as $FeCl_3$ or H_2O_2 to form very pure conductive polymer particles. Enzymatic synthesis is based on "green" reactions by applying oxidoreductases or redox compounds formed by enzymes to generate conductive polymers. Microbiological synthesis has also been reported, in which microorganisms are used to form the polymers while retaining their activity during the life cycle compared to enzymes. Electrochemical deposition is widely used due to the low solubility of conductive polymers in most solvents. It allows the deposition of conductive layers directly on the electrodes, adapting their electrochemical properties by varying the monomer concentration, pH and dopant concentration, and their morphological and thickness properties by varying the pH and potential profile [68]. These polymers have also been used to develop molecularly imprinted polymer (MIP)-based biosensors that use the target as a template, do not require bioreceptors for analyte detection and have been designed mainly from methacrylic acid, acrylamide and acrylic acid [68].

Within the immunosensors, hybrids with Ppy and gold have been investigated to detect human IgG, and Ppy has also been modified with ZnS nanocrystals to detect C-reactive protein [67].

2.2.1.4. Noble metals and metal oxides

Noble metals have been commonly incorporated in biosensing formats due to their simplicity, physicochemical malleability and high surface area. Most of their properties depend on sizes, such as quantum confinement and surface plasmon resonance. Silver and gold are the most widely studied, mainly in molecular diagnostic, imaging, drug delivery and therapeutic applications. They have been synthesized by different methods, including chemical reduction, photochemical reduction, coprecipitation, thermal decomposition, hydrolysis, and physical methods such as vapor deposition, laser ablation and milling [69].

Nanostructured iron oxides have been of interest as immobilizing matrices. Zinc, iron, cerium, tin, zirconium, titanium and magnesium oxides exhibit nano morphological, biocompatible, non-toxic and catalytic properties and offer improved electron transfer kinetics and strong adsorption capacity in biosensors. Nanostructures have been synthesized by different techniques depending on the desired morphology, such as soft templating to prepare nanorods and nanofibers, sol-gel and radiofrequency sputtering methods for ordered rough nanostructures, and hydrothermal deposition for shape-controlled nanoparticles [70].

In general, metal nanoparticles act as immobilizing platforms, accelerating electron transfer and catalysis. In electrochemical biosensors, metal nanoparticles have been used as labels or to increase the loading of electroactive species [37].

2.2.2. Characterization

The unique and enhanced properties of nanomaterials can be tested by comprehensive characterization, which is currently possible thanks to several highly reliable and sensitive techniques [71]. Size, shape, composition, surface charge, optical, magnetic and electrical characteristics are some of the most studied [72], as they promote understanding of their properties, broadening the range of possible applications. The following describes some of the most interest characterization techniques, classifying them according to properties.

2.2.2.1. Size, shape and morphology

Size, shape and aggregation state are of great relevance in determining the physicochemical properties of nanomaterials [73]. Several techniques allow a complete visualization and analysis of their morphology. Electron microscopy allows one to observe the nanostructures

with atomic resolution because it uses electrons instead of photons, which have a shorter wavelength [73]. For example, scanning electron microscopy (SEM) allows microstructure and nanostructure analysis of the sample surface's composition, topography, morphology, and crystallographic information from high-resolution images. [72]. Besides that, Transmission Electron Microscopy (TEM) also allows us to observe the sample's internal structure and crystallographic profile [72]. Another microscopy technique widely used in the characterization of nanomaterials is atomic force microscopy (AFM), in which a cantilever scans the surface of the sample, obtaining information on the 3D topography of the surface, depending on the interaction force in the tip-sample atoms [72], [73].

To characterize the size of nanoparticles in suspension, dynamic light scattering (DLS) measures the frequency of light scattering dependent on the Brownian motion of the nanoparticles [74]. This motion varies with particle size, i.e., smaller nanoparticles move faster than larger particles [71]. This technique provides information on nanoparticles' hydrodynamic size, size distribution, and aggregation state in a short time and with high sensitivity [72].

2.2.2.2. Composition

The chemical composition and structure of nanomaterials can be analyzed by techniques such as Energy Dispersive X-Ray Spectroscopy (EDS), which is a complementary technique to SEM, allowing the identification and quantification of the elemental composition of the sample since each element has an atomic structure that emits characteristic x-rays after being excited by an electron beam [75]. Thermal analysis techniques such as thermogravimetric analysis (TGA) or differential scanning calorimetry (DSC) have also been used for composition characterization. TGA analyzes the change in the weight of the sample upon time and temperature, which allows knowing the sample's composition and evaluating its thermal stability, the moisture content and volatile components, and the oxidation and reduction products [75], [76]. DSC measures the difference in heat flux between the sample and a reference, allowing qualitative and quantitative information to be obtained on the physical and chemical changes in the sample's endothermic or exothermic processes. In addition, it provides quantitative information on amorphous and crystalline phases and analysis of the presence of nanoparticles and the influence of nanofillers [75], [77].

Fourier transform infrared spectroscopy (FTIR) allows the characterization of the nanomaterial structure at the molecular scale, providing information on the chemical composition, bond arrangement, crystallinity and molecular tension, thanks to the vibrational motions of the components and their bonds induced by infrared radiation [78].

2.2.2.3. Surface charge

Surface charge is highly related to nanoparticles' dispersion stability and aggregation state. Particles with high surface charge, negative or positive, tend to repel each other, generating a stable colloidal dispersion, while nanoparticles with low surface charge attract each other, causing them to agglomerate and lose stability [71]. This property can be determined by the zeta potential, which is the charge on the surface of the electric double layer, which depends on the surface chemistry, concentration, particle size and ionic strength [79]. The zeta potential can be analyzed by electrophoretic light scattering (ELS) by measuring the movement of nanoparticles in the presence of an electric field, which is related to the surface charge of the nanomaterials. It also serves to evaluate the presence of coatings and stability upon the pH of the medium [80].

2.2.2.4. Optical properties

The optical properties of nanomaterials are sensitive to size, shape, agglomeration state and concentration and can provide information on the size, shape and surface properties of nanostructures in suspension. The most commonly used techniques to characterize the optical properties of nanoparticles are ultraviolet-visible spectroscopy (UV-Vis) and fluorescence spectroscopy. UV-Vis spectroscopy measures the light absorbed by the sample, which provides information on the size, oxidation state, and shape of metallic nanoparticles and the concentration of compounds and nanomaterials, dependent on the sample's absorbance following the Beer-Lambert law [71], [72].

Fluorescence spectroscopy allows the characterization of fluorescence dyes, fluorophores and fluorescent nanomaterials, such as quantum dots (QDs), by measuring the photons emitted by the sample as it moves from an excited electronic state to a quiescent state. In

addition, the fluorescence intensity can provide information on the concentration of the compound or surface modification of nanomaterials [71], [72].

2.2.2.5. Electrochemical

Electrochemistry allows nanomaterials to be fabricated and characterized, analyzing their corrosion mechanisms, catalytic properties and electron transfer capabilities. The most commonly used electrochemical techniques are cyclic voltammetry (CV), differential pulse voltammetry (DPV), EIS and chronoamperometry. These and other techniques allow the analysis of chemical properties of the electrode/solution interface, which can be current, potential or impedance, etc [81].

CV allows the analysis of the mechanisms of redox reactions, the reversibility of a reaction and the kinetics of electron transfer by measuring the resulting current when sweeping a cyclic potential window [81]. EIS evaluates the electron transfer properties and chemical transformation at the electrode/solution interface, which depend on the electrolyte's ohmic resistance, the double layer's resistance and charge transfer resistance [81]. Chronoamperometry records the current resulting from oxidoreduction processes of electroactive species at the electrode surface upon time after applying a fixed potential [51]. It can be selective by adequately selecting the working potential and enjoys high sensitivity and simplicity [52]. Therefore, chronoamperometry is the preferred technique to follow electrochemical reactions and catalytic processes on nanomaterial-based electrodes once the electrochemical process has been well-characterized by other electrochemical techniques.

2.3. Biosensors for SARS-CoV-2

In the last two years, different strategies have been investigated to detect SARS-CoV-2, desirable at the point of care in a rapid and ultrasensitive manner. Among the electrochemical biosensors, Seo et. al. [82] developed a field-effect transistor (FET)-based biosensor device to detect the S protein of the SARS-CoV-2 within months of the onset of the pandemic. After applying an input voltage, FET-based biosensors translated the biological signal into an electrical signal generated in a channel. The channel was coated with graphene sheets due to its high electrical conductivity, high carrier mobility, large surface area, and a captured antibody that interacted specifically with S protein immobilized on the graphene sheets. The

output signal was measured from FET transfer (current-voltage (I-V) curves), showing a limit of detection (LOD) of 1 fg/mL in phosphate-buffered saline and 2.42 x 10^2 copies/ mL in culture medium and patient samples, with the great advantage of being adaptable for the diagnosis of other emerging diseases.

Vadlamani et. al. [83] developed an electrochemical biosensor based on TiO_2 nanotubes functionalized with cobalt (Co), making it inexpensive, simple, cost-effective and highly sensitive. The detection was based on forming a Co-S protein complex at a specific bias voltage due to Co ions' reduction and S protein oxidation. This biosensor was designed to detect the RBD from protein S by amperometry with LOD of 12 nM, within a broad linear detection region and in only 30 s.

Fabiani et. al. [84] developed an electrochemical immunoassay to detect virus S and N proteins in saliva, using magnetic beads modified with an IgG anti-mouse as a carrier to immobilize a monoclonal capture antibody. A polyclonal antibody coupled to a secondary antibody conjugated with alkaline phosphatase was used to produce the signal. Detection was performed on screen-printed electrodes modified with carbon black nanomaterial by DPV using a portable potentiostat. The biosensor detected virus S and N proteins in buffer solution and saliva with LOD of 19 ng/mL and 8 ng/mL, respectively, in only 30 min, so they considered it to have great potential for commercialization. However, studies are required to improve the signal-to-noise ratio of the device.

Zhao et. al. [85] designed an electrochemical biosensor based on calixarene-functionalized graphene oxide and an Au@Fe_3O_4 nanocomposite to detect SARS-CoV-2 genetic material using a supersandwich strategy (capture probe coupled to Au@ Fe_3O_4 and the signal probe coupled to the functionalized graphene oxide) by DPV. This biosensor demonstrated high specificity and selectivity *in silico* tests and real samples with 200 copies/mL LOD. Moreover, this biosensor was integrated with a smartphone for point-of-care analysis of the results.

Torrente et. al [86] developed a low-cost, portable and wireless multiplexed biosensor platform that enabled the rapid and ultra-sensitive detection of three COVID-19-specific biomolecules. The device determined not only viral antigen nucleocapsid protein (indicative of viral infection) and IgG and IgM antibodies (immune response) that provide information on disease stage, but also C-reactive protein as an indicator of disease severity. Bioreceptors

were immobilized on laser-etched graphene electrodes and measured by DPV and open-circuit (OPC)-EIS. Blood and saliva samples were analyzed, showing a highly selective and rapid response, between 1 and 10 min in relevant physiological ranges.

Idili et. al [87] developed an aptamer-based electrochemical sensor that detected SARS-CoV-2 S protein rapidly, specifically, sensitively and reagent-free. The sensor response was produced by a conformational change induced by the binding of the modified aptamer to a methylene blue derivative immobilized on a gold electrode surface. This response was so fast that it could recognize the target in a single step and 15 s, within a range of S protein concentrations from 760 pg/mL to 76 ng/mL.

Among optical biosensors, Ahmadivand et. al. [88] designed a toroidal plasmonic metasensor to diagnose COVID-19, with the ability to harness electromagnetic fields in frequency, time and space at the same time. This biosensor had gold nanoparticles functionalized with an antibody specific to the SARS-CoV-2 S protein, whose response measured by toroidal resonance had a LOD of 4.2 fmol. Although they did not evaluate its performance on patient samples, the researchers highlighted the usability of the highly sensitive and highly accurate miniaturized device, which detected the SARS-CoV-2 protein in very diluted solutions and approximately 80 min.

Funari et. al. [89] developed a biosensor based on localized surface plasmon resonance using an opto-microfluidic sensing platform modified with gold nanoprobes to detect the presence and concentration of SARS-CoV-2 S protein with sample volumes of only 1 µL and in as little as 30 min. This label-free platform achieved a LOD of 0.08 ng/mL and the authors indicated its potential use as a promising tool for easy, inexpensive and rapid point-of-care detection of S protein.

Finally, within a few examples, Moitra et. al. [90] developed a colorimetric assay based on gold nanoparticles functionalized with antisense oligonucleotides modified with a thiol group, specifically designed for the N gene or also called SARS-CoV-2 nucleocapsid phosphoprotein. Detection was performed by optical methods, by changes in surface plasmon resonance in response to interaction with the analyte. The biosensor allowed the detection of isolated RNA with a detection limit of 0.18 ng/mL and in only 10 min.

Although significant advances have been made in this area, only a few biosensors have been reported for SARS-CoV-2, as summarized in Table 1. Only one biosensor for detecting this virus has been reported in Colombia [91].

Table 1. Biosensors designed for the detection of SARS-CoV-2.

	PLATFORM	***ANALITE***	***LIMIT OF DETECTION***	***REF***
Electrochemical	SPCE + pABA	S protein	1.065 fg / mL	[91]
	Graphene + FET	S protein	1 fg/mL	[82]
	TiO_2 nanotubes	S protein	0.7 nM	[83]
	Electrode + PFDT	S protein	38.6 copies/mL	[92]
	Graphene electrode	S protein	260 nM	[93]
	Electrode + DNA-antibody complex	S protein	1 pg/mL	[94]
	GCE-Pd-Au nanosheet + Magnetic beads	S protein	0.0072 ng/mL	[95]
	SPE – Cu_2O	S protein	0.04 fg/mL	[96]
	In_2O_3/ZnO transistors	S protein	865×10^{-18} M	[97]
	Au-TFME + MIP	S protein	4.8 pg/ml	[98]
	Capacitive interdigitated electrode + L Cysteine	S protein	750 pg / μL / mm^2	[99]
	SPCE + MBs + AuNPs	S protein	0.35 ag/mL	[100]
	Interdigitated Au electrode + carboxymethyl chitosan	S protein	0.179 fg/mL	[101]
	FTO - AuNPs	S protein	0.63 fM	[102]
	Glucometer	S and N protein	0.71 pM (N), 0.34 pM (S)	[103]
	FET- SWCNT	S and N protein	0.55 fg/mL (S), 0.016 fg/mL (N)	[104]
	MBs + SPE	S and N protein	19 ng/mL (S), 8 ng/mL (N)	[84]
	MIP – Au electrode	N protein	15 fM	[105]
	microelectrode array, microfluidic	N protein	3.16 fg/mL	[106]
	PI, Graphene	N protein, CRP, IgG e IgM	Depends on the biomolecule	[86]
	SPE-GO-AuNPs	Virus glycoproteins	1.68×10^{-22} μg/mL	[107]
	CNT/WO_3 -MIP	Viral particle	57 pg/mL	[108]
	AuNPs- ssDNA	RNA	6.9 copies/ μL	[109]

	CPE-Chitosan	RNA	0.3 pM	[110]
	SPE-RGO-TB + $Au@Fe_3O_4$	RNA	200 copies/mL	[85]
Optical	SWCNTs-Fluorescence	S protein	35 mg/L	[111]
	Plasmonic Metasensor	S protein	4.2 fmol	[88]
	Colorimetric - AuNPs	S, E and M protein	36.5 copies/mL	[112]
	Thermoplasmonic	RNA	0.22 pM	[113]
	AuNPs – SERS, fluorescence, colorimetric	RNA	160 fM	[114]
	LSPR- AuNPs	RNA	6.9 copies / μL	[90]
	SiO_2 @Ag Microfluidic-SERS	IgG, IgM	$1/1.28 \times 10^7$	[115]
	Opto-microfluidics, nanospikes	IgG, IgM	0.5 pM (0.08 ng/mL)	[89]
	Colorimetric - Magnetic particles	IgG - IgM		[116]
	Microfluidics-fluorescence	IgG, IgM		[117]
Of paper	Chemiluminescent	S protein	0.1 ng/mL	[118]
	Electrochemical paper	IgG-IgM	1 ng/mL	[119]
	AuNPs - colorimetric	IL -6	1.3 pg/mL	[120]

SPCE, screen-printed carbon electrode; pABA, p-Aminobenzoic acid; FET, field-effect transistor; PFDT, perfluorodecanethiol; GCE, glassy carbon electrode; SPE, screen-printed electrode; TFME, thin-film metal electrode; MIP, molecularly imprinted polymer; MBs, magnetic beads; AuNPs, gold nanoparticles; FTO, fluorinated tin oxide; SWCNT, Single-walled carbon nanotube; PI, polyimide; GO, graphene oxide; CNT, carbon nanotube; WO_3, tungsten oxide; CPE: carbon paste electrode; RGO, reduced graphene oxide; SERS, surface-enhanced raman scattering; LSPR, localized surface plasmon resonance.

CHAPTER III: Assembly, analytical characterization and performance of the immunosensor

Abstract

A rapid, straightforward, and massive diagnosis of COVID-19 is one of the more important measures to mitigate the current pandemics. This work reports on an immunosensor to rapidly detect the spike protein from the severe acute respiratory syndrome coronavirus 2 (SARS-CoV-2). The immunosensing device entraps the spike protein linked to angiotensin-converting enzyme host receptor (ACE2) protein in a sandwich arrangement between carboxylated magnetic beads functionalized with an anti-spike antibody and an anti-ACE2 antibody, further labeled with streptavidin (poly)horseradish peroxidase (HRP) reporter enzyme. The particles were confined at the surface of screen-printed gold electrodes, whose signal resulting from the interaction of the enzyme with a mediator was recorded in a portable potentiostat. The immunosensor showed a sensitivity of 0.83 µA*mL/µg and a limit of detection of 22.5 ng/mL of spike protein, with high reproducibility. As a proof-of-concept, it detected commercial spike protein-supplemented buffer solutions, pseudovirions, isolated viral particles and ten nasopharyngeal swab samples from infected patients compared to samples from three healthy individuals paving the way to detect the virus closer to the patient.

KEYWORDS: SARS-CoV-2, spike protein, ACE2, immunosensor, coronavirus, magnetic beads.

1. Introduction

COVID-19, caused by SARS-CoV-2, is an infectious disease [21] with severe symptoms (mainly respiratory failure) that may lead to death, affecting people worldwide regardless of race or gender, age, or social status. [5].

The SARS-CoV-2 structure consists of its genome that is a single strand +RNA of 29903 nucleotides [121], and of a cellular-derived bilipid membrane and a set of the structural proteins spike (S), membrane (M), envelope (E) and nucleocapsid (N). The M, E and S

proteins are located on the virion's envelope, and the N protein is associated with the viral genome. Protein S is a highly N-glycosylated 180 KDa trimeric class I fusion glycoprotein that consists of two subunits known as S1 and S2 [18],[22] and is responsible for binding to the ACE2 protein in the cell membrane. The receptor-binding domain (RBD) with the S1 subunit is responsible for interaction with the ACE2 receptor, while the S2 subunit facilitates virus-cell membrane fusion and forms the spike stem [21],[22],[8],[12]. The RBD region of the SARS-CoV-2 binds to the ACE2 receptor with a 10-20 fold higher affinity than SARS-CoV, which facilitates viral entry and provides an explanation for the easiness of virus spread from person to person [26],[122], thereby generating significant concern throughout the whole world population.

Rapid, simple and specific detection of the virus is paramount to decreasing its speed of spread. Standard diagnostics are time-consuming and have highly qualified personnel and specialized equipment requirements. Biosensor-based devices are amenable to miniaturization and integration into portable analysis systems using minimal volumes of reagents and samples for fast and user-friendly assays [123]. Electrochemical biosensors are the most extended. A complete characterization of the electrochemical process at an electrode surface is achieved readily by electrochemical techniques. Chronoamperometry can be specific by adequately selecting the working potential and enjoys high sensitivity and simplicity [51], [52]; therefore, it is the preferred technique to follow electrochemical reactions once the electrochemical process has been well-characterized. Outstanding features of biosensors have been used in the detection of bacterial pathogens [124], infections [125], cancer biomarkers [15],[16], autoimmune diseases [128] and virus identification [18],[19], including SARS-CoV-2 immunosensors [83],[92],[93],[94],[96], [103],[104],[131],[132],[133],[134],[135],[136], and genosensors [85],[109],[110],[137], being up-and-coming detection tools that promise to solve diagnosis limitations in this and coming pandemics [138].

Here, we report an electrochemical immunosensor for the straightforward detection of the spike protein from SARS-CoV-2. This is the first sandwich-type assay based on an anti-spike antibody immobilized on carboxylated MBs that capture the spike-ACE2 complex. The immunocomplex is further linked to a biotinylated anti-ACE2 antibody and an enzymatic system based on streptavidin (poly)HRP for amplification and reading. All variables involved

in the immunosensor development were rapidly screened by spectrophotometry. The analytical performance was finally evaluated by chronoamperometry using commercial solutions of spike protein, SARS-CoV-2 pseudovirions, and SARS-CoV-2 viral particles obtained from cell culture isolation and nasopharyngeal swabs samples from infected patients. Overall, the approach rapidly and straightforwardly detected the spike protein, offering opportunities to detect SARS-CoV-2 closer to the patient in remote settings and minimizing people and samples displacement and thus virus spreading.

2. Experimental

2.1. Reagents and solutions

Dynabeads™ MyOne™ carboxylic acid (Ref. 65011) and Pierce™BCA Protein Assay Kit (Ref. 23225) were obtained from Thermo Fisher Scientific. SARS-CoV-2 (2019-nCoV) spike antibody, Rabbit PAb (Ref. 40591-T62); SARS-CoV-2 (2019-nCoV) spike S1-His Recombinant Protein (Ref. 40591-V08H) and ACE2 Protein, Human, Recombinant (Ref. 10108-H05H) were obtained from Sino Biological. Human ACE2 Biotinylated Antibody (Ref. BAF933) was obtained from R&D systems. Streptavidin-HRP conjugate (Ref. OR3L-200UG) and soluble TMB (Ref. 613544-100ML) were obtained from Merck. N-(3-dimethylaminopropyl)-N'-ethylcarbodiimide hydrochloride (EDC) (Ref. E6383-5G), N-Hydroxysuccinimide (NHS) (Ref. 130672-5G) and 2-(N-morpholino) ethanesulfonic acid sodium salt (MES) were purchased from Sigma-Aldrich. Streptavidin-poly-HRP-20 (Ref. 85R-200) and streptavidin-poly-HRP-80 (Ref. 65R-S105PHRP) were obtained from Fitzgerald. SARS-CoV-2 (COVID-19) spike antibody (Ref. GTX135356) was obtained from GeneTex. SARS-CoV-2 spike antibodies (Ref. AM038105, AM002414, AM043105, AM001414 and AM009105) were obtained from Active Motif. Potassium hydrogen phosphate (K_2HPO_4) and disodium hydrogen phosphate (Na_2HPO_4) were acquired from PanReac AppliChem. Potassium dihydrogen phosphate (KH_2PO_4), potassium chloride (KCl) and sodium chloride (NaCl) were obtained from J.T.Baker®. Sulphuric acid (H_2SO_4) was purchased from Honeywell FlukaTM. RT-qPCR commercial kit (Maxima SyBR Green/Rox qPCR master mix, Thermo Scientific), HEK-293 cell line (Ref. CRL-1573) and Vero-E6 cells were kindly donated by the Immunovirology Group from the University of Antioquia. Miniprep (250 reactions) (Ref. FAPDE 300) was purchased in Favorgen and linear

polyethyleneimine (PEI), MW 25000, transfection grade was obtained from Polysciences. 50 mm Tris–HCl (pH 7.4), 100 mm NaCl, 0.1 mm EDTA (TNE buffer) was prepared.
20 mM MES buffer pH 6.5 was used to activate MBs and conjugate anti-spike antibodies. 0.15 M PBS buffer 1X pH 7.4 (PBS) was used to conjugate the spike-ACE2 complex and anti-ACE2 antibodies, and 0. 15 M buffer PBS 1X pH 7.4 with 0.05% Tween 20 (PBST) for each of the washing steps. 0.15 M buffer PBS 1X pH 7.4 with 0.05% Tween 20 and 1% casein (PBST-C) was used to block the particles after anti-spike conjugation and conjugation of the streptavidin-(poly) HRP 80 enzyme complex. 15 M buffer PBS 1X pH 7.4 with 0.05% Tween 20 and 1% BSA (PBST-B) was used for blocking the particles after anti-spike conjugation and for conjugation of the streptavidin-HRP and streptavidin-(poly) HRP 20 enzyme complex. ChemCruz Radioimmunoprecipitation lysis buffer (RIPA, Ref. sc-24948) with 1% phenylmethylsulfonyl fluoride (PMSF), 1% sodium orthovanadate and 2% protease inhibitor cocktail were used for lysing viral particles and samples.

2.2. Apparatus and chips

The electrochemical measurements were performed with a three-electrode cell configuration SPAuE (Ref. 220BT, from DropSens) in a PalmSens4 potentiostat with a PS Trace software analyzer and a Sensit Smart smartphone workstation. The chips consist of a 4 mm gold working electrode, a gold counter electrode, and a silver pseudo-reference electrode printed on the same strip.

2.3. Production of pseudovirions

Pseudovirions were assembled by co-transfection of HEK-293 cells with three plasmids: murine leukemia virus (MLV)-Gag-Pol encoding the Gag and Pol proteins of MLV, luciferase plasmid encoding the luciferase reporter gene, the packaging signal and the 5'/3' long repetitive sequences of MLV and SARS-CoV-2 S plasmid encoding the spike protein of SARS-CoV-2, which were donated by Gary Whittaker at Cornell University, USA. HEK-293 cells were seeded in a 6-well plate, 800000 cells per well, and incubated at 37 ºC and 5% CO_2 overnight. Co-transfection was achieved using 800 ng of SARS 2 S plasmid, 600 ng of MLV-Gag-Pol plasmid and 600 ng of luciferase plasmid per well in the presence of 1 g/L PEI. Then culture medium was added and the cells were incubated at 37 °C and 5% CO_2 for 72 h and the supernatant of the transfected cells was collected and stored in aliquots previous

centrifugation at 25000 rpm and filtration with a 0.45 μm filter [139]. Following the same protocol, pseudovirions expressing the spike protein of MERS-CoV, SARS-CoV and the glycoprotein of the vesicular stomatitis virus (VSV) were obtained as controls to evaluate the biosensor's specificity using a MERS-CoV S, SARS-CoV S and VSV plasmid, respectively.

2.4. Characterization of pseudovirions

The infectivity of pseudovirions was assessed by Vero-E6 cell transduction using 10-fold serial dilutions of the supernatant obtained from cotransfected HEK-293. Luciferase activity was determined at 72 h after transduction, and the expression level was quantified using a commercial kit (Promega) after cell lysis. The luminescence signal was determined by each dilution, evaluated by triplicate, using a Varioskan. In addition, pseudovirions were quantified in copies/ml by RT-qPCR using the primers CTCACTGAGACTACATCAGC and TCCAGATCCACAACCTTCGC and a commercial kit (Maxima SyBR Green/Rox qPCR master mix, Thermo Scientific), previous RNA extraction. Besides, Spike protein expression was demonstrated in transfected HEK-293 cells by western blot using polyclonal anti-SARS-CoV-2 Spike antibody and HRP-conjugated secondary antibody.

2.5. Assembly of the immunosensor

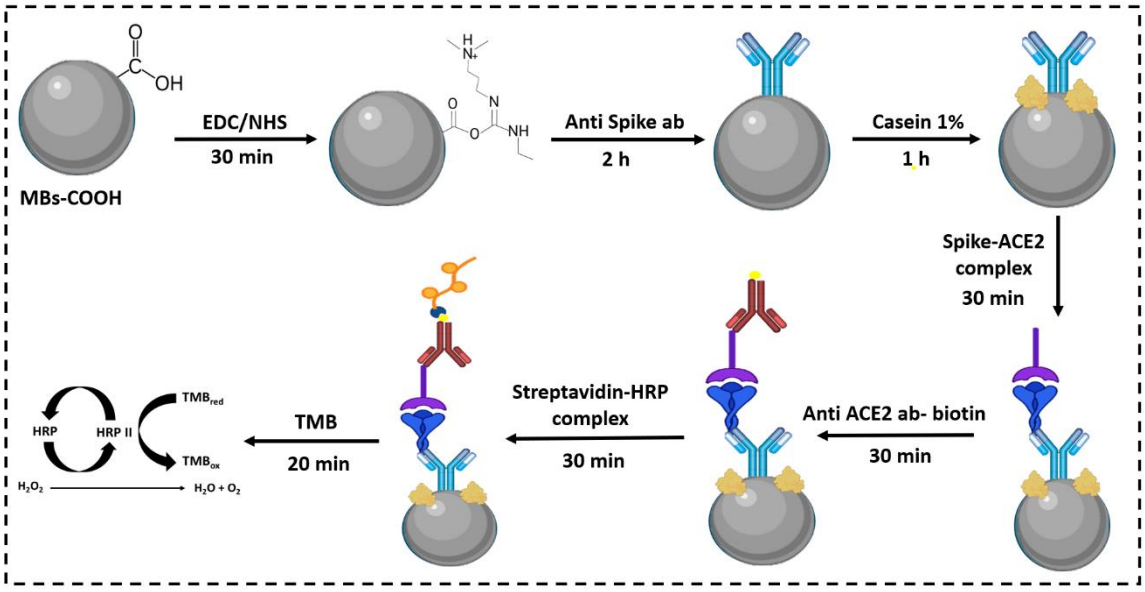

Figure 3. Methodology of assembly of immunosensor

As shown in Figure 3, 1 mL of carboxylated MBs was functionalized with an anti-spike antibody by transferring 40 µL of commercial MBs to a 1.5 mL vial, washing twice with 1 mL of MES, placing the vial in a magnetic rack for 2 min and removing the supernatant. Subsequently, the carboxylated MBs were activated with 15.4 mg of EDC (400 mM) and 2.2 mg of NHS (100 mM) dissolved in 200 µL of MES for 30 minutes at room temperature under 1000 rpm constant stirring. After removing the supernatant, the activated MBs were incubated with 200 µL of 12 µg/mL anti-spike solution in MES for 2 h at room temperature under constant stirring. The antibody-coated MBs were washed thrice with 1 mL of PBST and resuspended in 1 mL PBS. For each sensor, 50 µL of functionalized particles were transferred to a 1.5 mL vial and removed the supernatant. 50 µL of PBST-C was added as a blockage agent, incubated for 1 h at 37°C and washed with 200 µL of PBST.

Separately, 0.1-2 µg/mL of commercial spike protein and 2 µg/mL ACE2 protein were mixed in a total volume of 50 µL of PBS and incubated at 37°C for 45 minutes under stirring. On the other hand, 1 µL of inactivated viral particles at $1x10^{11}$ copies/mL were diluted in 99 µL RIPA, vortexed for 1.5 min and sonicated in a sonication bath for 1 min. Dilutions of viral particles were prepared from 1 $x10^{7}$ to 1 $x10^{5}$ copies/mL. Subsequently, 25 µL of diluted viral particles were mixed with 2 µg/mL ACE2 protein and completed the volume up to 50 µL with PBS. In either case, all the Spike-containing solution volume was added to the antibody-coated MBs button and incubated for 30 min at 37°C under constant stirring, followed by washing twice with 200 µL of PBST. The captured spike-ACE2 complex was incubated with 50 µL of 2 µg/mL anti-ACE2-biotin in PBS for 30 minutes at 37°C under stirring and washed thrice with PBST. 50 µL of 50 ng/mL of streptavidin(poly) HRP in PBST-C were later incubated for 30 minutes at 37°C, followed by five washing steps with PBST and finally, the immunocomplex was resuspended in 10 µL of PBST. The total immunosensor assembly time was approximately 90 min; once MBs were modified with the anti-spike antibody and blocked, the stock solution was stable for 20 days at 4°C.

2.6. Characterization of surface coverage

The amount of anti-spike antibodies at the surface of the MBs was calculated indirectly, i.e., estimating the one in the supernatant. For this purpose, 25 µL of the supernatant was added to a 96-well plate, and 200 µL of BCA working reagent was added, incubated at 37°C for 30

min and after cooling to room temperature, the absorbance was measured at 562 nm. In addition, known concentrations of anti-spike antibodies were assessed to calculate the antibody concentration from a calibration curve.

2.7. Electrochemical measurements

For the electrochemical reading, the SPAuE was activated by CV in 0.1 M sulfuric acid from 1.6 to - 0.2 V at 0.05 V/s scan rate for 11 consecutive cycles (when the peak reached about -1.5 V). A baseline was established with only TMB commercial solution containing H_2O_2. The immunocomplex was then confined at the working electrode, placing a magnet behind it. After removing the supernatant, 50 µL of TMB was added and the resultant current was measured by chronoamperometry at a potential of -150 mV for 65 s.

2.8. Measurement of pseudovirions and viral particles

Viral particles were isolated after culturing a nasopharyngeal swab sample from an infected patient donated by the Immunovirology Group from the University of Antioquia following established biosafety and ethical standards in a biosafety level (BSL)-3 facility. The viral particles were inactivated by ultraviolet (UV)-light exposure for 30 min with a 6-watt power lamp.

Both pseudovirions and viral particles were diluted to a concentration of $1x10^6$ copies/mL in RIPA buffer, then vortexed for 1 min and 30 s and sonicated for 1 min. The respective concentrations from this stock solution were achieved by diluting in PBS buffer before being tested. It is important to note that diluting the pseudovirions or viral particles is not necessary. The starting stock solution was $10.6x10^8$ copies/mL and $4.3x10^7$ copies/mL, respectively. Following the established protocol in which a previous incubation with the ACE2 protein is performed and maintaining the conditions of standardized volumes, the maximum concentration of $1x10^6$ copies/mL was used as a starting point, followed by serial dilutions in PBS buffer to obtain the calibration curve.

2.9. Measurement of patient samples

The Tropical Diseases Study and Control Program (PECET-by its Spanish acronym) laboratory from the Universidad de Antioquia kindly donated nasopharyngeal swab samples.

For analysis by RT-PCR in a BSL-2 facility following established ethical and biosafety standards, they were inactivated by UV light and the RT-PCR protocol briefly described below was followed.

Samples obtained by nasopharyngeal swabs were immediately deposited in a transport medium, followed by RNA extraction from 200-300 µL samples on the same day. The extraction was done by extraction using the kingFisher Flex robot and the MagMAXTM Viral/Pathogen II (MVP II) Nucleic Acid Isolation kit (Thermo Fisher) or using manual extraction with the Quick RNA Viral Kit (Zymo Research). The amplification reaction was done using the Berlin protocol, with some modifications. For this, the Luna® Universal Probe One-Step RT-qPCR Kit (New England BioRad) was used following the manufacturer's instructions. Primers were used to detect the E gene and primers and a probe for the Human RNAsaP gene were also used as control. Some borderline positivity samples were confirmed by amplifying the N gene described in the Berlin protocol or the GeneFinder™ COVID-19 Plus RealAmp Kit (OSANG Healthcare Co., Ltd, Korea). The primers, probes and the respective concentrations used for the Berlin protocol are in the following reference [140]. Additionally, a negative control was included in all runs in which water was added to replace the sample. The RT-PCR reactions were performed in a BioRad, CFX96 thermal cycler using 55 °C for 10 min for reverse transcription, followed by 95 °C for 3 min and then 45 cycles at 95 °C for 15 s and 58 °C for 30 s. Extracts were frozen at -80 ºC until use.

For testing the samples with the immunosensor, the nasopharyngeal swabs non-inactivated were progressively thawed and lysed in RIPA buffer at 1/10 dilution by vortexing for 1 minute and 30 s, followed by sonication for 1 min. All sample assays were performed in a BSL-2 laboratory following established biosafety and ethical standards.

2.10. Statistical analysis

Statistical analysis on the specificity of results and evaluation of patient samples used R studio software. Data were analyzed using the variance method (ANOVA) and the samples were compared using the least significant difference (LSD) and Tukey methods with a confidence level 95 %. *** indicates a significance level *p* less than 0.001, ** values between 0.001 and 0.01, * values between 0.01 and 0.05; and - values greater than 0.05.

3. Results and discussion

3.1. Optimization of the immunosensor

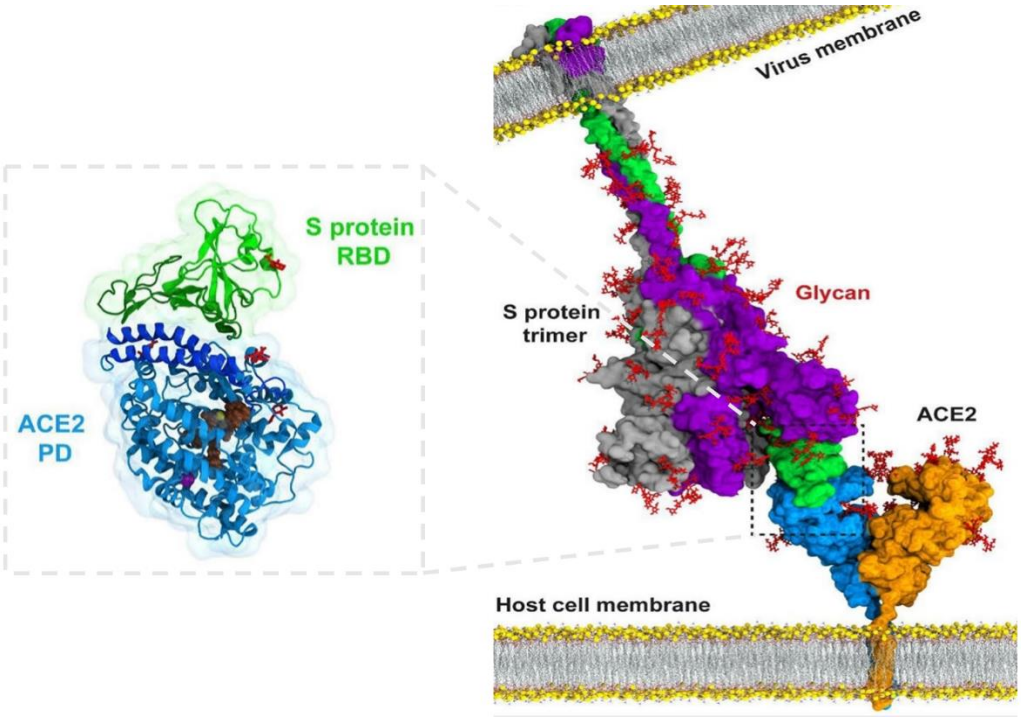

Figure 4. ACE2-Spike proteins interaction [141]

Spike protein is repeated 50-200 times on the viral surface [142] and consists of approximately 1273 amino acids [143], of which around 200 correspond to the RBD region (amino acid residues 331-524) located in the S1 subunit of the protein [144]. ACE2 is a protein of 805 amino acids formed by the N-terminal peptidase and the C-terminal choleric domains. The peptidase domain is the one that binds tightly to the RBD fragment of the spike protein (see Figure 4) [3],[40] and this interaction occurs with a 10-20 fold higher affinity compared to SARS-CoV [26],[25], making ACE2 a potential biorecognition element for virus detection. Although the spike-ACE2 protein interaction occurs, forming the complex, the spike protein still has several epitopes to be detected by a polyclonal anti-spike antibody [145]. Therefore, we used these features to assemble an immunosensor based on the spike-ACE2 protein complex in a sandwich between the corresponding antibodies with high efficiency while minimizing unspecific interactions [146]. In addition, magnetic particles pre-concentrated the spike protein directly from the samples, facilitating washing steps and decreasing the effects of potential interferents present in the complex matrix while confining

the immunocomplex at the SPAuEs [147]. In this context, the immunosensor response further interrogated in a portable potentiostat offers a versatile and cost-affordable but robust alternative to detect the virus.

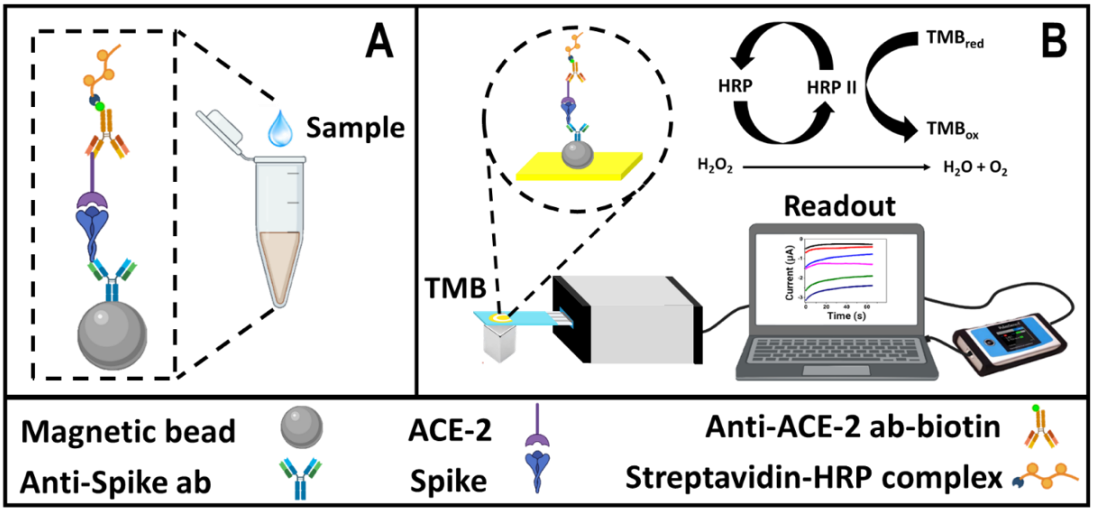

Scheme 1. Conceptual schematic of the immunosensor design based on the Spike-ACE-2 complex. A) Sandwich immunosensor assembly on the magnetic bead-based platform and B) enzyme-amplified electrochemical reaction and chronoamperometric signal readout [148].

The immunosensor assembly design is described in Scheme 1A. It consists of carboxylated magnetic particles as a support platform to bind primary amine groups from the anti-spike antibodies by covalent coupling with N-ethyl-N′-(3-(dimethylamino)propyl)carbodiimide (EDC) and N-hydroxysuccinimide (NHS). Some of the anchored antibodies eventually have the Fab region exposed and available to interact with the spike protein epitope from the spike-ACE2 complex with high affinity. Afterward, this ACE2 protein interacts with a biotinylated anti-ACE2 antibody and the streptavidin-(HRP) complex reporter. Finally, the immunocomplex is transferred to an SPAuE. After adding TMB as a substrate of the HRP enzyme in the presence of H_2O_2, it generates a change in current over time detectable by chronoamperometry that correlates well with changes in the concentration of the spike protein (pseudovirions and viral particles) analyzed as depicted in Scheme 1B.

As preliminary steps, each parameter involved in the immunosensor development was screened rapidly and systematically by spectrophotometry (absorbance at 650 nm). As indicated above, carboxylated magnetic beads served as a platform to covalently couple the anti-spike antibody using the carbodiimide chemistry [48],[49], following a slightly modified

protocol reported by the manufacturer but expecting a high yield surface coverage [149]. A higher signal-to-noise ratio was evident when incubating the activated particles with the anti-spike antibody in MES buffer pH 6.0 for 2 h compared to 12 h, or PBS buffer pH 7.4 for 12 h (recommended by the manufacturer) or 2 h, respectively (see Figure S 1, A), as expected from the instability of the acyl urea intermediate of EDC in PBS [151]. The effect of 1% casein and 1% bovine serum albumin (BSA) on the immunosensor response was evaluated based on the signal-to-noise ratio and determined casein as the optimal blocking agent (see Figure S 1, B).

The amount of MBs supporting the immunoassay was tested between 5 and 40 µg, and the maximum signal reached 20 µg (Figure S 2, A). Subsequently, the MBs' maximum coating capacity was evaluated empirically from 6 to 48 µg/mL anti-spike antibody based on the signal response (see Figure S 2, B). Although the maximum screened signal was obtained with 24 µg/mL, it didn't represent a significant increase concerning 12 µg/mL, which is more cost-efficient; therefore, the last-mentioned concentration was selected as optimal for further steps (see Figure S 2, B). Surface coverage was estimated by indirectly quantifying the antibody concentration in the supernatant after conjugation to the magnetic particles using a BCA kit (see Figure S 3). 3 µg/mL was determined as the concentration immobilized at the MBs, which is 75% efficiency in the coupling reaction compared to the one reported by the manufacturer (4-6 µg/mL) [150], indicating a proper bioconjugation process. Besides, having empirically found the MB-based supporting platform's optimal surface coverage will ensure optimal electrochemical and optical readout. Remarkably, when different references of commercially available anti-spike antibodies were evaluated, it was found that the spike S1-His Recombinant Protein (Ref. 40591-V08H) used herein interacted only with the corresponding antibody of the same commercial company (see Figure S 4). Although the antibodies were kept at the storage conditions recommended by the manufacturer, they did not have the expected stability. Yet, the mentioned protein-antibody marriage was used in the following steps.

The ACE2 protein and anti-ACE2 antibody concentrations were assessed between 0.5 and 3 µg/mL, obtaining 2 µg/mL as optimal in both cases (see Figure S 2, C and D). Finally, the concentration of streptavidin-HRP, also crucial for getting a higher signal response while minimizing the noise, was evaluated between 50 and 200 ng/mL. Although the signal seems

to reach a plateau at 100 ng/mL (Figure S 2, E), 50 ng/mL produced a higher signal/noise ratio, so this was selected as the optimal condition (Figure S 2, F).

Once the optimal conditions were screened, the MB-based immunoplatform was confined at the SPAuE surface by placing a magnet behind the working electrode to check its performance with an electrochemical readout. It was achieved by chronoamperometry by applying a fixed potential of -150 mV and using a commercial TMB solution, as detailed in the experimental section. Once the performance was confirmed, the immunosensor was challenged with a buffer supplemented with concentrations of commercial spike protein ranging from 0 to 3 µg/mL to construct a calibration curve. Figure 5A shows the electrochemical signal response was concentration-dependent in a linear range between 0 and 2 µg/mL, with a sensitivity of 1.13 µA*mL/µg, a LOD of 100 ng/mL and high linearity (R^2 = 0.9948). The optical signal response was linear in the same range, with a sensitivity of 0.86 mL/µg, LOD of 17 ng/mL and R^2 of 0.9883 (see Figure 5B). Although the optical method is slightly more sensitive than the electrochemical one, the signals were well-correlated (R^2 = 0.9814), as shown in Figure 5C, indicating the great potential of the immunosensor not only for spectrophotometric bench laboratory testing but for electrochemical detection closer to the patient and remote settings. Despite being more time-consuming than our immunosensor, the ELISA-like assay permits more samples to be detected simultaneously, but both techniques have high reproducibility.

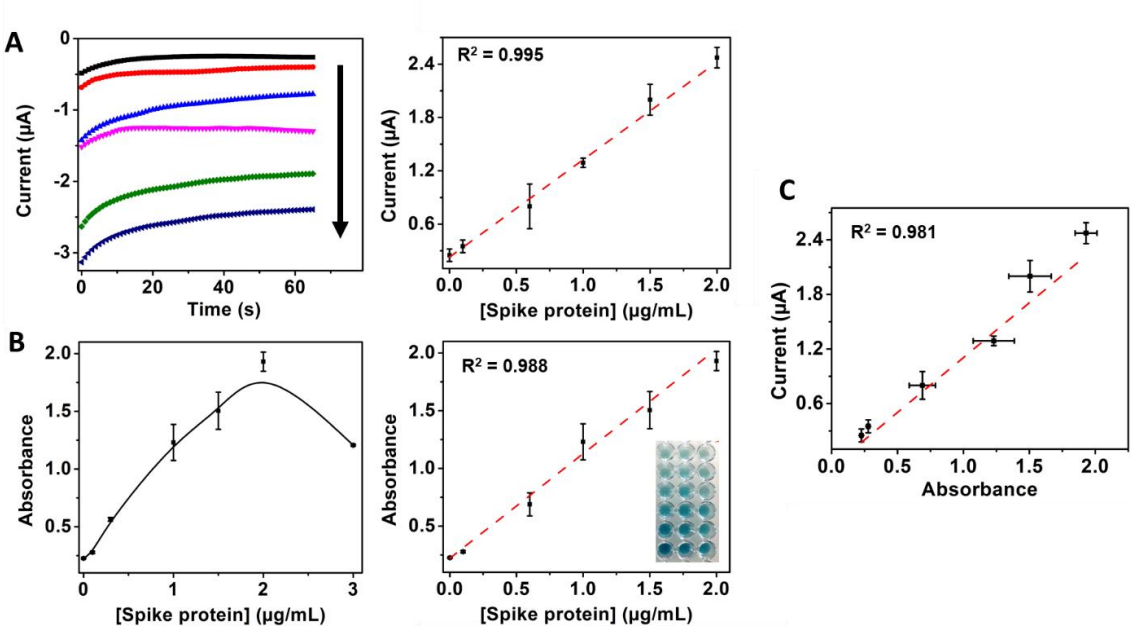

Figure 5. Immunosensor response with increasing concentrations of spike protein amplified with streptavidin-HRP. A) chronoamperometry at a potential of -150 mV for 65 s and B) spectrophotometric response by absorbance at 650 nm with 0, 0.1, 0.6, 1, 1.5 and 2 µg/mL spike protein, C) Correlation between electrochemical and optical reading.

Streptavidin (poly) HRP-20 and streptavidin (poly) HRP-80 bioconjugated enzymatic complexes, with 100 and 400 HRP molecules per streptavidin molecule and the same concentration of streptavidin HRP were coupled to the immunosensor format in an attempt to increase its analytical performance. It was observed that there was a significant improvement in the signal while keeping the corresponding background signal constant, as reported for this kind of complex [152]. Therefore, based on the signal-to-noise ratio, 50 ng/mL streptavidin (poly) HRP-80 complex was optimal (see Figure S 5). With the new enzymatic complex, the enhanced immunosensor format produced a signal that was spike protein concentration-dependent in a linear range between 0 to 1.0 µg/ml, with a sensitivity of 0.83 µA*mL/µg, a LOD of 22.55 ng/mL and R^2 = 0.997 (see Figure 6). By replacing the standard streptavidin HRP with the streptavidin (poly) HRP-80 bioconjugated enzymatic complex, the LOD of the resulting immunosensor was lowered more than 4-fold mainly due to an increased signal without increasing the background. Such a low LOD is comparable to other SARS-CoV-2 spike protein immunosensors reported in the literature [136] and lower than other reports [93],[83]. Furthermore, it highlights the potential of the immunosensor for the detection of the spike protein in infected patients, considering that the viral loading in samples from infected patients has been reported to be between 10^4 and 10^{11} copies/mL, with

an average loading of 10^5 copies/mL [153],[154],[155]. Therefore, based on approximately 100 copies of spike protein per virion [154] and the 180-200 kDa molecular weight of spike protein [156], we can expect a concentration of approximately 0.3 pg/mL to 3 µg/mL spike protein in samples from patients for the reported viral loading (10^4 to 10^{11} copies/mL).

Although other biosensors with slightly lower LODs have been reported in the literature [89][95], our immunosensor has good enough analytical properties for practical applications being advantageous in terms of easiness of sample processing without the need to modify electrodes and using robust and specialized equipment. Remarkably, MBs preconcentrate the spike protein at the surface of the SPAuEs, simplifying washing steps and reducing assay time. Such electrodes are expected to be of similar performance to those from carbonaceous materials but worst than those modified with nanomaterials such as graphene and Pusian blue, plausible approaches to improve the analytical performance of the resultant biosensors [136].

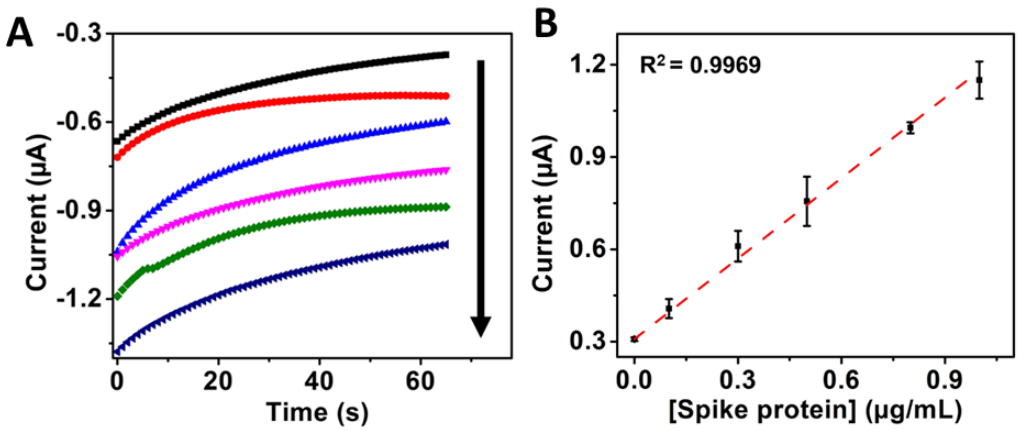

Figure 6. A) Immunosensor electrochemical response with increasing concentrations of 0, 0.1, 0.3, 0.5, 0.8 and 1 µg/mL of the spike protein amplified with streptavidin-HRP (poly) 80 and B) Corresponding calibration curve.

3.2. Detection of pseudovirions

Developing protocols and devices to detect hazardous pathogens may represent a risk for researchers when evaluating samples with active pathogens, requiring BSL-3 settings. In contrast, pseudovirions expressing the spike protein and heterologous viral proteins reduce the risk, requiring only BSL-2 facilities [139]. Pseudovirions have been proposed to investigate virus-host interaction but herein were used as a good substitute for virions for biosensor characterization to speed up the process while protecting the safety of researchers [157]. Pseudovirions were assembled by co-transfection of three plasmids carrying the genes

MLV gal-pol, luciferase and SARS-CoV-2 S into the HEK-293T cell line and characterized by luciferase expression and RT-qPCR.

Pseudoviral particles harboring the SARS-CoV-2 spike glycoprotein were then produced in cell culture following the protocol detailed in the experimental methods section. The viability of pseudovirions was demonstrated by transduction of Vero-E6 cells by luciferase expression after 72 h post-transduction. The assay confirmed the viability of the pseudovirions (see Figure S 6, A), with high efficiency and reproducible results being higher for SARS-CoV-2 (7.76 x 10^8 URL/mL) than for MERS-CoV pseudovirions (5.66 x 10^7 URL/mL) but lower than the VSV (8.74 x 10^{10} URL/mL) counterparts used as controls. A western blot assay confirmed the presence of SARS-CoV-2 spike protein in the HEK-293 cells cotransfected with MLV Gag-Pol, luciferase and SARS-CoV-2 spike plasmids and control HEK-293 cells (see Figure S 6, B). Finally, pseudovirions were quantified in copies/mL by a real-time PCR (RT-PCR) assay. Table S 1 of the S.I. file shows a 3.7-fold higher concentration of pseudovirions after ultracentrifugation (25.000 rpm 90 min 4 ºC TNE in buffer) than untreated pseudovirions. Furthermore, concentrations of 1.1 x10^9, 5.2 x10^8 and 3.3 x 10^8 copies/mL were obtained for SARS-CoV-2, SARS-CoV and MERS-CoV pseudovirions, respectively.

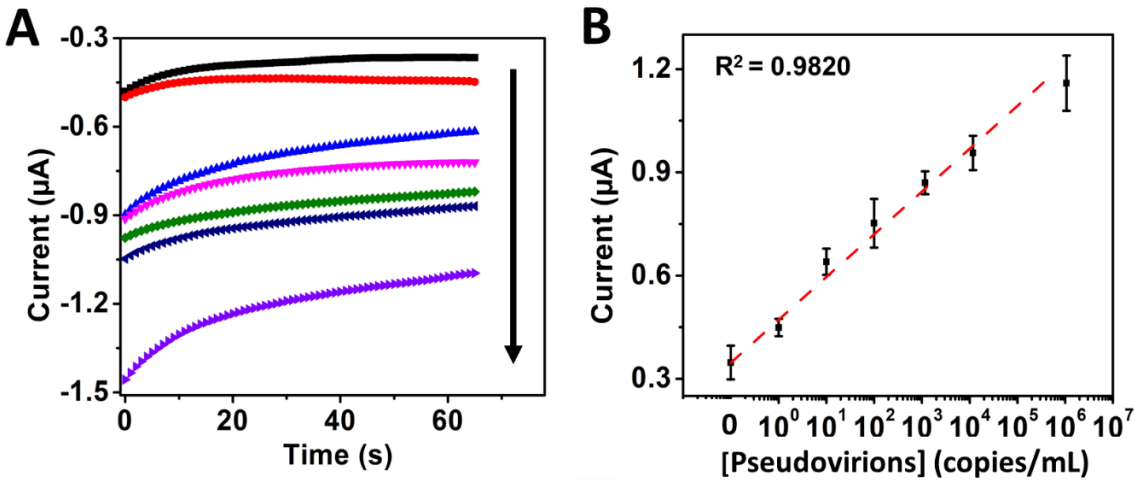

Figure 7. Immunosensor electrochemical response with increasing concentrations of 0, 1, 10, 10^2, 10^3, 10^4, and 10^6 copies/mL pseudovirions amplified with streptavidin-HRP (poly) 80 and B) Corresponding calibration curve.

The immunosensor was then tested with 1 to 1x10^6 copies/mL of artificially assembled pseudovirions, which resultant electrochemical signal was viral particle-dependent in this

range, with a sensitivity of 1.28 µA*mL/copies, a LOD of 0.12 copies/mL, and high linearity, *i.e.*, R^2 = 0.982 (see Figure 7). However, the immunosensor responded with lower sensitivity $6.0x10^{-7}$ µA*mL/copies and worst LOD of $4.17x10^4$ copies/mL (R^2=0.987) in a range between 1 to $5x10^5$ copies/mL of viral particles cultured from an infected patient inactivated by UV-light exposure for 30 min and lysed with RIPA buffer before the measurements (see Figure S 7). Inactivation of the viral particles was explained by [158] and [159]. They reported that UV-light irradiation could cause damage to genetic material and other viral components, potentially decreasing the RBD's binding capacity from the spike protein to the ACE2 protein, in agreement with the decreased sensitivity of our immunosensor in UV-inactivated viral particles. Therefore, inactivation (denaturalization) of viral particles only by lysis would be a better strategy for pretreatment and interrogation of clinical samples, achieving detection limits lower than the gold standard that has been reported to be approximately 100 copies/mL [160], [161]. Furthermore, although such a protocol breaks the viral particle membrane, it does not damage the spike protein, thus maintaining its binding capacity to the ACE2 protein.

3.3. Specificity of the immunosensor

Since specificity is a highly desired feature in a biosensor to obtain reliable results, this feature was evaluated later. Figure 8 shows the 1 µg/mL spike protein signal compared to the commercial RBD at the same concentration and $1x10^5$ copies/mL of lysed SARS-CoV-2 pseudovirions. Although the commercial spike protein signal was 1.35-fold and 1.2-fold higher than those of the RBD region and lysed pseudovirions, they had statistically significant differences from the negative control without analyte (***p <0.001). Statistically significant differences were also observed when comparing the signals from the same number of pseudovirions of SARS-CoV-2, SARS-CoV and MERS-CoV (***p <0.001). Since SARS-CoV-2 shares 79.9% homology with SARS-CoV and 40% homology with MERS-CoV, the anti-spike antibody bound to the MBs may present cross interactions, which explain the small current signals obtained. Specificity was also evaluated with another glycoprotein (β-1.4-GALT-5) and VSV pseudovirions as controls. In both cases, there were statistically significant differences (***p<0.001) with commercial spike protein and SARS-CoV-2 pseudovirions and very low significance (**p<0.01 and - p>0.05) with the negative control,

respectively. These results demonstrated that the immunosensor efficiently detected SARS-CoV-2 spike protein with higher affinity than glycoproteins from other coronaviruses and VSV.

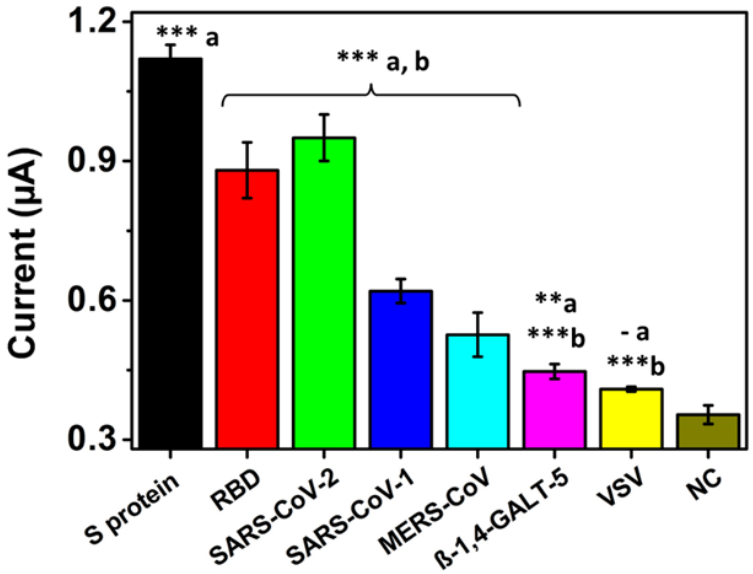

*Figure 8. Immunosensor specificity when detecting 1 µg/mL spike, RBD and β-1,4-GALT-5 proteins and 1 x 10^5 copies/mL MERS, SARS-CoV-1, SARS-CoV-2 and VSV pseudovirions supernatants. Statistically significant differences (a) with respect to the negative control and (b) with respect to the commercial spike protein, ***($p < 0.001$), **($p<0.01$), *($p<0.05$) and – ($p>0,05$).*

3.4. Detection of SARS-COV-2 spike protein in clinical samples

Once the specificity was proved, the immunosensor was challenged by detecting the spike protein in samples obtained from ten patients and results compared to three samples from healthy individuals, positive and negative by RT-PCR, respectively. The samples were obtained by nasopharyngeal swabbing, kindly donated by the PECET group from the University of Antioquia and classified based on the cycle threshold (C.T.) measured values (as higher the C.T., the lower the viral loading, see Table S 2 in the S.I. file). The immunosensor signal of 1 µg/mL commercial spike protein was compared with three negative samples, three samples with high, three with medium and four with low C.T. values. The samples were measured at a 1/10 dilution and lysed in RIPA buffer, using only 5 µL of sample for the electrochemical measurement. The 90% of samples positive by RT-PCR had statistically significant differences (*$p<0.05$, ** $p<0.01$, *** $p<0.001$) concerning the negative control. Similarly, samples negative by RT-PCR had no statistically significant

differences from the negative control (p >0.05). Furthermore, the results were consistent with the C.T. reported for each sample, *i.e.*, all the ten positive samples by RT-PCR and the three negative ones were positive and negative, respectively, with our immunosensor, demonstrating the excellent detection capability of the as-developed immunosensor even in samples with high C.T. (see Figure 9). An estimation of the concentration of the spike protein in each sample is in Table S2. Yet, rather than an exact amount of spike protein found, it must be interpreted as negative samples or positive samples with low, middle or high viral loading. To avoid the sample preparation and simplify the assay, samples with low C.T. were evaluated both lysed and raw. It was observed that detection of the spike protein from SARS-CoV-2 could be achieved with statistically significant differences with the negative control (*p <0.05) even without sample pretreatment (see Figure S 8). It is important to highlight that the number of samples is low and clinical validation with samples from a cohort of patients positive for SARS-CoV-2 and healthy individuals by the RT-PCR gold standard is required. Yet, this proof-of-concept opens the way to sensitive detection of SARS-CoV-2 using simpler sample handling, i.e., the availability of a portable, easy-to-use device that may offer the possibility of point-of-care implementation.

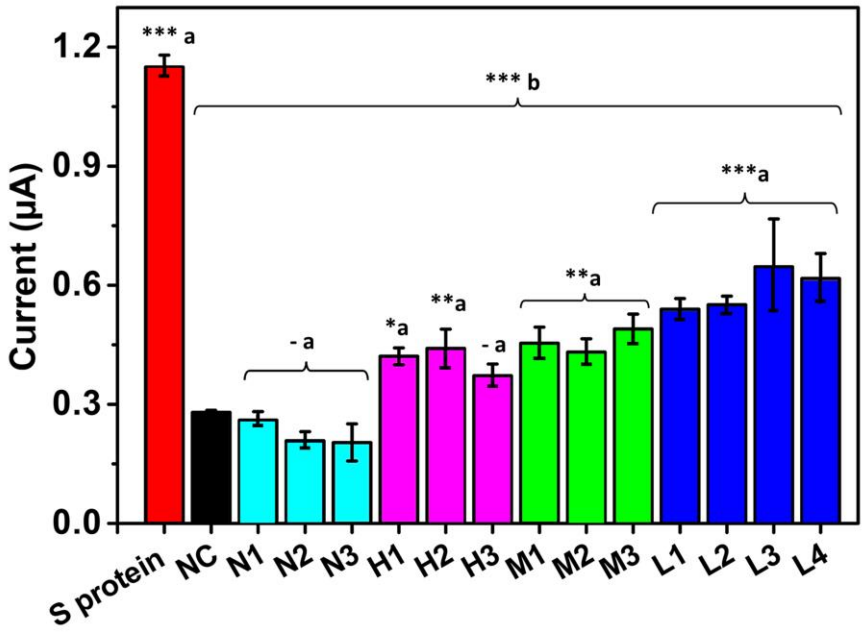

*Figure 9. Immunosensor response of different lysed patient samples compared to a commercial spike protein-positive control and a negative control without the target protein. Cyan, purple, green and blue columns correspond to negative samples and high, medium and low C.T positive samples. Statistically significant differences (a) with respect to the negative control and (b) with respect to the commercial Spike protein, ***(p < 0.001), **(p<0.01), *(p<0.05) and – (p>0,05).*

3.5. Detection with Sensit Smart smartphone potentiostat

We compared the signal obtained with the PalmSens4 potentiostat with a Sensit Smart pocket potentiostat to detect the virus closer to the patient. Figure S 9 shows both the positive and negative controls have a similar signal in both potentiostats, without statistically significant differences (p >0.05), evidencing the possibility of implementing the immunosensor assay in this Sensitive Smart potentiostat, maintaining the high detection performance.

4. Conclusion

A proof of concept of the immunosensor was developed to detect the SARS-CoV-2 spike protein by electrochemical reading. The immunosensor takes advantage of the high-affinity interaction between the spike protein and the ACE2 human host protein used herein as bioreceptor-like for the first time, forming a spike-ACE2 protein complex. The immunosensor showed outstanding analytical performance with a sensitivity of 0.83 µA*mL/µg and a LOD of 22.55 ng/mL, using the streptavidin (poly) HRP-80 enzymatic complex as an amplification system. In addition, the immunosensor specifically detected pseudovirions synthetically assembled herein with spike protein expressed on their outermost surface with LOD of 0.12 copies/mL, but with lower sensitivity with UV-light inactivated viral particles. Finally, the high detection capacity of the immunosensor was demonstrated in raw and lysed samples from infected patients and compared with samples from healthy individuals using only 5 µL of the sample. The approach does not need RNA extraction, complex, robust equipment, or specialized personnel compared to RT-PCR, highlighting the device's potential for SARS-CoV-2 detection closer to the patient and minimizing sample volume, displacement and virus spreading.

5. Acknowledgments

The authors acknowledge MinCiencias for funding the project Nanobiosensors to detect SARS-CoV-2 rapidly (Cod. 1115101576765). J.O acknowledges financial support from the Minciencias, the University of Antioquia and the Max Planck Society through the Cooperation agreement 566-1, 2014. In addition, the authors are thankful to the PECET and the Immunovirology Group from the University of Antioquia for donations of patient

samples and viral particles and Vero cells, respectively and CECOLTEC for the Sensit Smart pocket potentiostat donation. The authors also thank the technical assistance of Maria Camila Lopez-Osorio and Melissa Montoya-Guzman of the Gastrohepatology Group from the University of Antioquia and EPM and Ruta N for hosting the Max Planck Tandem Groups. Finally, the authors want to acknowledge Gary Whittaker at Cornell University for providing the plasmids needed for the pseudovirion system.

CHAPTER IV: Conclusions and perspectives

CONCLUSIONS

This master thesis developed an electrochemical immunosensor to detect SARS-CoV-2 protein S, taking advantage of the high-affinity interaction of protein S with ACE2 protein. Each of the amounts or concentrations of the immunosensor components was rapidly screened by spectrophotometry, obtaining 20 µg of magnetic particles, 12 µg/mL of anti-Spike antibody, and 2 µg/mL of ACE protein and anti ACE2 antibody, and 50 ng/mL of streptavidin-HRP as optimal. In addition, it demonstrated the broad utility of implementing amplification systems by improving the LOD 5-fold using the streptavidin (poly) HRP 80 enzyme complex concerning the streptavidin-HRP system counterpart. Additionally, the use of protein A and anti-Spike antibodies differently from the commercial brand of the protein of interest was discarded.

The optimized electrochemical immunosensor showed an analytical performance comparable to commercial methods, with a sensitivity of 0.83 µA*mL/µg and a LOD of 22.55 ng/mL in detecting commercial protein S. Also, the immunosensor detected synthetically assembled pseudovirions and real viral particles, with lower sensitivity in inactivated viral particles than pseudovirions, achieving a LOD of 0.12 copies/mL. Finally, the high detection capacity of the immunosensor was demonstrated by discriminating the level of protein S in ten crude and lysed samples from infected patients and compared with three samples from healthy individuals concerning the conventional method based on RT-PCR.

The immunosensor showed a high potential to detect SARS-CoV-2 in a sensitive, selective, and specific manner with high reproducibility and in real samples, without the need for RNA extraction, complex and robust equipment, or specialized personnel compared to RT-PCR, and with only 5 µL of the sample.

PERSPECTIVES

Although the potential of the immunosensor developed in detecting SARS-CoV-2 in ten samples of infected patients was evident, the next step to follow would be to validate the

device in a statistically significant number of samples, which would allow greater certainty of its detection capacity in a real scenario.

With the above and considering that the immunosensor developed evidenced the possibility of being implemented at the point of care by achieving detection in a pocket potentiostat such as the Sensit Smart, the next step would be the development of an easy-to-use and portable kit to reach remote settings. Furthermore, this detection platform could serve as a basis for developing biosensors to detect other emerging viruses to reduce the detection time and screening of infected patients, isolating them at the right time and reducing the possibility of spreading and thus future crises such as the COVID 19 pandemic.

Another perspective of great interest is the development of multiparametric devices that allow the detection of several biomolecules of interest simultaneously. For example, in the case of COVID 19, a large group of inflammatory, hematological, biochemical, and genetic biomarkers has been found of interest as they are closely related to susceptibility to infection and severity of the disease. Therefore, it would be of great interest to implement this immunosensor as part of a multiparametric system, in which the detection of SARS-CoV-2 is achieved together with the detection of specific biomarkers such as C-reactive protein, interleukin-6, procalcitonin, ferritin, vitamin D, dimer D, cardiac troponin that are highly correlated not only to the disease diagnosis but prognosis and curse of the disease. The multiparametric system would open the door to the diagnosis, prognosis, and evaluation of the progress and severity of COVID-19 using a single device, paving the way toward personalized medicine.

REFERENCES

[1] J. Wan *et al.*, "Human-IgG-Neutralizing Monoclonal Antibodies Block the SARS-CoV-2 Infection," *Cell Rep.*, vol. 32, no. 3, p. 107918, Jul. 2020, doi: 10.1016/j.celrep.2020.107918.

[2] A. C. Walls, Y. J. Park, M. A. Tortorici, A. Wall, A. T. McGuire, and D. Veesler, "Structure, Function, and Antigenicity of the SARS-CoV-2 Spike Glycoprotein," *Cell*, vol. 181, no. 2, pp. 281-292.e6, 2020, doi: 10.1016/j.cell.2020.02.058.

[3] NanoB2A, "Técnicas y sistemas de diagnóstico para COVID-19 : clasificación , características , ventajas y limitaciones Diagnóstico de COVID-19 SARS-CoV-2," *NanoB2A - ICN2*, pp. 1–10, 2020, [Online]. Available: http://www.ciencia.gob.es/stfls/MICINN/Ministerio/FICHEROS/TecnicasDiagnosticoCOVID19-ICN2.pdf.

[4] "Preguntas y respuestas sobre la enfermedad por coronavirus (COVID-19)." https://www.who.int/es/emergencies/diseases/novel-coronavirus-2019/advice-for-public/q-a-coronaviruses (accessed Nov. 29, 2020).

[5] K. G. Andersen, A. Rambaut, W. I. Lipkin, E. C. Holmes, and R. F. Garry, "The proximal origin of SARS-CoV-2," *Nat. Med.*, vol. 26, no. 4, pp. 450–452, 2020, doi: 10.1038/s41591-020-0820-9.

[6] Revista El país, "Coronavirus: ccu cgg cgg gca: las doce letras que cambiaron el mundo | Ciencia | EL PAÍS," May 11, 2020. https://elpais.com/elpais/2020/05/09/ciencia/1589059080_203445.html (accessed Nov. 05, 2020).

[7] "Invitación a presentar proyectos que contribuyan a la solución de problemáticas actuales de salud relacionadas con la pandemia de COVID-19 | Convocatoria | Minciencias." https://minciencias.gov.co/convocatorias/invitacion-para-presentacion-propuestas/invitacion-presentar-proyectos-que-contribuyan (accessed Mar. 02, 2022).

[8] L. Zhang and H. Guo, "Biomarkers of COVID-19 and technologies to combat SARS-CoV-2," *Adv. Biomark. Sci. Technol.*, vol. 2, pp. 1–23, Jan. 2020, doi: 10.1016/j.abst.2020.08.001.

[9] M. C. Collivignarelli, C. Collivignarelli, M. Carnevale Miino, A. Abbà, R. Pedrazzani, and G. Bertanza, "SARS-CoV-2 in sewer systems and connected facilities," *Process Saf. Environ. Prot.*, vol. 143, pp. 196–203, 2020, doi: 10.1016/j.psep.2020.06.049.

[10] M. A. Shereen, S. Khan, A. Kazmi, N. Bashir, and R. Siddique, "COVID-19 infection: Origin, transmission, and characteristics of human coronaviruses," *Journal of Advanced Research*, vol. 24. Elsevier B.V., pp. 91–98, Jul. 01, 2020, doi: 10.1016/j.jare.2020.03.005.

[11] A. Wu *et al.*, "Genome Composition and Divergence of the Novel Coronavirus (2019-nCoV) Originating in China," *Cell Host Microbe*, vol. 27, no. 3, pp. 325–328, 2020, doi: 10.1016/j.chom.2020.02.001.

[12] Z. Luo *et al.*, "Combating the Coronavirus Pandemic: Early Detection, Medical Treatment, and a Concerted Effort by the Global Community," *Research*, vol. 2020, pp. 1–35, Jun. 2020, doi: 10.34133/2020/6925296.

[13] A. G. Wrobel *et al.*, "SARS-CoV-2 and bat RaTG13 spike glycoprotein structures inform on virus evolution and furin-cleavage effects," *Nat. Struct. Mol. Biol.*, vol. 27,

no. 8, pp. 763–767, 2020, doi: 10.1038/s41594-020-0468-7.
[14] J. Yang *et al.*, “Molecular interaction and inhibition of SARS-CoV-2 binding to the ACE2 receptor,” *Res. Sq.*, May 2020, doi: 10.21203/rs.3.rs-30468/v1.
[15] Statista, “• Coronavirus: número acumulado mundial de casos 2020-2022 | Statista,” Feb. 06, 2022. https://es.statista.com/estadisticas/1104227/numero-acumulado-de-casos-de-coronavirus-covid-19-en-el-mundo-enero-marzo/ (accessed Feb. 09, 2022).
[16] E. Mathieu *et al.*, “Coronavirus Pandemic (COVID-19),” *Our World Data*, vol. 5, no. 7, pp. 947–953, Mar. 2020, doi: 10.1038/S41562-021-01122-8.
[17] Sino Biological, “Reactivos de antígeno SARS-Cov-2 (2019-nCoV),” 2020. https://www.sinobiological.com/research/virus/2019-ncov-antigen (accessed Nov. 05, 2020).
[18] A. A. Rabaan *et al.*, “SARS-CoV-2, SARS-CoV, and MERS-CoV: a comparative overview,” 2020. [Online]. Available: https://www.infezmed.it/media/journal/Vol_28_2_2020_7.pdf.
[19] N. Chams *et al.*, “COVID-19: A Multidisciplinary Review,” *Front. Public Heal.*, vol. 8, no. July, pp. 1–20, 2020, doi: 10.3389/fpubh.2020.00383.
[20] R. Kubina and A. Dziedzic, “Molecular and serological tests for COVID-19. A comparative review of SARS-CoV-2 coronavirus laboratory and point-of-care diagnostics,” *Diagnostics*, vol. 10, no. 6, 2020, doi: 10.3390/diagnostics10060434.
[21] Y. A. Malik, “Properties of Coronavirus and SARS-CoV-2,” Malaysia, pp. 3–11, 2020.
[22] Sino Biological, “Human Coronavirus Spike,” 2020. https://www.sinobiological.com/research/virus/human-coronavirus-spike (accessed Nov. 05, 2020).
[23] H. Esakandari, M. Nabi-Afjadi, J. Fakkari-Afjadi, N. Farahmandian, S. M. Miresmaeili, and E. Bahreini, “A comprehensive review of COVID-19 characteristics,” *Biol. Proced. Online*, vol. 22, no. 1, pp. 1–10, 2020, doi: 10.1186/s12575-020-00128-2.
[24] S. Wang *et al.*, “AXL is a candidate receptor for SARS-CoV-2 that promotes infection of pulmonary and bronchial epithelial cells,” *Cell Res. 2021 312*, vol. 31, no. 2, pp. 126–140, Jan. 2021, doi: 10.1038/s41422-020-00460-y.
[25] J. M. Delgado, N. Duro, D. M. Rogers, A. Tkatchenko, S. A. Pandit, and S. Varma, “Molecular basis for higher affinity of SARS-CoV-2 spike RBD for human ACE2 receptor,” *Proteins Struct. Funct. Bioinforma.*, vol. 89, no. 9, pp. 1134–1144, Sep. 2021, doi: 10.1002/PROT.26086.
[26] J. Lu and P. D. Sun, “High affinity binding of SARS-CoV-2 spike protein enhances ACE2 carboxypeptidase activity,” *J. Biol. Chem.*, vol. 295, no. 52, pp. 18579–18588, Dec. 2020, doi: 10.1074/JBC.RA120.015303.
[27] M. A. Al-Azzawi and M. A. Sakr, “Co-Evolution between New Coronavirus (SARS-CoV-2) and Genetic Diversity: Insights on Population Susceptibility and Potential Therapeutic Innovations,” in *Genetic Diversity [Working Title]*, IntechOpen, 2020.
[28] Q. Wang *et al.*, “Structural and Functional Basis of SARS-CoV-2 Entry by Using Human ACE2,” *Cell*, vol. 181, no. 4, pp. 894-904.e9, 2020, doi: 10.1016/j.cell.2020.03.045.
[29] R. Yan, Y. Zhang, Y. Li, L. Xia, Y. Guo, and Q. Zhou, “Structural basis for the recognition of SARS-CoV-2 by full-length human ACE2,” *Science (80-.).*, vol. 367, no. 6485, pp. 1444–1448, Mar. 2020, doi: 10.1126/science.abb2762.

[30] G. Pastrian-Soto, “Bases Genéticas y Moleculares del COVID-19 (SARS-CoV-2). Mecanismos de Patogénesis y de Respuesta Inmune,” *Int. J. Odontostomatol.*, vol. 14, no. 3, pp. 331–337, Sep. 2020, doi: 10.4067/s0718-381x2020000300331.

[31] S. Mahapatra and P. Chandra, “Clinically practiced and commercially viable nanobio engineered analytical methods for COVID-19 diagnosis,” *Biosens. Bioelectron.*, vol. 165, no. June, p. 112361, 2020, doi: 10.1016/j.bios.2020.112361.

[32] N. Ravi, D. L. Cortade, E. Ng, and S. X. Wang, “Diagnostics for SARS-CoV-2 detection: A comprehensive review of the FDA-EUA COVID-19 testing landscape,” *Biosens. Bioelectron.*, vol. 165, p. 112454, Oct. 2020, doi: 10.1016/j.bios.2020.112454.

[33] A. Y. R. Saenz and J. M. C. Valero, “Enfermedad por Coronavirus 2019: diagnostico por el laboratorio,” *Salud Soc.*, vol. 5, no. 1, p. ...-..., Oct. 2020, Accessed: Nov. 05, 2020. [Online]. Available: https://revistas.uptc.edu.co/index.php/salud_sociedad/article/view/11944.

[34] J. M. Meza Calvache, A. D. Estrada Rodríguez, C. B. Chabusa Chabusa, and V. A. Velasco Paucar, “Utilidad de Pruebas de cadena de polimerasa, pruebas rápidas y Tomografías en pacientes con Covid-19,” *J. Am. Heal.*, vol. 3, no. 2, pp. 32–39, Jul. 2020, doi: 10.37958/jah.v3i2.28.

[35] P. Aguilar Ramírez, Y. Enriquez Valencia, C. Quiroz Carrillo, E. Valencia Ayala, J. de León Delgado, and A. Pareja Cruz, “Pruebas diagnósticas para la COVID-19: la importancia del antes y el después,” *Horiz. Médico*, vol. 20, no. 2, p. e1231, Jun. 2020, doi: 10.24265/horizmed.2020.v20n2.14.

[36] Minsalud, “PROCESO GESTIÓN DE LAS INTERVENCIONES INDIVIDUALES Y COLECTIVAS PARA LA PROMOCIÓN DE LA SALUD Y PREVENCIÓN DE LA ENFERMEDAD. Código GIPS21 DOCUMENTO SOPORTE LINEAMIENTOS PARA EL USO DE PRUEBAS MOLECULARES RT-PCR Y PRUEBAS DE ANTÍGENO Y SEROLÓGICAS PARA SA,” 2020. Accessed: Nov. 05, 2020. [Online]. Available: https://www.minsalud.gov.co/Ministerio/Institucional/Procesos y procedimientos/GIPS21.pdf.

[37] H. Malekzad, P. S. Zangabad, H. Mirshekari, M. Karimi, and M. R. Hamblin, “Noble metal nanoparticles in biosensors: recent studies and applications,” *Nanotechnol. Rev.*, vol. 6, no. 3, pp. 301–329, Jun. 2017, doi: 10.1515/NTREV-2016-0014.

[38] N. Debnath and S. Das, “Nanobiosensor: Current trends and applications,” in *NanoBioMedicine*, Springer Singapore, 2020, pp. 389–409.

[39] H. H. Nguyen, S. H. Lee, U. J. Lee, C. D. Fermin, and M. Kim, “Immobilized enzymes in biosensor applications,” *Materials*, vol. 12, no. 1. MDPI AG, p. 121, Jan. 02, 2019, doi: 10.3390/ma12010121.

[40] S. Patel, R. Nanda, S. Sahoo, and E. Mohapatra, “Biosensors in health care: The milestones achieved in their development towards lab-on-chip-analysis,” *Biochemistry Research International*, vol. 2016. Hindawi Publishing Corporation, 2016, doi: 10.1155/2016/3130469.

[41] S. K. Saxena and S. M. P. Khurana, Eds., *NanoBioMedicine*. Singapore: Springer Singapore, 2020.

[42] N. Wongkaew, M. Simsek, C. Griesche, and A. J. Baeumner, “Functional Nanomaterials and Nanostructures Enhancing Electrochemical Biosensors and Lab-on-a-Chip Performances: Recent Progress, Applications, and Future Perspective,” *Chem. Rev.*, vol. 119, no. 1, pp. 120–194, 2019, doi: 10.1021/acs.chemrev.8b00172.

[43] C. Sabu, T. K. Henna, V. R. Raphey, K. P. Nivitha, and K. Pramod, "Advanced biosensors for glucose and insulin," *Biosensors and Bioelectronics*, vol. 141. Elsevier Ltd, p. 111201, Sep. 15, 2019, doi: 10.1016/j.bios.2019.03.034.
[44] G. Palestino, I. García-Silva, O. González-Ortega, and S. Rosales-Mendoza, "Can nanotechnology help in the fight against COVID-19?," *Expert Rev. Anti. Infect. Ther.*, vol. 00, no. 00, pp. 1–16, 2020, doi: 10.1080/14787210.2020.1776115.
[45] M. Sharifi *et al.*, "Cancer diagnosis using nanomaterials based electrochemical nanobiosensors," *Biosensors and Bioelectronics*, vol. 126. Elsevier Ltd, pp. 773–784, Feb. 01, 2019, doi: 10.1016/j.bios.2018.11.026.
[46] J. Quinchia, D. Echeverri, A. F. Cruz-Pacheco, M. E. Maldonado, and J. A. Orozco, "Electrochemical biosensors for determination of colorectal tumor biomarkers," *Micromachines*, vol. 11, no. 4, pp. 1–46, 2020, doi: 10.3390/MI11040411.
[47] G. Dutta, "Nanobiosensor-based diagnostic system: Transducers and surface materials," in *Nanobiomaterial Engineering: Concepts and Their Applications in Biomedicine and Diagnostics*, Springer Singapore, 2020, pp. 1–13.
[48] P. Díez Sánchez, R. Villalonga Santana, and J. M. Pingarrón Carrazón, "Nuevos nanomateriales para el diseño de Biosensores Electroquímicos y Sistemas de liberación controlada," p. 479, 2016, [Online]. Available: https://eprints.ucm.es/45583/1/T39408.pdf.
[49] J. D. Ospina, "Los aptámeros como novedosa herramienta diagnóstica y terapéutica y su potencial uso en parasitología," *Biomédica*, vol. 40, no. Suppl 1, p. 148, 2020, doi: 10.7705/BIOMEDICA.4765.
[50] S. S. Shankar, R. M. Shereema, V. Ramachandran, T. V. Sruthi, V. B. S. Kumar, and R. B. Rakhi, "Carbon Quantum Dot-Modified Carbon Paste Electrode-Based Sensor for Selective and Sensitive Determination of Adrenaline," *ACS Omega*, vol. 4, no. 4, pp. 7903–7910, Apr. 2019, doi: 10.1021/ACSOMEGA.9B00230.
[51] O. J. Guy and K. A. D. Walker, "Graphene Functionalization for Biosensor Applications," *Silicon Carbide Biotechnol. A Biocompatible Semicond. Adv. Biomed. Devices Appl. Second Ed.*, pp. 85–141, Jan. 2016, doi: 10.1016/B978-0-12-802993-0.00004-6.
[52] R. K. Franklin, S. M. Martin, T. D. Strong, and R. B. Brown, "Chemical and Biological Systems: Chemical Sensing Systems for Liquids," *Ref. Modul. Mater. Sci. Mater. Eng.*, Jan. 2016, doi: 10.1016/B978-0-12-803581-8.00549-X.
[53] B. Rezaei and N. Irannejad, "Electrochemical detection techniques in biosensor applications," *Electrochem. Biosens.*, pp. 11–43, Jan. 2019, doi: 10.1016/B978-0-12-816491-4.00002-4.
[54] Bboujakhrout Abderrahmane, "Nanomateriales hibridos para el diseño de biosensores enzimáticos electroquímicos ," *Tesis Doctoral , Uuniversidad Complutense de Madrid*, 2018. https://eprints.ucm.es/id/eprint/49182/1/T40176.pdf (accessed Sep. 29, 2021).
[55] C. Ji, Y. Zhou, R. M. Leblanc, and Z. Peng, "Recent Developments of Carbon Dots in Biosensing: A Review," *ACS Sensors*, vol. 5, no. 9, pp. 2724–2741, Sep. 2020, doi: 10.1021/ACSSENSORS.0C01556.
[56] I. Bravo Segura, "Interacción de nanoestructuras de carbono o metálicas con (bio)moléculas y su aplicación al desarrollo de sensores," p. 1, 2017, [Online]. Available: https://dialnet.unirioja.es/servlet/tesis?codigo=135986.
[57] A. Chamorro-Garcia and A. Merkoçi, "Nanobiosensors in diagnostics,"

Nanobiomedicine, vol. 3, pp. 1–26, 2016, doi: 10.1177/1849543516663574.
[58] "Dynabeads Magnetic Separation Technology | Thermo Fisher Scientific - CO." https://www.thermofisher.com/co/en/home/brands/product-brand/dynal.html (accessed Nov. 03, 2021).
[59] M. A. Islam and M. Z. Ahsan, "To cite this article: Md. Aminul Islam, Md. Ziaul Ahsan. Plausible Approach for Rapid Detection of SARS-CoV-2 Virus by Magnetic Nanoparticle Based Biosensors," *Am. J. Nanosci.*, vol. 6, no. 2, pp. 6–13, 2020, doi: 10.11648/j.ajn.20200602.11.
[60] M. Li, T. Chen, J. J. Gooding, and J. Liu, "Review of Carbon and Graphene Quantum Dots for Sensing," *ACS Sensors*, vol. 4, no. 7, pp. 1732–1748, Jul. 2019, doi: 10.1021/ACSSENSORS.9B00514.
[61] B. Gayen, S. Palchoudhury, and J. Chowdhury, "Carbon dots: A mystic star in the world of nanoscience," *J. Nanomater.*, vol. 2019, 2019, doi: 10.1155/2019/3451307.
[62] L. Ansari, S. Hallaj, T. Hallaj, and M. Amjadi, "Doped-carbon dots: Recent advances in their biosensing, bioimaging and therapy applications," *Colloids Surfaces B Biointerfaces*, vol. 203, p. 111743, Jul. 2021, doi: 10.1016/J.COLSURFB.2021.111743.
[63] T. K. Henna and K. Pramod, "Graphene quantum dots redefine nanobiomedicine," *Mater. Sci. Eng. C*, vol. 110, p. 110651, May 2020, doi: 10.1016/J.MSEC.2020.110651.
[64] Q. Huang, X. Lin, J. J. Zhu, and Q. X. Tong, "Pd-Au@carbon dots nanocomposite: Facile synthesis and application as an ultrasensitive electrochemical biosensor for determination of colitoxin DNA in human serum," *Biosens. Bioelectron.*, vol. 94, pp. 507–512, Aug. 2017, doi: 10.1016/J.BIOS.2017.03.048.
[65] A. Mathur *et al.*, "An Enzymatic Multiplexed Impedimetric Sensor Based on α-MnO2/GQD Nano-Composite for the Detection of Diabetes and Diabetic Foot Ulcer Using Micro-Fluidic Platform," *Chemosens. 2021, Vol. 9, Page 339*, vol. 9, no. 12, p. 339, Dec. 2021, doi: 10.3390/CHEMOSENSORS9120339.
[66] J. Yang *et al.*, "Simple synthesis of the Au-GQDs@AgPt Yolk-shell nanostructures electrocatalyst for enhancing the methanol oxidation," *J. Alloys Compd.*, vol. 834, p. 155056, Sep. 2020, doi: 10.1016/J.JALLCOM.2020.155056.
[67] C. S. Park, C. Lee, and O. S. Kwon, "Conducting Polymer Based Nanobiosensors," *Polymers (Basel).*, vol. 8, no. 7, Jun. 2016, doi: 10.3390/POLYM8070249.
[68] S. Ramanavicius and A. Ramanavicius, "Conducting Polymers in the Design of Biosensors and Biofuel Cells," *Polym. 2021, Vol. 13, Page 49*, vol. 13, no. 1, p. 49, Dec. 2020, doi: 10.3390/POLYM13010049.
[69] G. Doria *et al.*, "Noble Metal Nanoparticles for Biosensing Applications," *Sensors 2012, Vol. 12, Pages 1657-1687*, vol. 12, no. 2, pp. 1657–1687, Feb. 2012, doi: 10.3390/S120201657.
[70] P. R. Solanki, A. Kaushik, V. V. Agrawal, and B. D. Malhotra, "Nanostructured metal oxide-based biosensors," *NPG Asia Mater. 2011 31*, vol. 3, no. 1, pp. 17–24, Jan. 2011, doi: 10.1038/asiamat.2010.137.
[71] M. Kaliva and M. Vamvakaki, "Nanomaterials characterization," *Polym. Sci. Nanotechnol.*, pp. 401–433, Jan. 2020, doi: 10.1016/B978-0-12-816806-6.00017-0.
[72] P. Senthil Kumar, K. Grace Pavithra, and M. Naushad, "Characterization techniques for nanomaterials," *Nanomater. Sol. Cell Appl.*, pp. 97–124, Jan. 2019, doi: 10.1016/B978-0-12-813337-8.00004-7.

[73] A. Mayeen, L. K. Shaji, A. K. Nair, and N. Kalarikkal, "Morphological Characterization of Nanomaterials," *Charact. Nanomater. Adv. Key Technol.*, pp. 335–364, Jan. 2018, doi: 10.1016/B978-0-08-101973-3.00012-2.
[74] "Dispersión de luz dinámica DLS | Malvern Panalytical." https://www.malvernpanalytical.com/es/products/technology/light-scattering/dynamic-light-scattering (accessed Sep. 12, 2021).
[75] S. Ebnesajjad, "Surface and Material Characterization Techniques," *Handb. Adhes. Surf. Prep.*, pp. 31–48, Jan. 2011, doi: 10.1016/B978-1-4377-4461-3.10004-5.
[76] S. Loganathan, R. B. Valapa, R. K. Mishra, G. Pugazhenthi, and S. Thomas, "Thermogravimetric Analysis for Characterization of Nanomaterials," *Therm. Rheol. Meas. Tech. Nanomater. Charact.*, vol. 3, pp. 67–108, Jan. 2017, doi: 10.1016/B978-0-323-46139-9.00004-9.
[77] A. Barhoum, M. Luisa García-Betancourt, H. Rahier, and G. Van Assche, "Chapter 9 - Physicochemical characterization of nanomaterials: polymorph, composition, wettability, and thermal stability," *Emerg. Appl. Nanoparticles Archit. Nanostructures*, p. 0, 2018, doi: 10.1016/B978-0-323-51254-1.00009-9.
[78] P. H. Salame, V. B. Pawade, and B. A. Bhanvase, "Chapter 3 - Characterization Tools and Techniques for Nanomaterials," 2018, doi: 10.1016/B978-0-12-813731-4.00003-5.
[79] T. Mudalige, H. Qu, D. Van Haute, S. M. Ansar, A. Paredes, and T. Ingle, "Characterization of Nanomaterials: Tools and Challenges," *Nanomater. Food Appl.*, pp. 313–353, Jan. 2019, doi: 10.1016/B978-0-12-814130-4.00011-7.
[80] "Electrophoretic Light Scattering ELS | Measure Electrophoretic Mobility | Malvern Panalytical." https://www.malvernpanalytical.com/en/products/technology/light-scattering/electrophoretic-light-scattering (accessed Feb. 21, 2022).
[81] P. S. Nnamchi and C. S. Obayi, "Electrochemical Characterization of Nanomaterials 4.1 INTRODUCTION TO AND OVERVIEW OF ELECTROCHEMICAL CHARACTERIZATION OF NANOMATERIALS," 2018, doi: 10.1016/B978-0-08-101973-3.00004-3.
[82] G. Seo *et al.*, "Rapid Detection of COVID-19 Causative Virus (SARS-CoV-2) in Human Nasopharyngeal Swab Specimens Using Field-Effect Transistor-Based Biosensor," *ACS Nano*, vol. 14, no. 4, pp. 5135–5142, 2020, doi: 10.1021/acsnano.0c02823.
[83] B. S. Vadlamani, T. Uppal, S. C. Verma, and M. Misra, "Functionalized tio2 nanotube-based electrochemical biosensor for rapid detection of sars-cov-2," *Sensors (Switzerland)*, vol. 20, no. 20. MDPI AG, pp. 1–10, Oct. 02, 2020, doi: 10.3390/s20205871.
[84] L. Fabiani *et al.*, "Magnetic beads combined with carbon black-based screen-printed electrodes for COVID-19: A reliable and miniaturized electrochemical immunosensor for SARS-CoV-2 detection in saliva," *Biosens. Bioelectron.*, vol. 171, p. 112686, Jan. 2021, doi: 10.1016/j.bios.2020.112686.
[85] H. Zhao *et al.*, "Ultrasensitive supersandwich-type electrochemical sensor for SARS-CoV-2 from the infected COVID-19 patients using a smartphone," *Sensors Actuators, B Chem.*, vol. 327, p. 128899, Jan. 2021, doi: 10.1016/j.snb.2020.128899.
[86] R. M. Torrente-Rodríguez, H. Lukas, J. Tu, C. Xu, H. B. Rossiter, and W. Gao, "SARS-CoV-2 RapidPlex: A Graphene-Based Multiplexed Telemedicine Platform for Rapid and Low-Cost COVID-19 Diagnosis and Monitoring," *Matter*, 2020, doi:

10.1016/j.matt.2020.09.027.
[87] A. Idili, C. Parolo, R. Alvarez-Diduk, and A. Merkoçi, “Rapid and Efficient Detection of the SARS-CoV-2 Spike Protein Using an Electrochemical Aptamer-Based Sensor,” *ACS Sensors*, p. acssensors.1c01222, Aug. 2021, doi: 10.1021/ACSSENSORS.1C01222.
[88] A. Ahmadivand, B. Gerislioglu, Z. Ramezani, A. Kaushik, P. Manickam, and S. A. Ghoreishi, “Femtomolar-level detection of SARS-CoV-2 spike proteins using toroidal plasmonic metasensors,” pp. 1–21, 2020, [Online]. Available: http://arxiv.org/abs/2006.08536.
[89] R. Funari, K. Y. Chu, and A. Q. Shen, “Detection of antibodies against SARS-CoV-2 spike protein by gold nanospikes in an opto-microfluidic chip,” *Biosens. Bioelectron.*, vol. 169, p. 112578, Dec. 2020, doi: 10.1016/j.bios.2020.112578.
[90] P. Moitra *et al.*, “Selective Naked-Eye Detection of SARS-CoV-2 Mediated by N Gene Targeted Antisense Oligonucleotide Capped Plasmonic Nanoparticles,” *ACS Nano*, vol. 14, no. 6, pp. 7617–7627, Jun. 2020, doi: 10.1021/acsnano.0c03822.
[91] S. A. Perdomo *et al.*, “SenSARS: A Low-Cost Portable Electrochemical System for Ultra-Sensitive, near Real-Time, Diagnostics of SARS-CoV-2 Infections,” *IEEE Trans. Instrum. Meas.*, vol. 70, 2021, doi: 10.1109/TIM.2021.3119147.
[92] V. J. Vezza *et al.*, “An electrochemical SARS-CoV-2 biosensor inspired by glucose test strip manufacturing processes.,” *Chem. Commun. (Camb).*, Mar. 2021, doi: 10.1039/d1cc00936b.
[93] B. Mojsoska, S. Larsen, D. A. Olsen, J. S. Madsen, I. Brandslund, and F. A. Alatraktchi, “Rapid SARS-CoV-2 Detection Using Electrochemical Immunosensor,” *Sensors*, vol. 21, no. 2, p. 390, Jan. 2021, doi: 10.3390/s21020390.
[94] H. Yousefi *et al.*, “Detection of SARS-CoV-2 Viral Particles Using Direct, Reagent-Free Electrochemical Sensing,” *J. Am. Chem. Soc.*, vol. 143, pp. 1722–1727, Feb. 2021, doi: 10.1021/jacs.0c10810.
[95] J. Zhao *et al.*, “Magnet-assisted electrochemical immunosensor based on surface-clean Pd-Au nanosheets for sensitive detection of SARS-CoV-2 spike protein,” *Electrochim. Acta*, vol. 404, p. 139766, Feb. 2022, doi: 10.1016/J.ELECTACTA.2021.139766.
[96] Z. Rahmati, M. Roushani, H. Hosseini, and H. Choobin, “Electrochemical immunosensor with Cu2O nanocube coating for detection of SARS-CoV-2 spike protein.,” *Mikrochim. Acta*, vol. 188, no. 3, p. 105, Mar. 2021, doi: 10.1007/s00604-021-04762-9.
[97] Y. H. Lin *et al.*, “A Tri-Channel Oxide Transistor Concept for the Rapid Detection of Biomolecules Including the SARS-CoV-2 Spike Protein,” *Adv. Mater.*, vol. 34, no. 3, p. 2104608, Jan. 2022, doi: 10.1002/ADMA.202104608.
[98] A. G. Ayankojo, R. Boroznjak, J. Reut, A. Öpik, and V. Syritski, “Molecularly imprinted polymer based electrochemical sensor for quantitative detection of SARS-CoV-2 spike protein,” *Sensors Actuators B Chem.*, vol. 353, p. 131160, Feb. 2022, doi: 10.1016/J.SNB.2021.131160.
[99] A. Georgas *et al.*, “ACE2-based capacitance sensor for rapid native SARS-CoV-2 detection in biological fluids and its correlation with real-time PCR,” *Biosens. Bioelectron.*, vol. 202, p. 114021, Apr. 2022, doi: 10.1016/J.BIOS.2022.114021.
[100] E. D. Nascimento *et al.*, “COVID-19 diagnosis by SARS-CoV-2 Spike protein detection in saliva using an ultrasensitive magneto-assay based on disposable

electrochemical sensor," *Sensors Actuators B Chem.*, vol. 353, p. 131128, Feb. 2022, doi: 10.1016/J.SNB.2021.131128.
[101] J. C. Soares *et al.*, "Diagnostics of SARS-CoV-2 infection using electrical impedance spectroscopy with an immunosensor to detect the spike protein," *Talanta*, vol. 239, p. 123076, Mar. 2022, doi: 10.1016/J.TALANTA.2021.123076.
[102] A. Roberts, S. Mahari, D. Shahdeo, and S. Gandhi, "Label-free detection of SARS-CoV-2 Spike S1 antigen triggered by electroactive gold nanoparticles on antibody coated fluorine-doped tin oxide (FTO) electrode," *Anal. Chim. Acta*, vol. 1188, p. 339207, Dec. 2021, doi: 10.1016/J.ACA.2021.339207.
[103] N. K. Singh *et al.*, "Hitting the diagnostic sweet spot: Point-of-care SARS-CoV-2 salivary antigen testing with an off-the-shelf glucometer," *Biosens. Bioelectron.*, vol. 180, p. 113111, May 2021, doi: 10.1016/j.bios.2021.113111.
[104] W. Shao, M. R. Shurin, S. E. Wheeler, X. He, and A. Star, "Rapid Detection of SARS-CoV-2 Antigens Using High-Purity Semiconducting Single-Walled Carbon Nanotube-Based Field-Effect Transistors.," *ACS Appl. Mater. Interfaces*, vol. 13, pp. 10321–10327, Feb. 2021, doi: 10.1021/acsami.0c22589.
[105] A. Raziq, A. Kidakova, R. Boroznjak, J. Reut, A. Öpik, and V. Syritski, "Development of a portable MIP-based electrochemical sensor for detection of SARS-CoV-2 antigen," *Biosens. Bioelectron.*, vol. 178, p. 113029, Apr. 2021, doi: 10.1016/j.bios.2021.113029.
[106] H. Qi *et al.*, "Capacitive Aptasensor Coupled with Microfluidic Enrichment for Real-Time Detection of Trace SARS-CoV-2 Nucleocapsid Protein," *Anal. Chem.*, 2021, doi: 10.1021/ACS.ANALCHEM.1C04296/SUPPL_FILE/AC1C04296_SI_001.PDF.
[107] S. A. Hashemi *et al.*, "Ultra-sensitive viral glycoprotein detection NanoSystem toward accurate tracing SARS-CoV-2 in biological/non-biological media," *Biosens. Bioelectron.*, vol. 171, p. 112731, Jan. 2021, doi: 10.1016/j.bios.2020.112731.
[108] H. A. Hussein, A. Kandeil, M. Gomaa, R. Mohamed El Nashar, I. M. El-Sherbiny, and R. Y. A. Hassan, "SARS-CoV-2-Impedimetric Biosensor: Virus-Imprinted Chips for Early and Rapid Diagnosis," *ACS Sensors*, vol. 6, no. 11, pp. 4098–4107, Nov. 2021, doi: 10.1021/ACSSENSORS.1C01614/SUPPL_FILE/SE1C01614_SI_001.PDF.
[109] M. Alafeef, K. Dighe, P. Moitra, and D. Pan, "Rapid, Ultrasensitive, and Quantitative Detection of SARS-CoV-2 Using Antisense Oligonucleotides Directed Electrochemical Biosensor Chip," *ACS Nano*, vol. 14, no. 12, pp. 17028–17045, Dec. 2020, doi: 10.1021/acsnano.0c06392.
[110] L. Farzin, S. Sadjadi, A. Sheini, and E. Mohagheghpour, "A nanoscale genosensor for early detection of COVID-19 by voltammetric determination of RNA-dependent RNA polymerase (RdRP) sequence of SARS-CoV-2 virus.," *Mikrochim. Acta*, vol. 188, no. 4, p. 121, Mar. 2021, doi: 10.1007/s00604-021-04773-6.
[111] R. L. Pinals *et al.*, "Rapid SARS-CoV-2 Spike Protein Detection by Carbon Nanotube-Based Near-Infrared Nanosensors," *Nano Lett.*, vol. 21, no. 5, pp. 2272–2280, Mar. 2021, doi: 10.1021/acs.nanolett.1c00118.
[112] B. Della Ventura *et al.*, "Colorimetric test for fast detection of SARS-COV-2 in nasal and throat swabs," *ACS Sensors*, vol. 5, no. 10, pp. 3043–3048, Oct. 2020, doi: 10.1021/acssensors.0c01742.
[113] G. Qiu, Z. Gai, Y. Tao, J. Schmitt, G. A. Kullak-Ublick, and J. Wang, "Dual-Functional Plasmonic Photothermal Biosensors for Highly Accurate Severe Acute

Respiratory Syndrome Coronavirus 2 Detection," *ACS Nano*, vol. 14, no. 5, pp. 5268–5277, 2020, doi: 10.1021/acsnano.0c02439.
[114] Y. Gao *et al.*, "Rapid and sensitive triple-mode detection of causative SARS-CoV-2 virus specific genes through interaction between genes and nanoparticles," *Anal. Chim. Acta*, vol. 1154, p. 338330, Apr. 2021, doi: 10.1016/j.aca.2021.338330.
[115] H. Liu *et al.*, "Development of a SERS-based lateral flow immunoassay for rapid and ultra-sensitive detection of anti-SARS-CoV-2 IgM/IgG in clinical samples," *Sensors Actuators, B Chem.*, vol. 329, p. 129196, Feb. 2021, doi: 10.1016/j.snb.2020.129196.
[116] L. F. Huergo *et al.*, "Magnetic Bead-Based Immunoassay Allows Rapid, Inexpensive, and Quantitative Detection of Human SARS-CoV-2 Antibodies," *ACS Sensors*, Jan. 2021, doi: 10.1021/acssensors.0c02544.
[117] Q. Lin *et al.*, "Microfluidic Immunoassays for Sensitive and Simultaneous Detection of IgG/IgM/Antigen of SARS-CoV-2 within 15 min," *Anal. Chem.*, vol. 92, no. 14, pp. 9454–9458, Jul. 2020, doi: 10.1021/acs.analchem.0c01635.
[118] D. Liu *et al.*, "Nanozyme chemiluminescence paper test for rapid and sensitive detection of SARS-CoV-2 antigen," *Biosens. Bioelectron.*, vol. 173, p. 112817, Feb. 2021, doi: 10.1016/j.bios.2020.112817.
[119] A. Yakoh, U. Pimpitak, S. Rengpipat, N. Hirankarn, O. Chailapakul, and S. Chaiyo, "Paper-based electrochemical biosensor for diagnosing COVID-19: Detection of SARS-CoV-2 antibodies and antigen," *Biosens. Bioelectron.*, vol. 176, p. 112912, Mar. 2021, doi: 10.1016/j.bios.2020.112912.
[120] C. Adrover-Jaume *et al.*, "Paper biosensors for detecting elevated IL-6 levels in blood and respiratory samples from COVID-19 patients," *Sensors Actuators, B Chem.*, vol. 330, p. 129333, Mar. 2021, doi: 10.1016/j.snb.2020.129333.
[121] R. Yan, Y. Zhang, Y. Li, L. Xia, Y. Guo, and Q. Zhou, "Structural basis for the recognition of SARS-CoV-2 by full-length human ACE2," *Science*, vol. 367, no. 6485, p. 1444, Mar. 2020, doi: 10.1126/SCIENCE.ABB2762.
[122] J. Yang *et al.*, "Molecular interaction and inhibition of SARS-CoV-2 binding to the ACE2 receptor," pp. 1–21, 2020, doi: 10.21203/rs.3.rs-30468/v1.
[123] S. Patel, R. Nanda, S. Sahoo, and E. Mohapatra, "Biosensors in health care: The milestones achieved in their development towards lab-on-chip-analysis," *Biochem. Res. Int.*, vol. 2016, 2016, doi: 10.1155/2016/3130469.
[124] G. Vásquez, A. Rey, C. Rivera, C. Iregui, and J. Orozco, "Amperometric biosensor based on a single antibody of dual function for rapid detection of Streptococcus agalactiae," *Biosens. Bioelectron.*, vol. 87, pp. 453–458, Jan. 2017, doi: 10.1016/J.BIOS.2016.08.082.
[125] D. Echeverri, M. Garg, D. Varón Silva, and J. Orozco, "Phosphoglycan-sensitized platform for specific detection of anti-glycan IgG and IgM antibodies in serum," *Talanta*, vol. 217, Sep. 2020, doi: 10.1016/j.talanta.2020.121117.
[126] S. Kumar *et al.*, "Electrochemical paper based cancer biosensor using iron oxide nanoparticles decorated PEDOT:PSS," *Anal. Chim. Acta*, vol. 1056, pp. 135–145, May 2019, doi: 10.1016/J.ACA.2018.12.053.
[127] S. Campuzano, M. Pedrero, and J. M. Pingarrón, "Non-Invasive Breast Cancer Diagnosis through Electrochemical Biosensing at Different Molecular Levels," *Sensors 2017, Vol. 17, Page 1993*, vol. 17, no. 9, p. 1993, Aug. 2017, doi: 10.3390/S17091993.
[128] F. Ghorbani, H. Abbaszadeh, A. Mehdizadeh, M. Ebrahimi-Warkiani, M. R. Rashidi,

and M. Yousefi, “Biosensors and nanobiosensors for rapid detection of autoimmune diseases: a review,” *Microchimica Acta*, vol. 186, no. 12. Springer, pp. 1–11, Dec. 01, 2019, doi: 10.1007/s00604-019-3844-4.

[129] S. Cajigas, D. Alzate, and J. Orozco, “Gold nanoparticle/DNA-based nanobioconjugate for electrochemical detection of Zika virus,” *Microchim. Acta 2020 18711*, vol. 187, no. 11, pp. 1–10, Oct. 2020, doi: 10.1007/S00604-020-04568-1.

[130] D. Alzate, S. Cajigas, S. Robledo, C. Muskus, and J. Orozco, “Genosensors for differential detection of Zika virus,” *Talanta*, vol. 210, p. 120648, Apr. 2020, doi: 10.1016/j.talanta.2019.120648.

[131] G. Seo *et al.*, “Rapid Detection of COVID-19 Causative Virus (SARS-CoV-2) in Human Nasopharyngeal Swab Specimens Using Field-Effect Transistor-Based Biosensor,” *ACS Nano*, vol. 14, no. 4, pp. 5135–5142, Apr. 2020, doi: 10.1021/acsnano.0c02823.

[132] J. Muñoz and M. Pumera, “3D-Printed COVID-19 immunosensors with electronic readout,” *Chem. Eng. J.*, vol. 425, p. 131433, Dec. 2021, doi: 10.1016/J.CEJ.2021.131433.

[133] E. Karakuş, E. Erdemir, N. Demirbilek, and L. Liv, “Colorimetric and electrochemical detection of SARS-CoV-2 spike antigen with a gold nanoparticle-based biosensor,” *Anal. Chim. Acta*, vol. 1182, p. 338939, Oct. 2021, doi: 10.1016/J.ACA.2021.338939.

[134] M. A. Ehsan, S. A. Khan, and A. Rehman, “Screen-Printed Graphene/Carbon Electrodes on Paper Substrates as Impedance Sensors for Detection of Coronavirus in Nasopharyngeal Fluid Samples,” *Diagnostics 2021, Vol. 11, Page 1030*, vol. 11, no. 6, p. 1030, Jun. 2021, doi: 10.3390/DIAGNOSTICS11061030.

[135] A. Idili, C. Parolo, R. Alvarez-Diduk, and A. Merkoçi, “Rapid and Efficient Detection of the SARS-CoV-2 Spike Protein Using an Electrochemical Aptamer-Based Sensor,” *ACS Sensors*, vol. 6, no. 8, pp. 3093–3101, Aug. 2021, doi: 10.1021/ACSSENSORS.1C01222.

[136] L. Fabiani *et al.*, “Magnetic beads combined with carbon black-based screen-printed electrodes for COVID-19: A reliable and miniaturized electrochemical immunosensor for SARS-CoV-2 detection in saliva,” *Biosens. Bioelectron.*, vol. 171, p. 112686, Jan. 2021, doi: 10.1016/j.bios.2020.112686.

[137] Y. Peng *et al.*, “An electrochemical biosensor for sensitive analysis of the SARS-CoV-2 RNA,” *Biosens. Bioelectron.*, vol. 186, p. 113309, Aug. 2021, doi: 10.1016/J.BIOS.2021.113309.

[138] V. Kumari, S. Rastogi, and V. Sharma, “Emerging Trends in Nanobiosensor,” Springer, Cham, 2019, pp. 419–447.

[139] J. K. Millet *et al.*, “Production of pseudotyped particles to study highly pathogenic coronaviruses in a biosafety level 2 setting,” *J. Vis. Exp.*, vol. 2019, no. 145, Mar. 2019, doi: 10.3791/59010.

[140] V. Corman *et al.*, “Users looking for a workflow protocol consult the last three pages of this document,” 2020, Accessed: Sep. 25, 2021. [Online]. Available: https://virologie-ccm.charite.de/en/.

[141] “Molecular dynamic simulations reveal detailed spike-ACE2 interactions.” https://www.news-medical.net/news/20200923/Molecular-dynamic-simulations-reveal-detailed-spike-ACE2-interactions.aspx (accessed Aug. 31, 2022).

[142] S. Szunerits *et al.*, “The role of the surface ligand on the performance of electrochemical SARS-CoV-2 antigen biosensors,” *Anal. Bioanal. Chem. 2021*, pp.

1–11, Feb. 2021, doi: 10.1007/S00216-020-03137-Y.
[143] M. Hussain *et al.*, "Structural variations in human ACE2 may influence its binding with SARS-CoV-2 spike protein," *J. Med. Virol.*, vol. 92, no. 9, pp. 1580–1586, Sep. 2020, doi: 10.1002/JMV.25832.
[144] A. Basu, A. Sarkar, and U. Maulik, "Molecular docking study of potential phytochemicals and their effects on the complex of SARS-CoV2 spike protein and human ACE2," *Sci. Reports 2020 101*, vol. 10, no. 1, pp. 1–15, Oct. 2020, doi: 10.1038/s41598-020-74715-4.
[145] S. Biological, "Anti-Coronavirus spike Antibody, 40591-T62 | Sino Biological," 2021. https://www.sinobiological.com/antibodies/cov-spike-40591-t62 (accessed Sep. 01, 2021).
[146] H. F. Stills, "Polyclonal Antibody Production," *Lab. Rabbit. Guinea Pig, Hamster, Other Rodents*, pp. 259–274, Jan. 2012, doi: 10.1016/B978-0-12-380920-9.00011-0.
[147] A. H. Haghighi, M. T. Khorasani, Z. Faghih, and F. Farjadian, "Effects of different quantities of antibody conjugated with magnetic nanoparticles on cell separation efficiency," *Heliyon*, vol. 6, no. 4, p. e03677, Apr. 2020, doi: 10.1016/J.HELIYON.2020.E03677.
[148] "BioRender." https://biorender.com/ (accessed Nov. 12, 2021).
[149] Thermo Fisher Scientific, "Dynabeads™ MyOne™ Carboxylic Acid," 2021. https://www.thermofisher.com/order/catalog/product/65012#/65012 (accessed Sep. 01, 2021).
[150] Thermo Fisher Scientific, "Surface-activated Dynabeads," 2021. https://www.thermofisher.com/document-connect/document-connect.html?url=https%3A%2F%2Fassets.thermofisher.com%2FTFS-Assets%2FLSG%2Fbrochures%2FSurface_Activated_Dynabeads.PDF (accessed Sep. 05, 2021).
[151] D. Sehgal and I. K. Vijay, "A Method for the High Efficiency of Water-Soluble Carbodiimide-Mediated Amidation," *Anal. Biochem.*, vol. 218, no. 1, pp. 87–91, Apr. 1994, doi: 10.1006/ABIO.1994.1144.
[152] I. Ojeda, M. Moreno-Guzmán, A. González-Cortés, P. Yáñez-Sedeño, and J. M. Pingarrón, "Electrochemical magnetoimmunosensor for the ultrasensitive determination of interleukin-6 in saliva and urine using poly-HRP streptavidin conjugates as labels for signal amplification," *Anal. Bioanal. Chem. 2014 40625*, vol. 406, no. 25, pp. 6363–6371, Aug. 2014, doi: 10.1007/S00216-014-8055-6.
[153] Y. Pan, D. Zhang, P. Yang, L. L. M. Poon, and Q. Wang, "Viral load of SARS-CoV-2 in clinical samples," *The Lancet Infectious Diseases*, 2020. https://alatorax.org/es/biblioteca/viral-load-of-sars-cov-2-in-clinical-samples (accessed Sep. 03, 2021).
[154] Y. M. Bar-On, A. Flamholz, R. Phillips, and R. Milo, "Sars-cov-2 (Covid-19) by the numbers," *Elife*, vol. 9, Mar. 2020, doi: 10.7554/ELIFE.57309.
[155] L. Liv, G. Çoban, N. Nakiboğlu, and T. Kocagöz, "A rapid, ultrasensitive voltammetric biosensor for determining SARS-CoV-2 spike protein in real samples," *Biosens. Bioelectron.*, vol. 192, p. 113497, Nov. 2021, doi: 10.1016/J.BIOS.2021.113497.
[156] Y. Huang, C. Yang, X. Xu, W. Xu, and S. Liu, "Structural and functional properties of SARS-CoV-2 spike protein: potential antivirus drug development for COVID-19," *Acta Pharmacol. Sin. 2020 419*, vol. 41, no. 9, pp. 1141–1149, Aug. 2020, doi:

10.1038/s41401-020-0485-4.
[157] J. Millet and G. Whittaker, “Murine Leukemia Virus (MLV)-based Coronavirus Spike-pseudotyped Particle Production and Infection,” *Bio-Protocol*, vol. 6, no. 23, 2016, doi: 10.21769/bioprotoc.2035.
[158] E. I. Patterson *et al.*, “Methods of inactivation of SARS-CoV-2 for downstream biological assays,” *bioRxiv*, May 2020, doi: 10.1101/2020.05.21.108035.
[159] J. Hadi, M. Dunowska, S. Wu, and G. Brightwell, “Control Measures for SARS-CoV-2: A Review on Light-Based Inactivation of Single-Stranded RNA Viruses,” *Pathog. 2020, Vol. 9, Page 737*, vol. 9, no. 9, p. 737, Sep. 2020, doi: 10.3390/PATHOGENS9090737.
[160] R. Arnaout *et al.*, “SARS-CoV2 Testing: The Limit of Detection Matters,” *bioRxiv*, pp. 617–667, Jun. 2020, doi: 10.1101/2020.06.02.131144.
[161] H. H. Mostafa, J. Hardick, E. Morehead, J. A. Miller, C. A. Gaydos, and Y. C. Manabe, “Comparison of the analytical sensitivity of seven commonly used commercial SARS-CoV-2 automated molecular assays,” *J. Clin. Virol.*, vol. 130, p. 104578, Sep. 2020, doi: 10.1016/J.JCV.2020.104578.
[162] G. V. Shrivastava A, “Methods for the determination of limit of detection and limit of quantitation of the analytical methods,” *Chronicles Young Sci.*, vol. 2, no. 1, pp. 21–25, 2011, Accessed: Jan. 17, 2022. [Online]. Available: https://ddtjournal.net/view-pdf/?article=973f8e026105878f115d4567452c5ccftMZFNQ==.

ANNEX 1

SUPPLEMENTARY INFORMATION CHAPTER III

The LOD was estimated from the equation:

$$LOD = \frac{3*SD}{b} \qquad \textit{Equation 1}$$

Where SD is the standard deviation of the blank and b is the slope of the concentration vs. signal response curve [162].

For example, from Figure 5A, 0.038 is the standard deviation of the blank, and the slope is estimated from the current vs. concentration graph (1.13 µA*mL/µg), with which the respective calculation yields a LOD of 100.15 ng/mL. Other LODs were calculated similarly but are not shown.

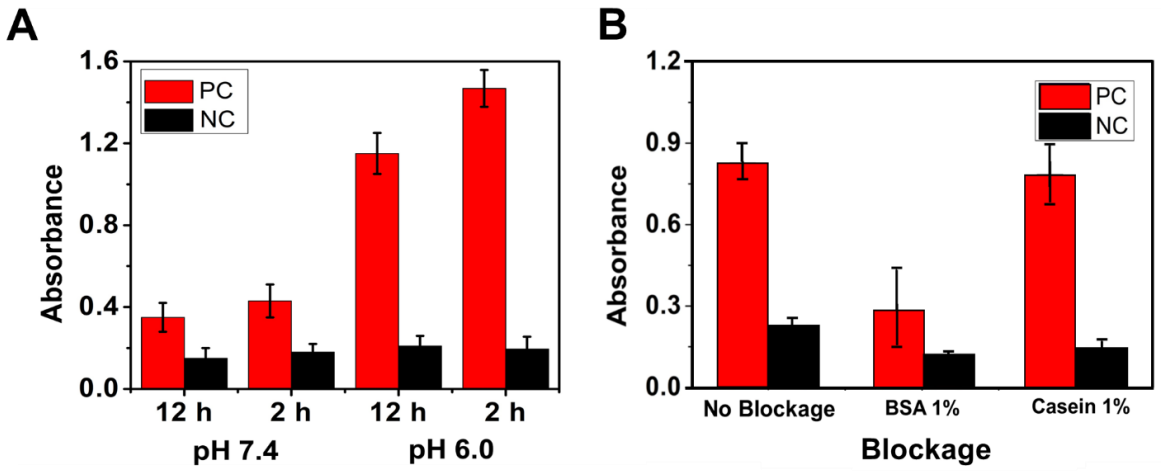

Figure S 1. Evaluation of the effect of A) pH and incubation time and B) different blocking agents in the signal response when conjugating anti-spike antibody on carboxylated magnetic beads and amplifying with streptavidin-HRP. (PC, Positive control and NC, Negative control)

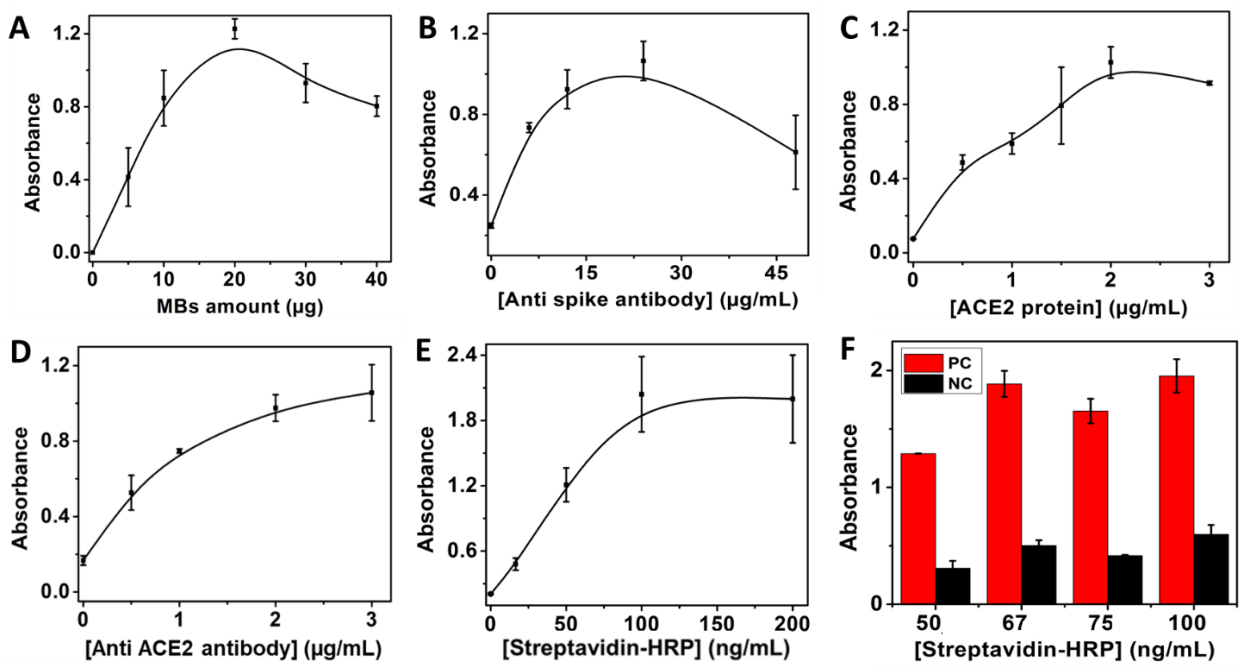

Figure S 2. Rapid screening of the variables involved in the immunosensor format by spectrophotometry. Optimization of A) carboxylated magnetic beads, B) anti-spike antibody, C) ACE-2 protein, D) anti-ACE-2 biotin antibody and E) streptavidin-HRP concentrations, respectively. F) Signal-to-noise ratio at different concentrations of streptavidin-HRP.

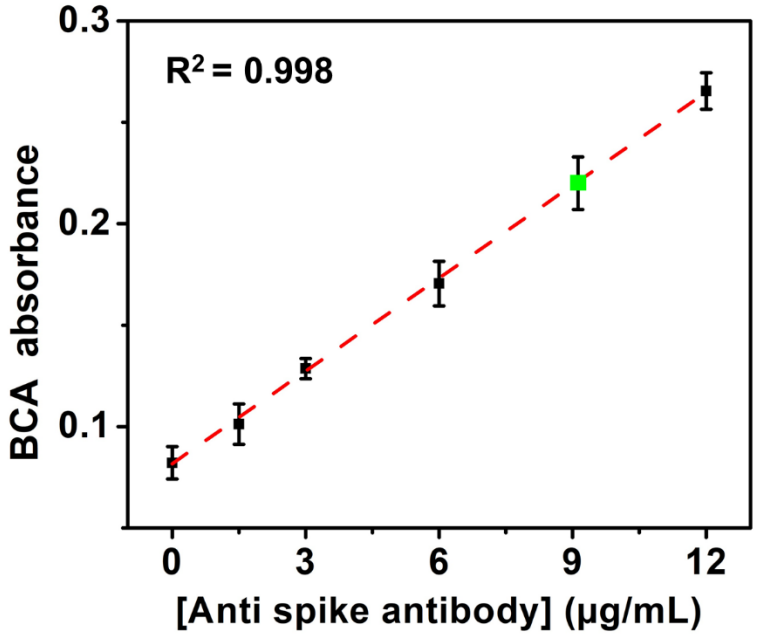

Figure S 3. Calibration curve of anti-spike antibody quantification using bicinchoninic acid and quantification of the supernatant after covalent antibody conjugation to magnetic beads (green dot).

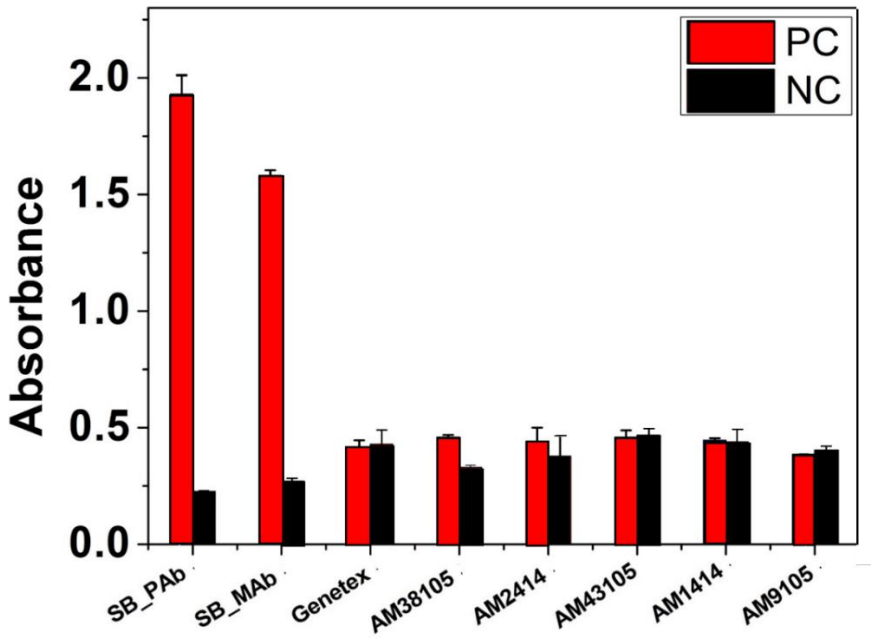

Figure S 4. Evaluation of different references of anti-spike antibody for the immunosensor assembly with the same commercial Spike protein. SB_PAb and SB_MAb are polyclonal and monoclonal antibodies from Sino Biological, respectively; the references AM038105, AM002414, AM043105, AM001414, AM009105 are anti Spike antibodies from Active Motif. (PC, Positive control and NC, Negative control).

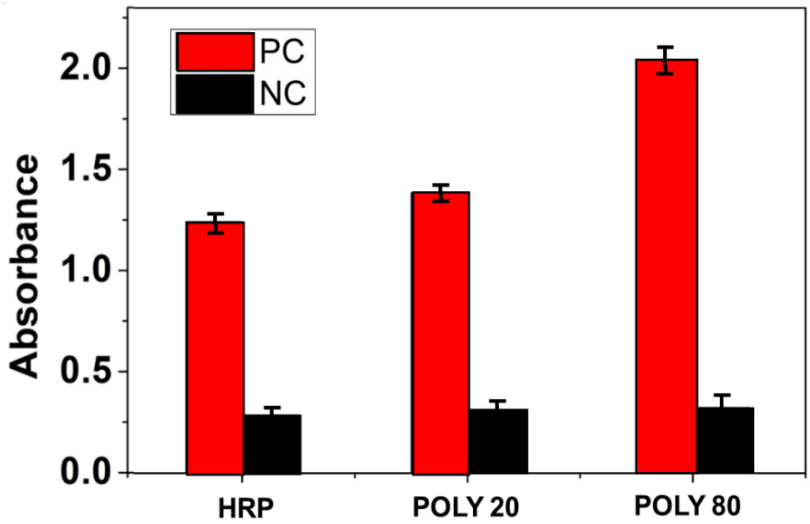

Figure S 5. Effect of three different enzyme complexes, i.e. streptavidin-HRP, streptavidin (poly) HRP-20 and streptavidin (poly) HRP-80, on the immunosensor signal response. (PC, Positive control and NC, Negative control).

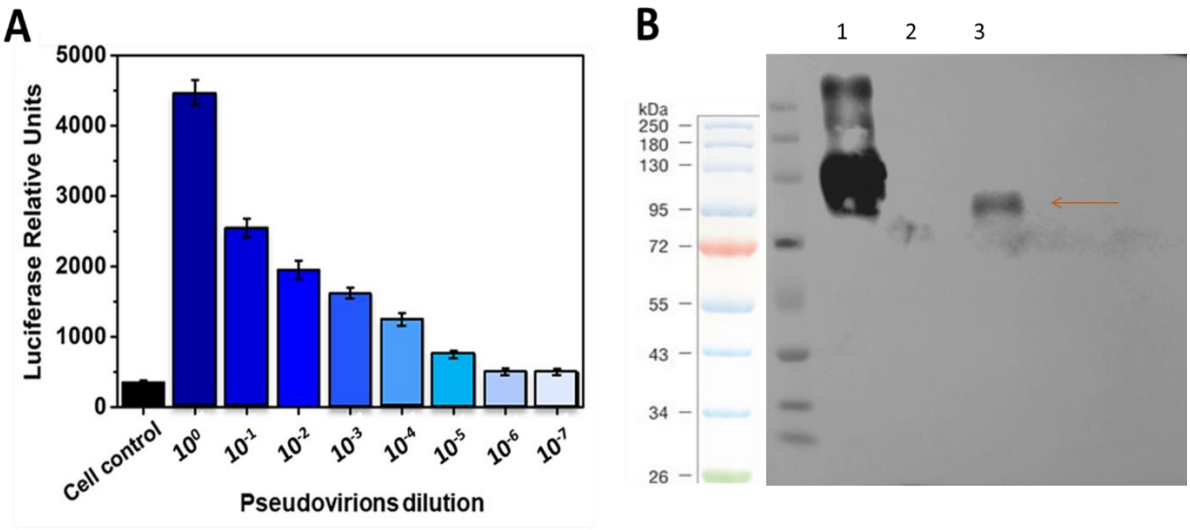

Figure S 6. A) Quantification of luciferase expression by transduction of pseudovirions expressing the SARS-CoV-2 Spike protein in Vero-E6 cells. Results of 10-fold serial dilutions of the stock (1/10 to 1/10^7). B) Detection of SARS-CoV-2 Spike protein in cotransfected HEK-293 cells. HEK-293 cells were co-transfected with 3 plasmids: SARS-CoV-2 S plasmid, MLV-gag-pol plasmid and Luciferase plasmid using linear Polyethylenimine. Cells were lysed 72 hours post-transfection and the lysates were fractionated by SDS-PAGE and analyzed using an antibody against Spike protein of SARS-CoV-2 (GTX135356) and a secondary Ab anti-Rabbit. MW Color Prestained Protein Standard Broad Range (10-250 Kda, 1) 500 ng commercial spike protein, 2) 60 µg HEK-293 control cells, 3) 60 µg transfected HEK-293 cells.

Table S 1. Quantifying copy number of the plasmid Firefly luciferase gene/MLV Y RNA / 5′/3′ MLV LTR by RT-PCR.

Pseudovirions	***C.T***	***Copies/µL***	***Pseudovirions/µL***
SARS-CoV-2	22.66	288631.78	144315.84
SARS-CoV-2 after ultra-centrifugation	19.80	1063462.99	531731.49
SARS-CoV	21.35	523929.16	261964.58
MERS-CoV	22.34	332799.47	166399.73

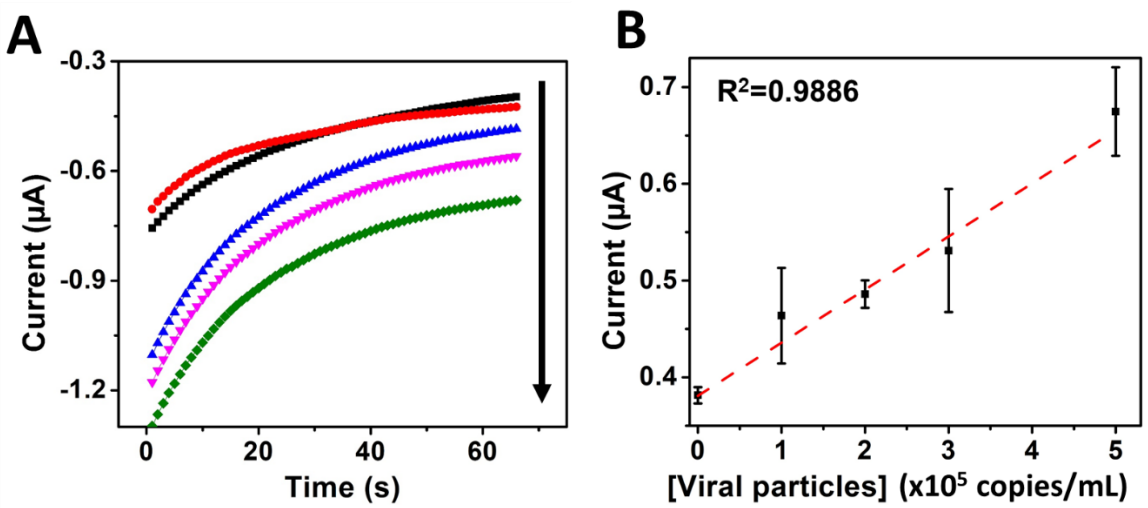

Figure S 7. A) Electrochemical response with increasing concentrations of 0, 1, 2, 3 and 5 x 10^5 copies/mL viral particles inactivated by UV-light for 30 minutes, lysed in RIPA buffer and amplified with streptavidin-HRP (poly) 80 and B) corresponding calibration curve

Table S 2. C.T of patient samples measured by RT-PCR and the spike protein concentration estimation from the calibration curve in Figure 2 with the immunosensor.

C.T level	***Sample***	***C.T***	***Estimation [Spike protein] (µg/mL)***
Zero	N1	>35	-
	N2	>35	-
	N3	>35	-
High	H1	33.07	1.11± 0.03
	H2	32.06	1.34 ± 0.05
	H3	31.97	0.52 ± 0.02
Medium	M1	27.80	1.49 ± 0.04
	M2	22.26	1.23 ± 0.03
	M3	20.01	1.93 ± 0.04
Low	L1	17.31	2.53 ± 0.03
	L2	15.10	2.67 ± 0.02
	L3	15.01	4.61 ± 0.21
	L4	11.20	3.46 ± 0.06

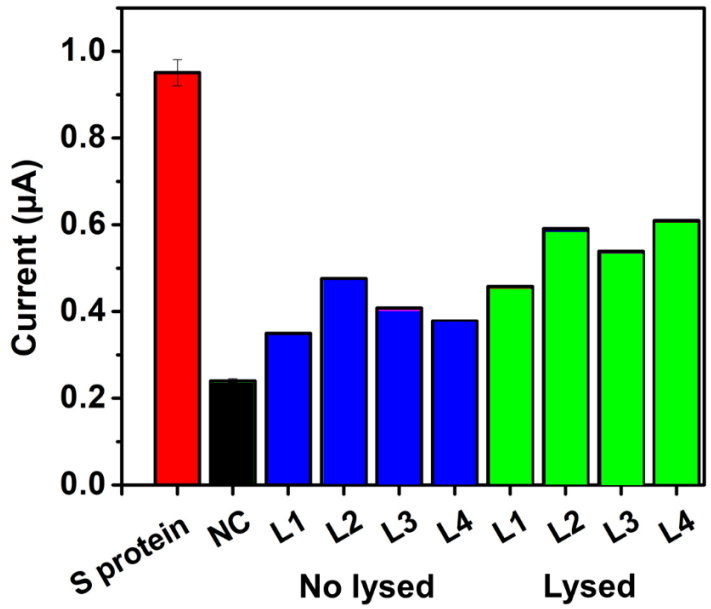

Figure S 8. Immunosensor response in raw and lysed samples from infected patients (positive by RT-PCR) compared to 1 µg/mL commercial Spike protein and a negative control without target protein.

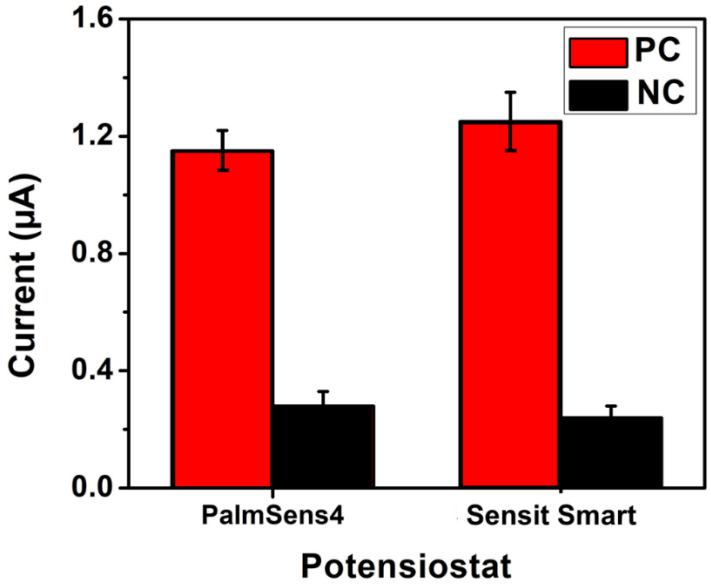

Figure S 9. Comparison of the electrochemical signal of the immunosensor using the PalmSens4 and Sensit smart potentiostat. (PC, Positive control and NC, Negative control).

ANNEX 2

RAPID SCREENING OF IMMUNOSENSOR COMPONENTS BY ELISA

A total of 100 µL of a 24 µg/mL protein A solution in PBS was transferred into each well of the 96-well plate and incubated overnight at 4°C, covering the plate with aluminum foil. Subsequently, the wells were washed with 200 µL PBST thrice, turning the plate over a clean towel or napkin, with several touches on the base of the plate for better washing. First, 100 µL of 3% casein in PBST was incubated for 1 h at 37°C under constant agitation to block the uncoated plate surface, followed by washing with PBST thrice. Then, 100 µL of 12 µg/mL anti-spike in PBS was incubated for 1 h at 37°C, followed by washing with PBST thrice. Subsequent, 100 µL of the cocktail of 0.1 - 2 µg/mL spike protein and 2 µg/mL ACE2 protein in PBS was incubated for 1 h at 37°C under agitation, followed by washing with PBST thrice. Next, 100 µL of 2 µg/mL anti-ACE2 in PBS was incubated for 1 h at 37°C under constant agitation, followed by washing with PBST thrice. Next, 100 µL of 50 ng/mL streptavidin-HRP in PBST was incubated for 30 min at 37°C under constant agitation, followed by five washing steps in PBST. Finally, 100 µL of a commercial TMB solution was incubated for twenty min at room temperature under stirring, and absorbance was measured at 650 nm.

Figure 10 shows the first design proposed to develop the immunosensor. First, protein A-coated magnetic particles were functionalized with the primary anti-spike antibody to bind to the preincubated spike-ACE2 protein complex. Next, the resultant immunocomplex was conjugated with an anti-ACE-2 secondary biotinylated antibody to form a sandwich-like structure, which was finally labeled by a streptavidin-HRP enzyme complex. In the presence of H_2O_2, the TMB substrate interacts with the enzyme producing a color change from transparent to blue detectable by spectrophotometry at 650 nm. Alternatively, a change in current over time is detectable by chronoamperometry when assembled the immunosensor. Both signals by spectrophotometry and chronoamperometry correlate directly with changes in the concentration of the spike protein analyzed.

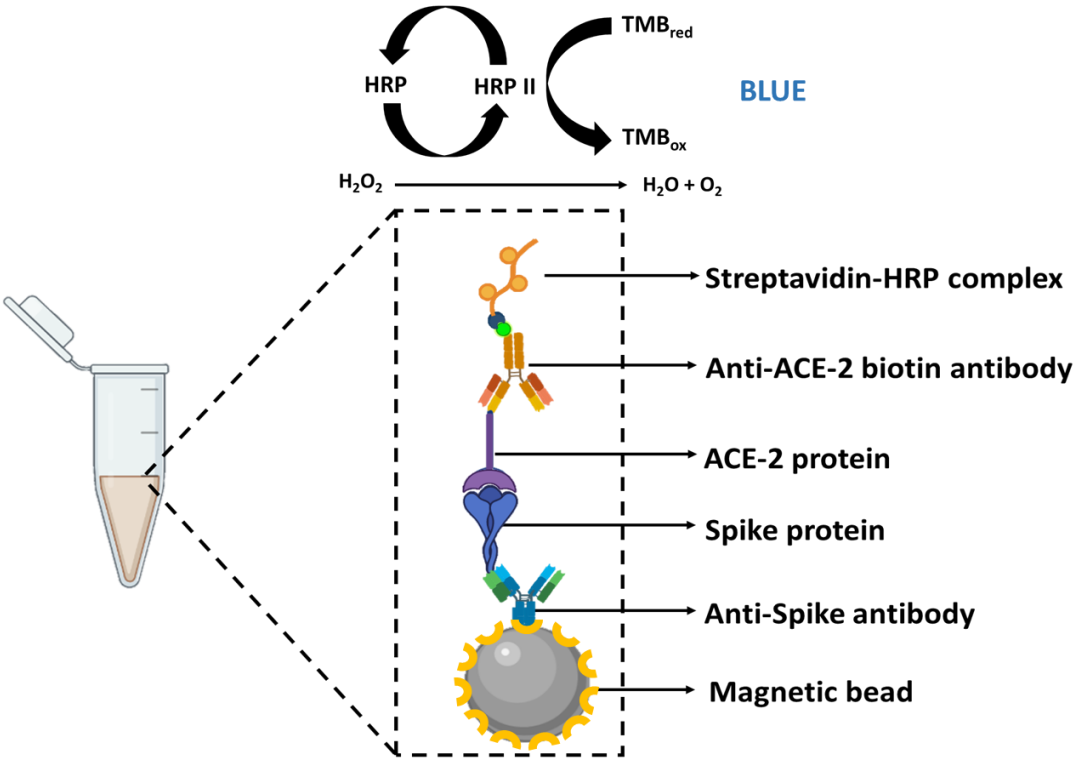

Figure 10. Immunosensor design based on protein A-coated MBs. The anti-spike capture antibody is immobilized at the MBs surface to interact with the Spike-ACE2 complex sandwiched with a biotinylated anti-ACE2 antibody and further linked to the streptavidin- HRP tag to react with the TMB substrate in the presence of H_2O_2 to produce a target-dependent signal.

The immunosensor was tested by incubating different concentrations of its components selected initially in the immunosensor design on the 96-well plates to rapidly evaluate their interaction by ELISA, as shown in Figure 11. A high interaction was evidenced at different concentrations of anti-ACE 2 antibody, ACE 2 protein, and spike protein (see Figure 11 A-C). Although an anti-spike antibody from Genetex did not interact with the Spike protein from Sino Biological, a high absorbance signal was obtained when changing this primary antibody for one from Sino Biological, selected for further experiments (see Figure 11 D). In addition, a high background was observed when anchoring the anti-spike antibody through the protein A due to interaction with other components of the immunosensor (see Figure 11 E), so another strategy based on covalent linking through carboxylic acids was assessed, as explained in the main text.

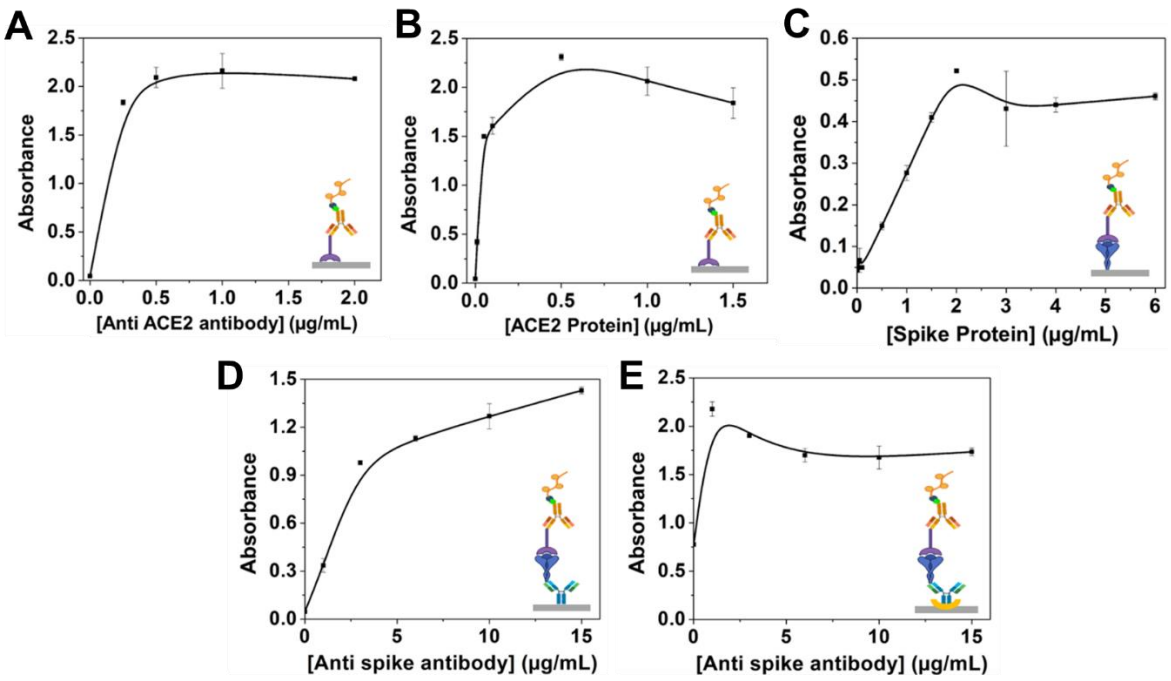

Figure 11. Evaluation of the interaction of the immunosensor components at different concentrations of A) anti-ACE 2 antibody, B) ACE 2 protein, C) spike protein, D) anti-spike antibody from Sino Biological and E) anti-spike in the presence of protein A by spectrophotometry at 650 nm.

It was observed that the Sino Biological anti-spike antibody seems to have lost the capacity to interact with the protein analyte after one month of storage at -20°C. Therefore, electrophoresis measurements of the antibody and the spike protein were performed to check their conformational stability (see Figure 12). While the formation of a band of spike protein at 180 kDa (line 1) and RBD protein at 35 kDa (line 3) is evident, the band for the stored anti-spike antibody (line 2) is absent compared to the one from a fresh solution of anti-spike antibody at 55 KDa (line 4). These results indicate a loss of the conformational structure of the antibody and confirm its poor stability.

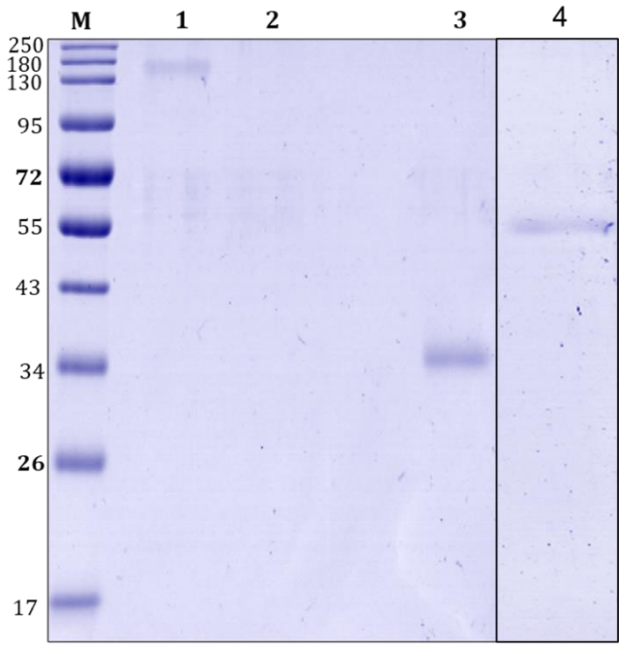

Figure 12. Evaluation of the 1) spike protein 2) anti-spike antibody after one month of storage at -20°C, 3) RBD protein and 4) fresh anti-spike in 12% SDS-PAGE electrophoresis with Chromassie R-250 staining.

ANNEX 3

SELECTIVITY, STABILITY AND REPRODUCIBILITY OF THE IMMUNOSENSOR

The stability of the immunosensor was evaluated by testing the ability of MBs conjugated with the antibody stored at 4°C to detect the spike protein by completing the immunosensor assembly at 3, 7, 15, 20, and 30 days of storage. Figure 13A shows a control chart that interrogates when the current intensity is less than that minus three-fold the standard deviation of the first day, i.e., approximately 70% of the signal is lost at 30 days of storage (see Figure 13A). Then, the reproducibility of the immunosensor was established by comparing the signal of five individual devices, showing signal differences lower than 10% (see Figure 13B).

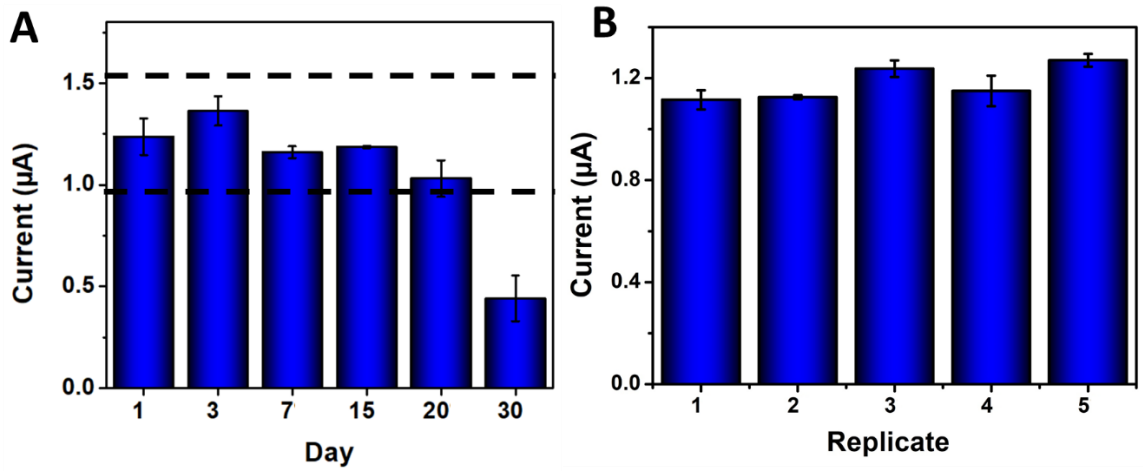

Figure 13. Evaluation of A) the stability of the immunosensor stored at 4°C and B) reproducibility of five individually assembled immunosensors.

Selectivity was tested by comparing the signal from a solution containing only SARS-CoV-2 concerning a cocktail with 1 x 10^5 copies/mL of SARS-CoV-2, SARS-CoV-1, and MERS-CoV pseudovirions. The initial signal from SARS-CoV-2 alone significantly decreased when interrogating it in the mix (see Figure 14). The cocktail was previously incubated with the ACE2 protein before being conjugated to the magnetic particles. Therefore, other

coronaviruses having high interaction with the ACE2 protein may be competing for linking the ACE2 protein leaving less concentration available to interact with the SARS-CoV-2 target pseudovirions. As a consequence, the resultant signal response was lower. Yet, the probability of finding several coronaviruses in the same patient is low.

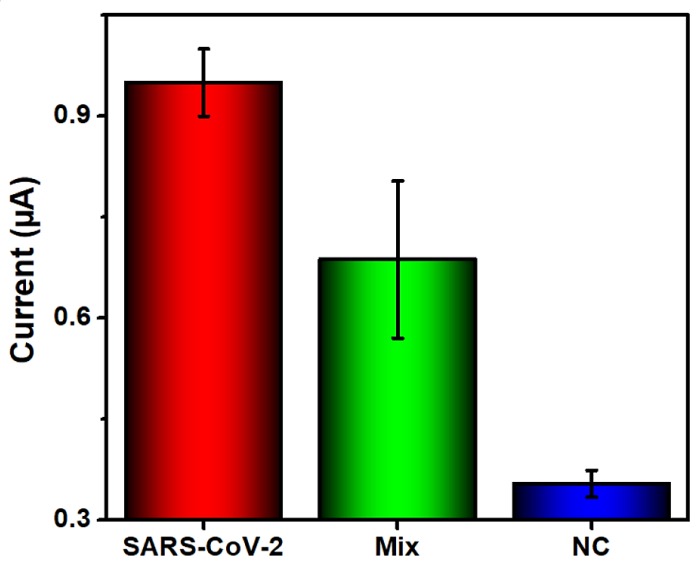

Figure 14. Immunosensor selectivity when detecting a cocktail of 1x10^5 copies/mL MERS, SARS-CoV-1, SARS-CoV-2 pseudovirions supernatants.

ANNEX 4

SARS-COV-2 BIOSENSOR BASED ON GQDs@AuPt-ANTIBODY HYBRID INTERFACE

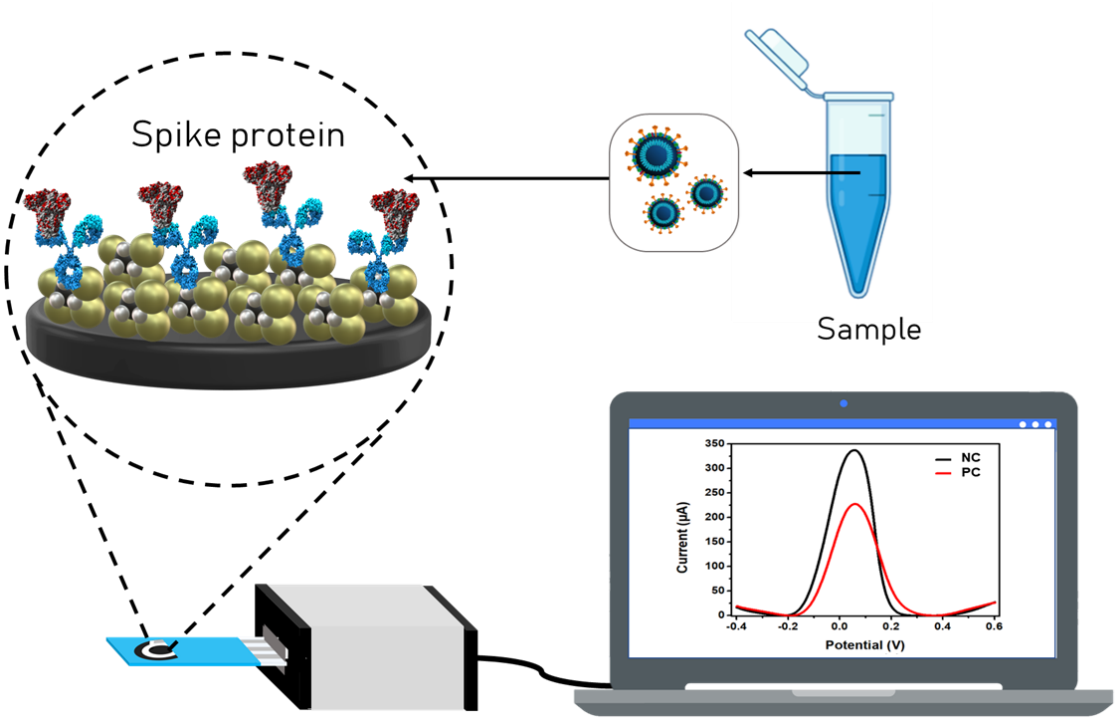

Figure 15. Graphical abstract Biosensor based on GQDs@AuPt

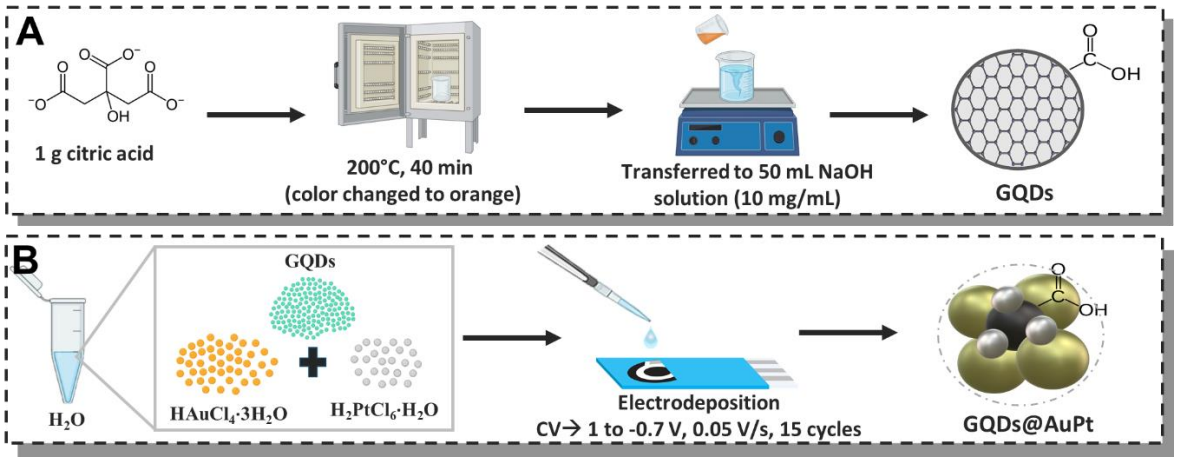

Figure 16. Methodology for the synthesis of A) GQDs and B) GQDs@AuPt

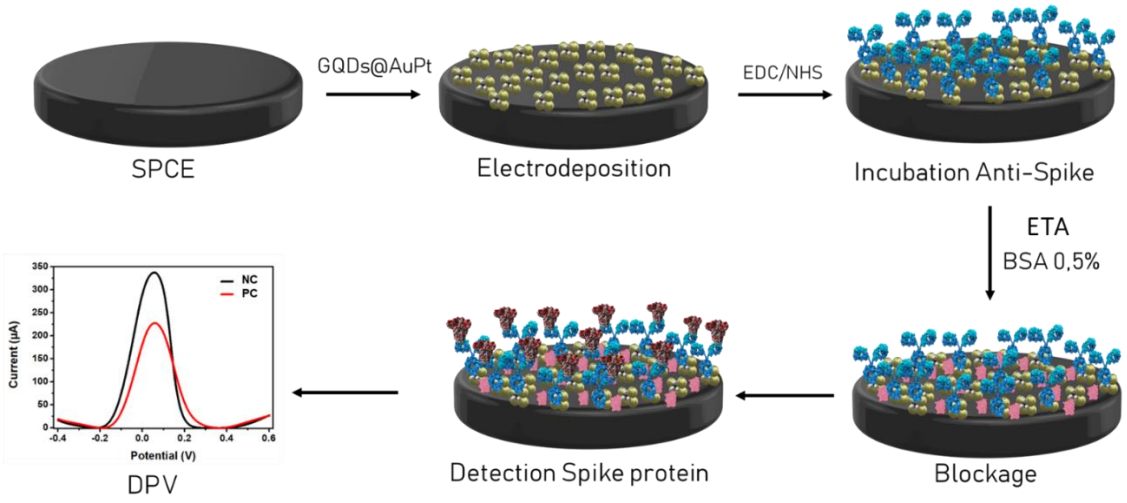

Figure 17. Conceptual schematic of the immunosensor

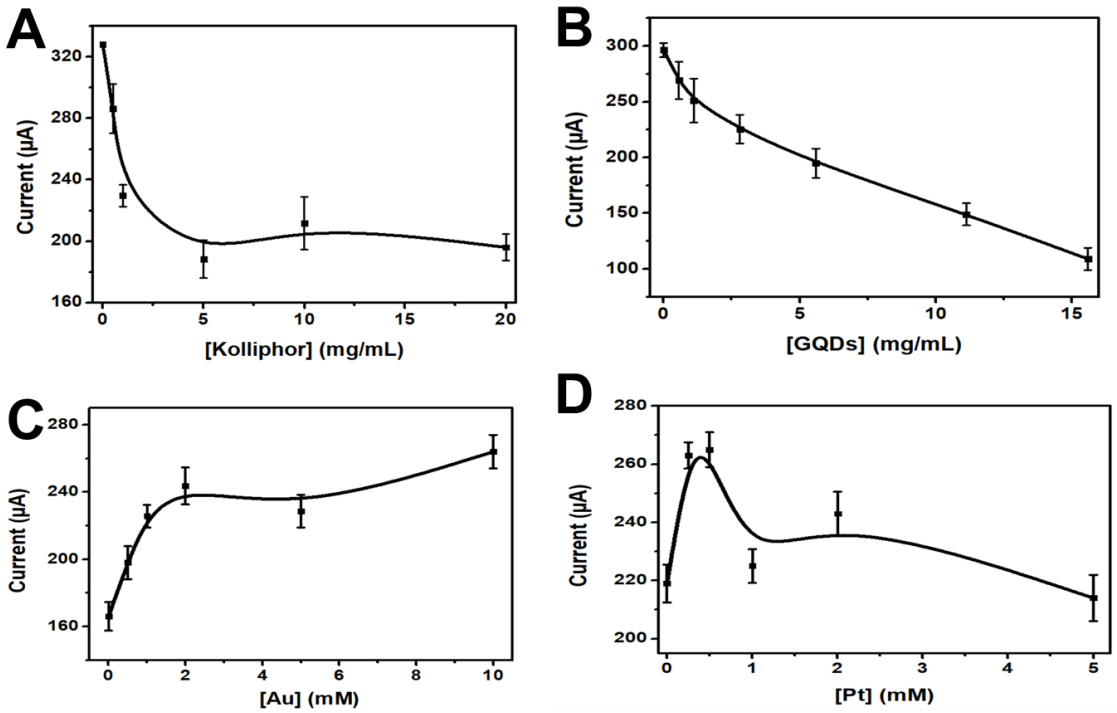

Figure 18. Optimization of A) Kolliphor, B) GQDs, C) Au and D) Pt concentrations in the biosensor platform. DPV at a potential window of -0.4 to 0.6 V, pulse potential to 0.125 V and scan rate to 0.05 V/s

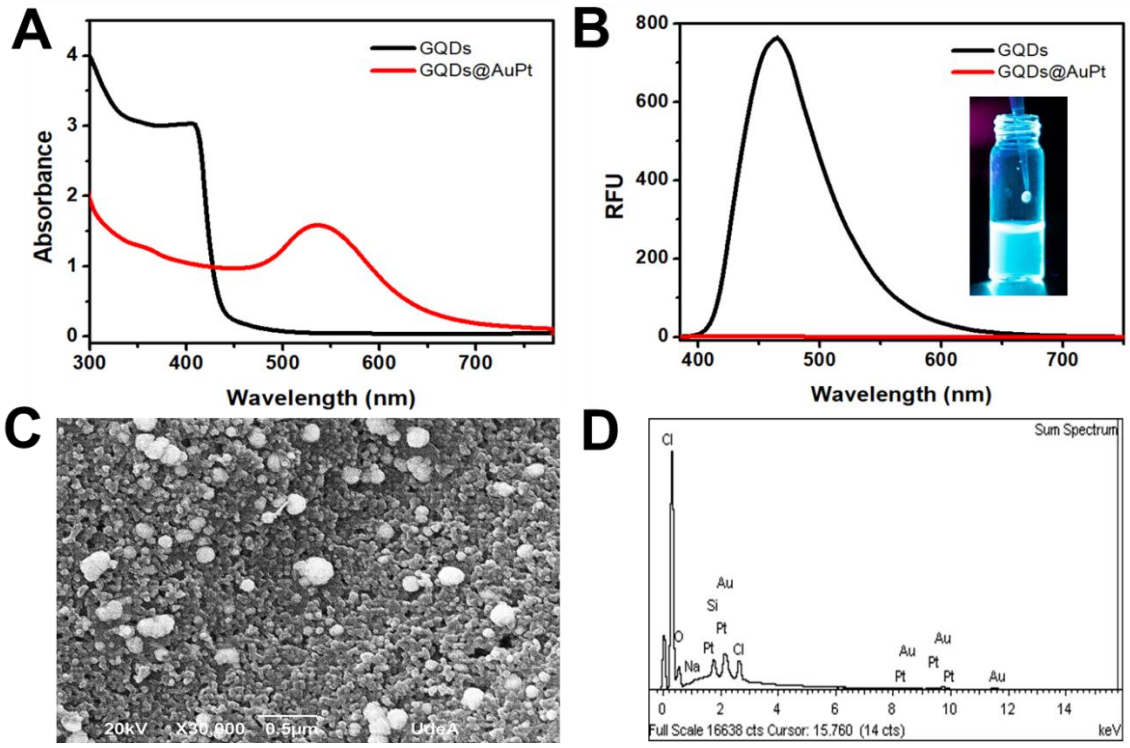

Figure 19. Characterization of A) absorbance, B) fluorescence of GQDs and GQDs@AuPt, C) SEM to 30.000X and D) EDS of modified electrodes

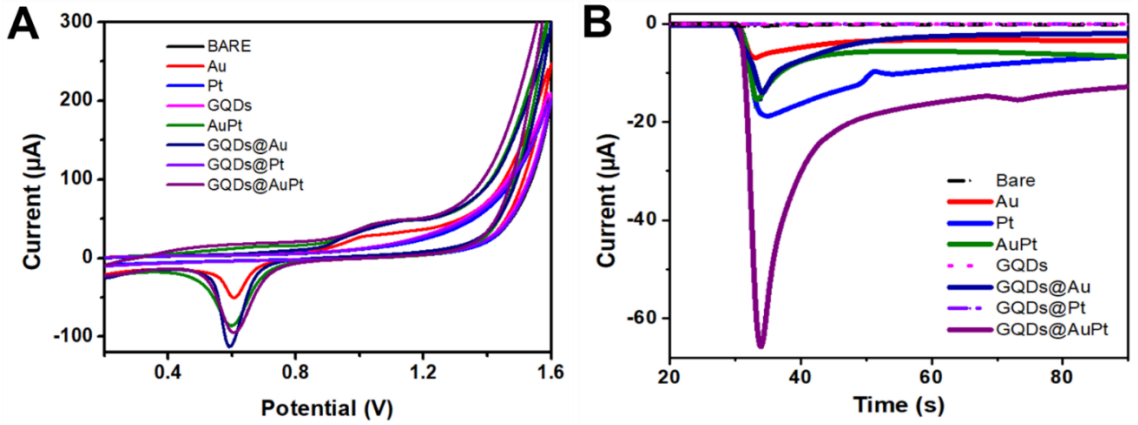

Figure 20. Electrochemical characterization of the bare electrode and controls of GQDs, Au and Pt, and the optimized GQDs@AuPt platform by A) CV in the presence of 0.1 M H_2SO_4 at a sweep rate of 0.1 V/s and a potential window of 0.6 V to 1.6 V and B) Chronoamperometry in the presence of H_20_2 10 mM at a potential

of -125 mV.

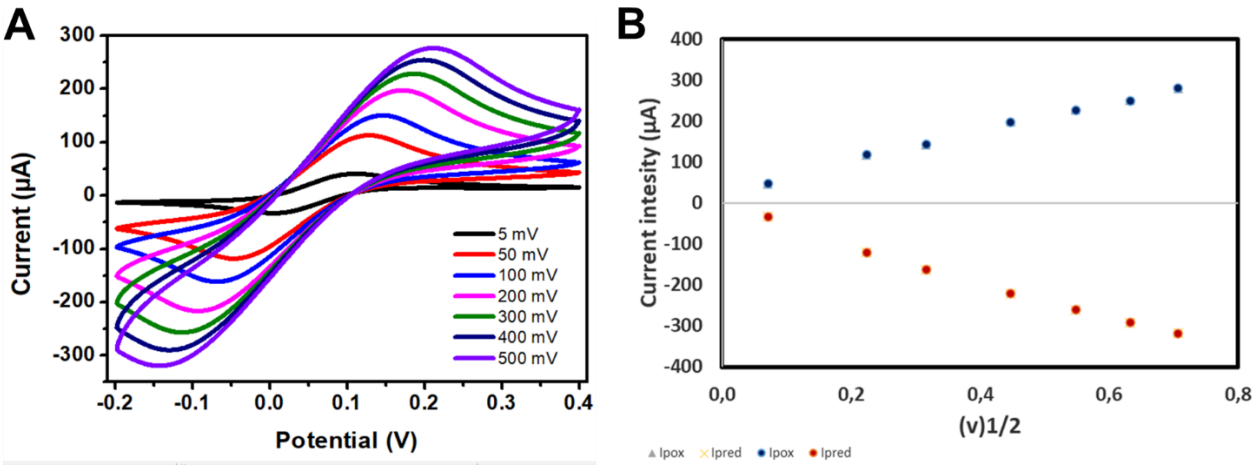

Figure 21. A) CV of the biosensor platform at different scanning speeds and its correlation with B) the response curve of peak current vs. the square root of the scan rate ($v^{1/2}$)

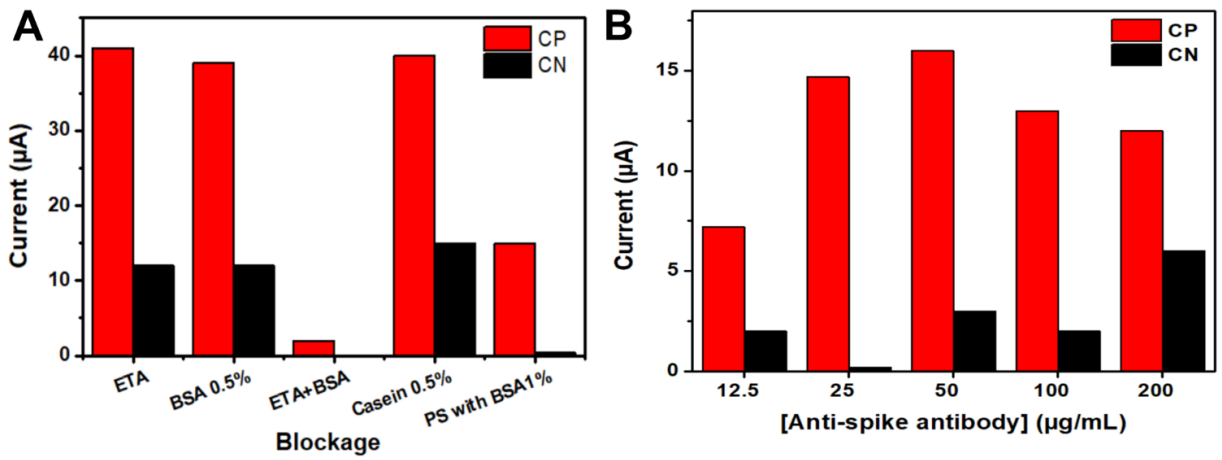

Figure 22. The effect of A) different blocking agents and B) different anti-Spike antibody concentrations in the signal response. (PC, Positive control and NC, Negative control) DPV at a potential window of -0.4 to 0.6 V, pulse potential to 0.125 V and scan rate to 0.05 V/s

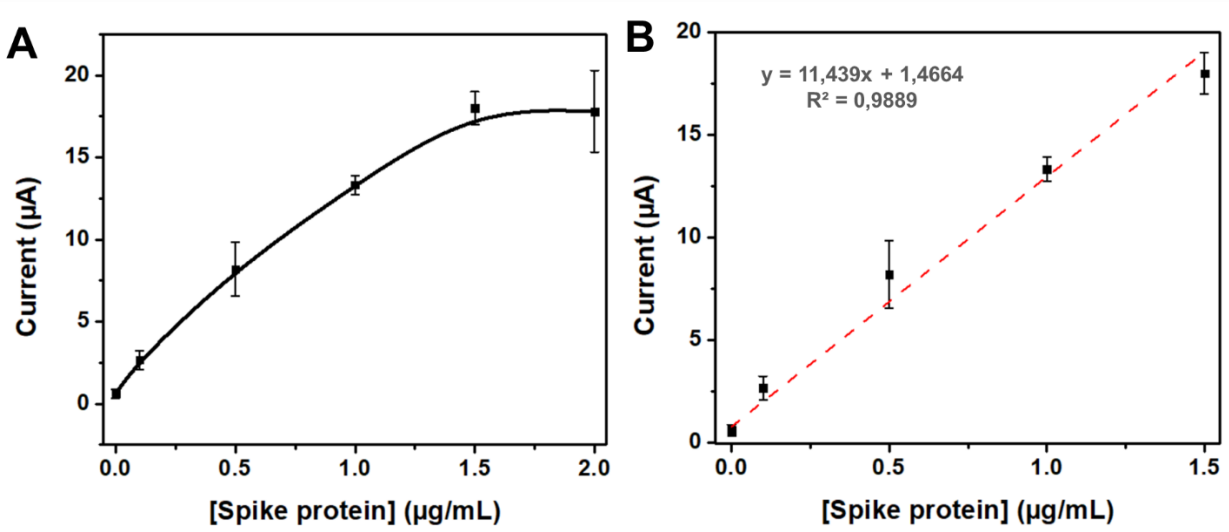

Figure 23. Electrochemical immunosensor response with increasing concentrations of spike protein by DPV at the potential window of -0.4 to 0.6 V, pulse potential to 0.125 V and scan rate to 0.05 V/s